CRUISE REPORT: P09

Created: March 2023, Updated June 2024

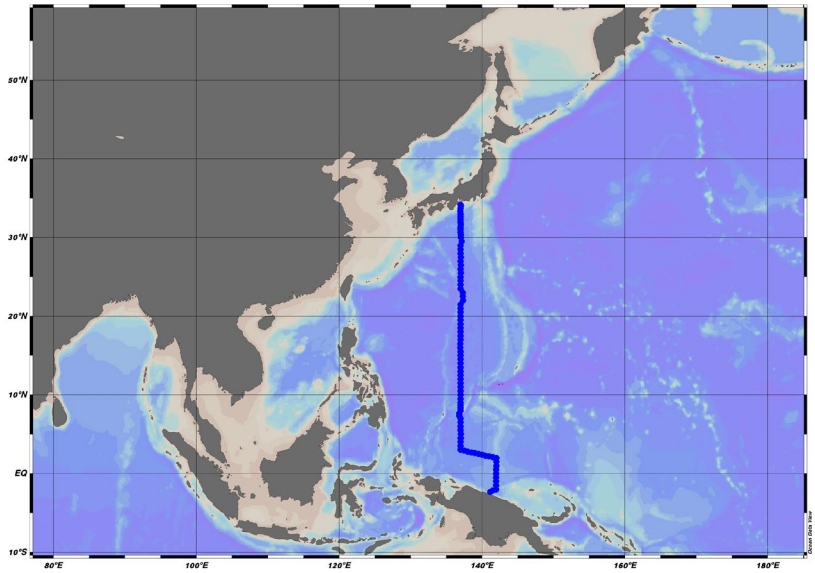

Cruise Summary Information

Section Designation	**P09** (RF22-05)
Expedition Designation (ExpoCode)	49UP20220727
Chief Scientist	NAGAI Naoki / JMA
Dates	**27 July 2022 – 20 August 2022**
Ship	R/V *Ryofu Maru*
Ports of Call	Tokyo, Japan to Tokyo, Japan
Geographic Boundaries	**34.17°N** **136.82°E** **142.01°E** **2.34°S**
Stations	93
Floats and Drifters Deployed	1 APEX Argo float (JAMSTEC) 4 ARVOR Argo floats (JMA)
Moorings Deployed and Recovered	0

Contact Information

HIBINO Sho

Atmospheric Environment and Ocean Division • Japan Meteorological Agency (JMA)

3-6-9, Toranomon, Minato-ku, Tokyo 105-8431, JAPAN

Tel: 81-3-6758-3900 (Ext. 4617) • Fax: +81-3-3434-9125• Email: seadata@met.kishou.go.jp

Report assembled by Savannah Lewis, UCSD/SIO

Links to Selected Topics

Shaded sections are not relevant to this cruise or were not available when this report was compiled.

Cruise Summary Information	Hydrographic Measurements
Description of Scientific Program	CTD Data:
Geographic Boundaries	Acquisition
Cruise Track (Figure): PI CCHDO	Processing
Description of Stations	Calibration
Description of Parameters Sampled	Temperature Pressure
Bottle Depth Distribution (figure)	Conductivity Oxygen
Deployments	Bottle Data
Moorings Deployed or Recovered	Salinity
	Oxygen
Programs and Principal Investigators	Nutrients
Scientific Personnel	Total CO_2
	CFCs and SF_6
Problems and Goals Not Achieved	Total Alkalinity
	pH
	Phytopigment
Underway Data Information	**Lowered Acoustic Doppler Current Profiler**
Navigation Bathymetry	
Acoustic Doppler Current Profiler	
Thermosalinograph	
XBT and/or XCTD	
pCO_2	Acknowledgements
Atmospheric Chemistry Data	
Meteorological Observations	
Chl-a	

Contents

A. Cruise narrative

Highlights
Cruise designation: RF22-05, RF22-06, RF22-07 (WHP-P09 revisit)

a. EXPOCODE: RF22-05 49UP20220727
RF22-06 49UP20220824
RF22-07 49UP20220929

b. Chief scientist: NAGAI Naoki
Atmospheric Environment and Ocean Division
Atmosphere and Ocean Department
Japan Meteorological Agency (JMA)

c. Ship name: R/V Ryofu Maru

d. Ports of call: RF22-05: Tokyo (Japan) – Tokyo (Japan)
RF22-06: Tokyo (Japan) – Tokyo (Japan)
RF22-07: Leg 1: Tokyo (Japan) – Kochi (Japan)
Leg 2: Kochi (Japan) – Tokyo (Japan)

e. Cruise dates (JST): RF22-05: 27 July 2022 – 20 August 2022
RF22-06: 24 August 2022 – 17 September 2022
RF22-07: Leg 1: 29 September 2022 – 19 October 2022
Leg 2: 23 October 2022 – 2 November 2022

f. Principal Investigator (Contact person):
HIBINO Sho
Atmospheric Environment and Ocean Division
Atmosphere and Ocean Department
Japan Meteorological Agency (JMA)
3-6-9, Toranomon, Minato-ku, Tokyo 105-8431, JAPAN
Phone: +81-3-6758-3900 Ext. 4617
FAX: +81-3-3434-9125
E-mail: seadata@met.kishou.go.jp

Cruise Summary

RF22-05, RF22-06 and RF22-07 cruises were carried out during the period from July 27 to November 2, 2022. The cruises started from the north of Papua New Guinea, and sailed towards north along approximately 137°E meridian. This line (WHP-P09) was observed by JMA in 1994 as WOCE (World Ocean Circulation Experiment) Hydrographic Programme and in 2010 and 2016 as CLIVAR (Climate Variability and Predictability Project) / GO-SHIP (Global Ocean Ship-based Hydrographic Investigations Program).

A total of 93 stations were occupied using a Sea-Bird Electronics (SBE) 36 position carousel equipped with 10-liter Niskin water sample bottles, a CTD system (SBE911plus) equipped with SBE35 deep ocean standards thermometer, JFE Advantech oxygen sensor (RINKO III), Valeport altimeter (VA500), and Teledyne RD Instruments L-ADCP (300kHz). To examine consistency of data, we carried out the observation repeatedly twice at stations of 4°30'N, 137°00'E (Stns.24 and 25) and 21°00'N, 137°00'E (Stns.61 and 62) at the cross points of each cruise. Station location and cruise track are shown in Figure A.1 (except Leg 2 at RF22-07).

At almost all station, full-depth CTDO$_2$ (temperature, conductivity (salinity) and dissolved oxygen) profile were taken, and up to 36 water samples were taken and analyzed. Water samples were obtained from 10 dbar to approximately 10 m above the bottom. In addition, surface water was sampled by a stainless steel bucket at each station. Sampling layer is designed as so-called staggered mesh as shown in Table A.1 (*Swift*, 2010). The bottle depth diagram is shown in Figure A.2.

Water samples were analyzed for salinity, dissolved oxygen, nutrients, dissolved inorganic carbon (DIC), total alkalinity (TA), pH, CFCs (CFC-11, CFC-12, and CFC-113), SF_6 and phytopigments (chlorophyll-a and phaeopigment). Underway measurements of partial pressure of carbon dioxide (pCO_2), temperature, salinity, chlorophyll-*a*, subsurface current, bathymetry and meteorological parameters were conducted along the cruise track.

At RF22-05, R/V Ryofu Maru departed from Tokyo (Japan) on July 27, 2022. The hydrographic cast of CTDO$_2$ was started at the first station (Stn.1 (2°20'S, 141°10'E; RF7041)) in the north of Papua New Guinea on August 5. RF22-05 consisted of 24 stations from Stn.1 to Stn.24 (4°30'N, 137°00'E; RF7064). Observation at Stn.24 was finished on August 13. She returned at Tokyo on August 20.

At RF22-06, she departed from Tokyo on August 24. The hydrographic cast of CTDO$_2$ restarted at the same station (Stn.25 (4°30'N, 137°00'E; RF7066)) with the RF22-05 last station on August 30. RF22-06 consisted of 37 stations from Stn.25 to Stn.61 (21°00'N, 137°00'E; RF7102). Observation at Stn.61 was finished on September 12. She returned at Tokyo on September 17.

At RF22-07, she departed from Tokyo on September 29. The hydrographic cast of CTDO$_2$ restarted at same station (Stn.62 (21°00'N, 137°00'E; RF7104)) with the RF22-06 last station on October 3. Observations from Stn.62 to Stn.86 (32°00'N, 137°00'E; RF7128) were carried out in order from the south. After observation at Stn.86, she evacuated to Suruga Bay in Shizuoka (Japan) for avoiding high waves expected in the observation area. She restarted from Stn.93 (34°10'N, 137°00'E; RF7129) on the coast of Japan on October 15 and observed southward to Stn.87 (32°20'N, 137°00'E; RF7136). Observation at Stn.87 was finished on October 16. RF22-07 consisted of 32 stations from Stn.62 to Stn.93. She entered at Kochi on October 19 (Leg 1). At Leg 2, she departed from Kochi on October 23, and observed the pCO2 and the surface layer temperature in the south of Japan, returned at Tokyo on November 2. Location data of stations is shown in Table A.2.

Five Argo floats were deployed along the cruise track. The information of deployed the float is listed in Table A.3.

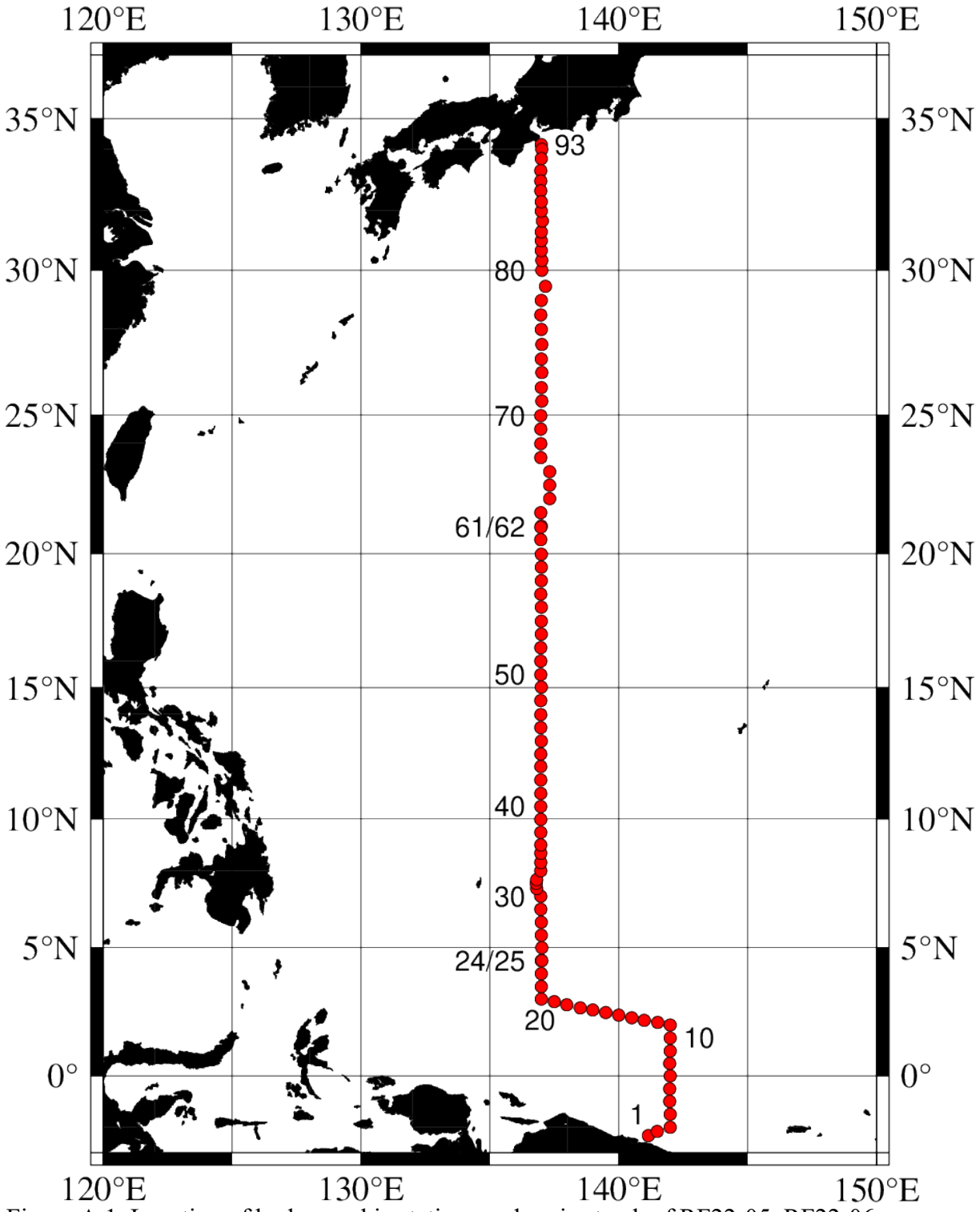

Figure A.1. Location of hydrographic stations and cruise track of RF22-05, RF22-06 and RF22-07. Circles indicate stations along WHP-09.

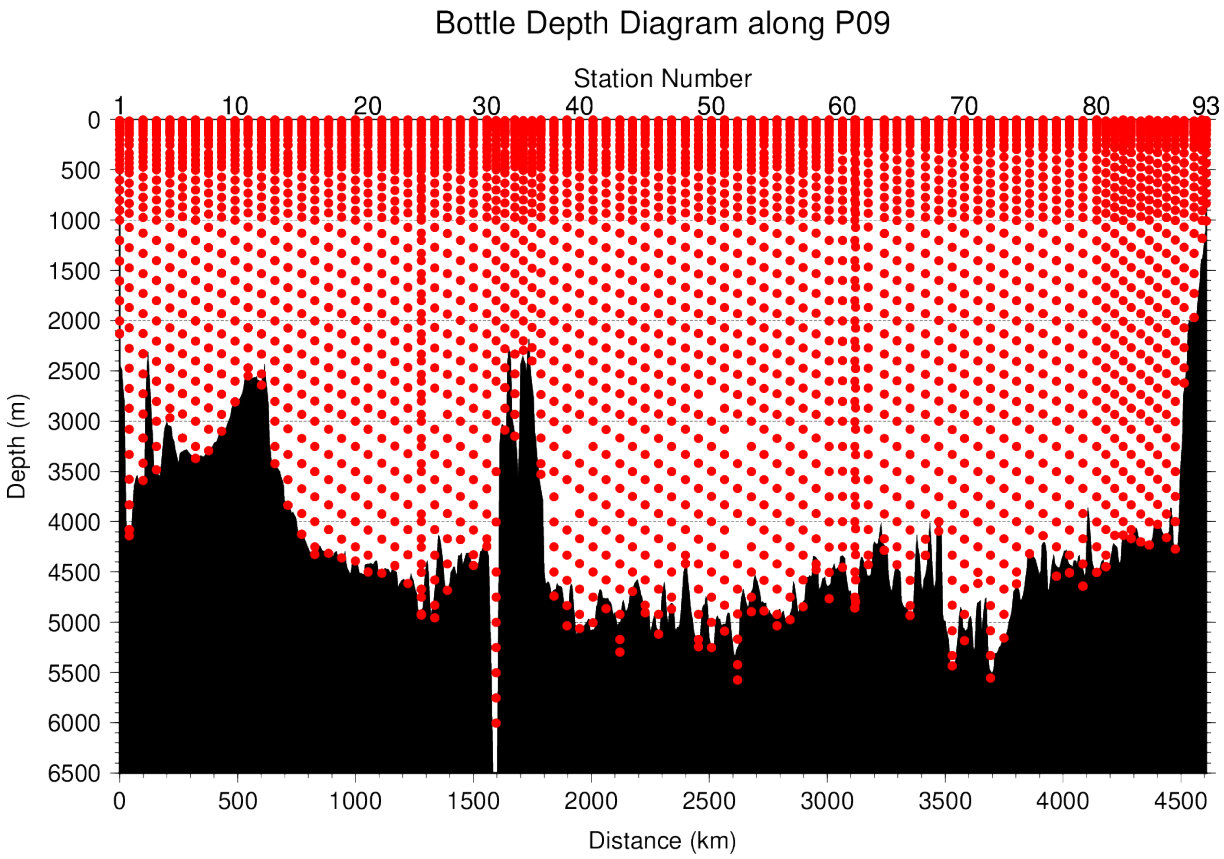

Figure A.2. The bottle depth diagram for WHP-P09 revisit.

Table A.1. The scheme of sampling layer in meters.

	North of 20°N (Stn.60–Stn.93)			South of 20°N (Stn.1–Stn.59)		
Bottle count	***Scheme 1***	***Scheme 2***	***Scheme 3***	***Scheme 4***	***Scheme 5***	***Scheme 6***
1	10	10	10	10	10	10
2	*25*	*25*	*25*	*25*	*25*	*25*
3	50	50	50	50	50	50
4	*75*	*75*	*75*	*75*	*75*	*75*
5	100	100	100	100	100	100
6	*125*	*125*	*125*	*125*	*125*	*125*
7	150	150	150	150	150	150
8	200	200	200	200	200	200
9	250	250	250	250	250	250
10	300	330	280	300	330	280
11	400	430	370	350	380	320
12	500	530	470	400	430	370
13	600	630	570	450	480	420
14	700	730	670	500	530	470
15	800	830	770	600	630	570
16	900	930	870	700	730	670
17	1000	1070	970	800	830	770
18	1200	1270	1130	900	930	870
19	1400	1470	1330	1000	1070	970
20	1600	1670	1530	1200	1270	1130
21	1800	1870	1730	1400	1470	1330
22	2000	2070	1930	1600	1670	1530
23	2200	2270	2130	1800	1870	1730
24	2400	2470	2330	2000	2070	1930
25	2600	2670	2530	2200	2270	2130
26	2800	2870	2730	2400	2470	2330
27	3000	3080	2930	2600	2670	2530
28	*3250*	*3330*	*3170*	*2800*	*2870*	*2730*
29	3500	3580	3420	3000	3080	2930
30	*3750*	*3830*	*3670*	*3250*	*3330*	*3170*
31	4000	4080	3920	3500	3580	3420
32	*4250*	*4330*	*4170*	*3750*	*3830*	*3670*
33	4500	4580	4420	4000	4080	3920
34	*4750*	*4830*	*4670*	*4250*	*4330*	*4170*
35	5000	5080	4920	4500	4580	4420
36	5250	5330	5170	4750	4830	4670
37	5500	5580	5420	5000	5080	4920
38	5750	5830	5670	5250	5330	5170
39	6000	6000	6000	5500	5580	5420
40				5750	5830	5670
41				6000	6000	6000

Scheme 1 to Scheme 3 are applied to the area north of 20°N, while Scheme 4 to Scheme 6 are applied to the area south of 20°N. At some deep stations over 36 layers, some layers shown in italic may be skipped.

Table A.2(a). Station lists of RF22-05 cruise. The 'RF' column indicates the JMA station identification number.

Station		***Location***		***Station***		***Location***	
Stn.	*RF*	*Latitude*	*Longitude*	*Stn.*	*RF*	*Latitude*	*Longitude*
1	7041	02-20.13 S	141-09.15 E	13	7053	02-11.50 N	140-59.64 E
2	7042	02-10.14 S	141-29.08 E	14	7054	02-16.10 N	140-30.17 E
3	7043	02-00.64 S	141-59.04 E	15	7055	02-23.44 N	140-00.04 E
4	7044	01-30.13 S	141-59.32 E	16	7056	02-29.21 N	139-30.50 E
5	7045	00-59.65 S	141-58.62 E	17	7057	02-35.79 N	138-59.40 E
6	7046	00-30.32 S	141-58.70 E	18	7058	02-40.99 N	138-30.23 E
7	7047	00-00.31 S	141-59.37 E	19	7059	02-47.67 N	137-59.50 E
8	7048	00-29.19 N	141-58.95 E	20	7060	02-54.57 N	137-30.73 E
9	7049	00-59.43 N	141-59.48 E	21	7061	03-00.56 N	137-00.19 E
10	7050	01-29.76 N	141-59.82 E	22	7062	03-30.53 N	137-00.96 E
11	7051	01-59.40 N	142-00.44 E	23	7063	04-00.55 N	137-00.86 E
12	7052	02-05.54 N	141-30.24 E	24	7064	04-30.80 N	137-00.95 E

Table A.2(b). Same as Table A.2(a) but for RF22-06 cruise.

Station		***Location***	
Stn.	*RF*	*Latitude*	*Longitude*
25	7066	04-30.84 N	137-01.30 E
26	7067	05-01.47 N	137-01.08 E
27	7068	05-30.42 N	137-00.06 E
28	7069	06-00.32 N	137-00.56 E
29	7070	06-30.58 N	136-59.24 E
30	7071	07-00.63 N	136-58.86 E
31	7072	07-19.80 N	136-49.15 E
32	7073	07-30.13 N	136-48.76 E
33	7074	07-39.71 N	136-49.44 E
34	7075	08-00.18 N	136-58.93 E
35	7076	08-19.91 N	136-59.77 E
36	7077	08-40.49 N	136-59.19 E
37	7078	09-00.28 N	136-59.51 E
38	7079	09-29.99 N	136-59.32 E
39	7080	09-59.93 N	136-59.43 E
40	7081	10-29.14 N	136-59.68 E
41	7082	10-59.88 N	136-58.72 E
42	7083	11-29.81 N	136-59.23 E
43	7084	12-00.68 N	136-59.21 E

Station		***Location***	
Stn.	*RF*	*Latitude*	*Longitude*
44	7085	12-29.79 N	136-59.62E
45	7086	12-59.13 N	137-00.42 E
46	7087	13-29.59 N	136-59.71 E
47	7088	13-59.76 N	136-59.36 E
48	7089	14-31.00 N	136-59.91 E
49	7090	15-01.07 N	137-00.41 E
50	7091	15-30.54 N	136-59.32 E
51	7092	16-00.19 N	136-58.59 E
52	7093	16-30.50 N	136-58.55 E
53	7094	17-01.83 N	137-00.22 E
54	7095	17-30.97 N	137-00.14 E
55	7096	18-01.11 N	137-00.10 E
56	7097	18-30.24 N	136-59.50 E
57	7098	19-00.30 N	137-00.14 E
58	7099	19-30.01 N	137-00.87 E
59	7100	19-59.90 N	137-00.62 E
60	7101	20-30.45 N	136-59.92 E
61	7102	21-00.13 N	137-00.88 E

Table A.2(c). Same as Table A.2(a) but for RF22-07 cruise.

Station		***Location***		***Station***		***Location***	
Stn.	*RF*	*Latitude*	*Longitude*	*Stn.*	*RF*	*Latitude*	*Longitude*
62	7104	20-58.77 N	136-59.83 E	78	7120	28-59.50 N	137-00.25 E
63	7105	21-29.28 N	136-59.23 E	79	7121	29-28.73 N	137-09.88 E
64	7106	22-00.24 N	137-19.80 E	80	7122	30-00.02 N	137-01.17 E
65	7107	22-29.79 N	137-19.12 E	81	7123	30-20.41 N	137-01.66 E
66	7108	22-59.46 N	137-19.00 E	82	7124	30-40.80 N	137-00.92 E
67	7109	23-29.33 N	136-59.47 E	83	7125	31-00.60 N	137-00.89 E
68	7110	23-59.83 N	136-59.22 E	84	7126	31-18.37 N	137-00.51 E
69	7111	24-30.90 N	136-59.26 E	85	7127	31-40.52 N	137-02.13 E
70	7112	24-59.01 N	136-59.41 E	86	7128	31-59.88 N	137-00.27 E
71	7113	25-29.33 N	137-01.01 E	87	7135	32-18.85 N	137-00.19 E
72	7114	25-58.35 N	137-00.90 E	88	7134	32-39.22 N	136-59.16 E
73	7115	26-29.23 N	137-01.76 E	89	7133	32-59.08 N	136-58.87 E
74	7116	26-58.04 N	137-00.96 E	90	7132	33-19.81 N	136-58.23 E
75	7117	27-28.52 N	137-01.12 E	91	7131	33-42.00 N	137-00.05 E
76	7118	27-59.29 N	137-00.39 E	92	7130	34-00.51 N	137-01.03 E
77	7119	28-29.67 N	136-59.61 E	93	7129	34-10.07 N	137-00.78 E

Table A.3. Information of deployed float.

Float WMO number	***Date and Time of Deployment (UTC)***	***Position of deployment*** *Latitude*	*Longitude*	***PI***	***Manufacturer***
5905872	September 4, 2022 00:27	9-59.83 N	136-58.85 E	JAMSTEC	APEX
2903708	September 11, 2022 02:18	20-01.60 N	137-03.39 E	JMA	ARVOR
2903712	October 7, 2022 10:31	27-57.75 N	137-00.04 E	JMA	ARVOR
2903714	October 9, 2022 06:37	30-00.04 N	137-02.38 E	JMA	ARVOR
2903716	October 11, 2022 03:38	31-59.68 N	137-01.45 E	JMA	ARVOR

ARVOR: NKE Instrumentation (France)
APEX: Teledyne Webb Research (USA)

List of Principal Investigators for Measurements

The principal investigators for each parameter are listed in Table A.4.

Table A.4. List of principal investigators for each parameter.

Hydrography	$CTDO_2$	MURAKAMI Kiyoshi
	Salinity	MURAKAMI Kiyoshi
	Dissolve oxygen	KITAGAWA Takahiro
	Nutrients	KITAGAWA Takahiro
	Phytopigments	KITAGAWA Takahiro
	DIC	ENYO Kazutaka
	TA	ENYO Kazutaka
	pH	ENYO Kazutaka
	CFCs	ENYO Kazutaka
	SF_6	ENYO Kazutaka
	LADCP	MURAKAMI Kiyoshi
Underway	Meteorology	NAGAI Naoki
	Thermo-Salinograph	ENYO Kazutaka
	pCO_2	ENYO Kazutaka
	Chlorophyll *a*	KITAGAWA Takahiro
	ADCP	MURAKAMI Kiyoshi
	Bathymetry	MURAKAMI Kiyoshi
Float	JMA	NAKAMURA Tetsuya
	JAMSTEC	HOSODA Shigeki

Reference

Swift, J. H. (2010): Reference-quality water sample data: Notes on acquisition, record keeping, and evaluation. *IOCCP Report No.**14**, ICPO Pub. 134, 2010 ver.1*

B. Underway measurements

1. Navigation

27 March 2024

(1) Personnel

MURAKAMI Kiyoshi (JMA)
SEGAWA Takahiro (JMA)

(2) Overview of the equipment

The ship's position was measured by navigation system manufactured by FURUNO ELECTRIC CO., LTD., Japan. The system has three 12-channels GPS receivers (GP-150, GP-170, JLR-7800).
GPS antennas were installed on the compass deck. We switched the receivers to choose better receiving state if the number of received GPS satellites was small or HDOP was large. The GPS data, gyro heading data and log speed data were integrated and delivered to two workstations. These workstations work as the primary and secondary NTP (Network Time Protocol) servers.
The navigation data were obtained approximately every one second and one minute data were extracted from one second data. These one minute data were recorded as "LOG data (GPS data)".

(3) Data Period

03:01, 27 Jul. 2022 to 22:59, 19 Aug. 2022 (UTC).
03:15, 24 Aug. 2022 to 00:00, 15 Sep. 2022 (UTC).
03:45, 29 Sep. 2022 to 00:00, 19 Oct. 2022 (UTC)

2. Bathymetry

27 March 2024

(1) Personnel

MURAKAMI Kiyoshi (JMA)
SEGAWA Takahiro (JMA)

(2) Overview of the equipment

R/V Ryofu Maru equipped a single beam echo sounder, EA 600 (Kongsberg Maritime, Norway). The main objective of the survey is to collect continuous bathymetry data along ship's track.
The sound speed to correct depth data was set to 1500 m/s during the cruise. Data interval was about 10 seconds in the measurement for 7500 m depth.

(3) System Configuration and Performance

System:	Kongsberg EA 600
Frequency:	12 kHz
Transmit power:	2 kW
Transmit pulse interval:	Within 20 seconds
Depth range:	5–15,000 m
Depth resolution:	1 cm
Depth accuracy (Assuming correct sound velocity, transducer depth and shortest pulse length):	Within 20 cm

(4) Data Period

03:01, 27 Jul. 2022 to 05:00, 03 Aug. 2022 (UTC).
21:20, 03 Aug. 2022 to 22:59, 19 Aug. 2022 (UTC).
03:15, 24 Aug. 2022 to 00:00, 15 Sep. 2022 (UTC).
03:45, 29 Sep. 2022 to 00:00, 19 Oct. 2022 (UTC)

Underway chlorophyll-a

31 March 2023

(1) Personnel

KITAGAWA Takahiro
FUJII Takuya
NAKAMURA Motohiro (RF22-05, RF22-06)
HASHIMOTO Susumu (RF22-06, RF22-07)
OCHIAI Naoko (RF22-05, RF22-07)
FUJIWARA Hiroyuki (RF22-05)
UEHARA Tomohiro (RF22-06)
KAKUYA Keita (RF22-07)

(2) Method

The Continuous Sea Surface Water Monitoring System of fluorescence (Nippon Kaiyo, Japan) automatically had been continuously measured seawater which is pumped from a depth of about 4.5 m below the maximum load line to the laboratory. The flow rate of the surface seawater was controlled by several valves and adjusted to about 0.6 L min^{-1}. The sensor in this system is a fluorometer 10-AU (S/N: 1100411 (RF22-05) and S/N 7063 (RF22-06 and RF22-07), Turner Designs, United States).

(3) Observation log

The chlorophyll-*a* continuous measurements were conducted during the entire cruise; from 27 Jul. to 19 Aug., 2022 in RF22-05, 24 Aug. to 15 Sep., 2022 in RF22-06, and from 29 Sep. to 17 Oct., 2022 in RF22-07.

(4) Water sampling

Surface seawater was corrected from outlet of water line of the system at nominally 1 day intervals. The seawater sample was measured in the same procedure as hydrographic samples of chlorophyll-*a* (see Chapter C9 “Phytopigments”).

(5) Calibration

At the beginning and the end of legs, a raw fluorescence value of sensor was adjusted in sensitivity of the sensor using deionized water and a rhodamine 0.1ppm solution measured.
After the cruise, the fluorescence value was converted to chlorophyll-*a* concentration by programs in the system based on nearby water sampling data (chlorophyll-*a* concentration and distance from location of sensor data).

(6) Data

Underway fluorescence and chlorophyll-*a* data is distributed in JMA format in “49UP20220727_P09_underway_chl.csv”. The record structure of the format is as follows;

Column1 DATE: Date (YYYYMMDD) [JST]
Column2 TIME: Time (HHMM) [JST] (= UTC + 9h)
Column3 LATITUDE: Latitude

Column4 LONGITUDE: Longitude
Column5 FLUOR: Fluorescence value (RFU)
Column6 CHLORA: Chlorophyll-*a* concentration (μg L^{-1})
Column7 BTLCHL: Chlorophyll-*a* concentration of water sampling (μg L^{-1}).

(7) Problems

On RF22-05, raw fluorescence values of sensor drifted over time. We determined that there was a problem with the quality of the observation data.
The fluorometer was replaced from RF22-06, and no problems occurred on RF22-06 and RF22-07.

7. Acoustic Doppler Current Profiler

27 March 2024

(1) Personnel

MURAKAMI Kiyoshi (GEMD/JMA)
WADA Kouichi (GEMD/JMA)

(2) Instruments and Methods

Current direction and speed were measured by the hull-mounted 38 kHz Ocean Surveyor ADCP (Teledyne RD Instruments, Inc., USA; hereafter TRDI). The transducer of the system was installed in a dome at 3 m left of center and 13 m aft of the bow at the water line. The firmware version was 23.19 and the data acquisition software was TRDI/VMDAS Version. 1.49. The instrument was used in water-tracking mode during the operations, and was recording each ping raw data in 20 m × 60 bin from about 36 m to 1200 m in depth. Sampling interval was variable as short as possible and typically 6.4 seconds. GPS navigation data and ship's gyrocompass data were recorded with the ADCP data. In addition to the raw data, 60 seconds and 300 seconds averaged data were stored as short term average (STA) and long term average (LTA) data, respectively. Current field based on the gyrocompass was used to check the operation and the performance on board.

(3) Performance and quick view of the ADCP data on board

The performance of the ADCP instrument was almost good throughout the cruise, and current profiles were usually reached about 1000 m. We monitored the current profiles based on LTA data in this cruise on board.

(4) Data Processing

LTA data were processed by CODAS (Common Oceanographic Data Access System) software, developed at the University of Hawaii (https://currents.soest.hawaii.edu/docs/adcp_doc/index.html). We used a standard CODAS processing including a PC time correction, a sound-speed correction based on the thermistor temperature at the transducers, and an amplitude and phase calibration constant applied to the measured velocities.

Calibration constants to be applied were evaluated for each leg using the water track data. The values of amplitude and phase applied to each leg are listed in Table B.7.1. Figure B.7.1 shows surface current at the depth of 36 m during the cruise.

Table B.7.1. The values of amplitude and phase applied to each leg (cruise).

	Amplitude	Phase
RF2205	1.0026	-0.4516
RF2206	1.0050	-0.4798
RF2207	1.0002	0.0181

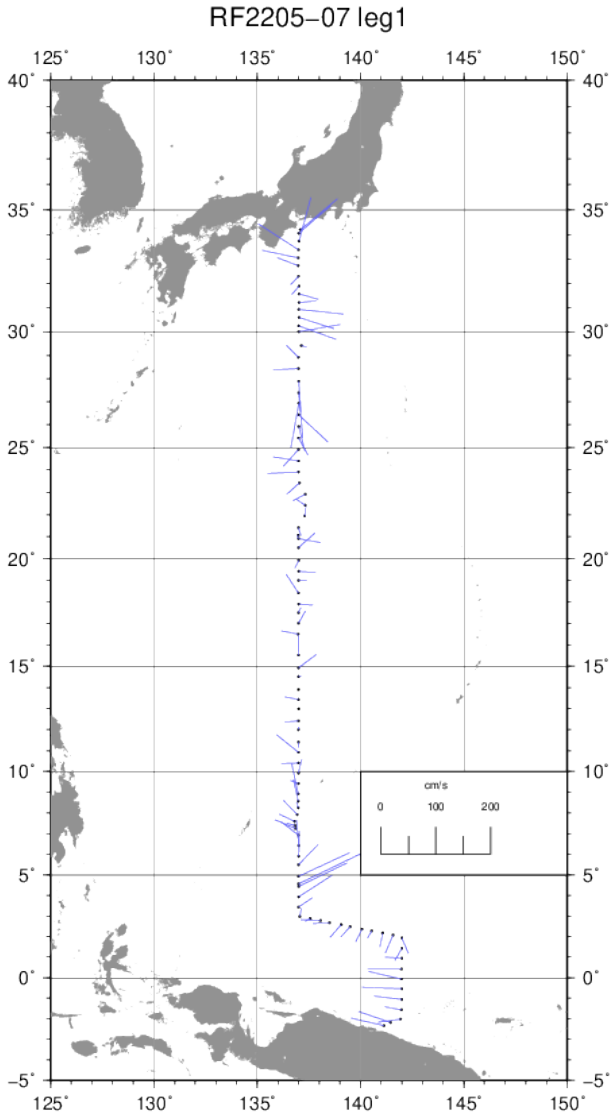

Figure B.7.1. Surface current at the depth of 36 m.

Reference

Joyce, T. M. (1988), On in-situ “calibration” of shipboard ADCPs. *J. Atmos. Oceanic Technol.*, 6, 169-172.

C. Hydrographic Measurement Techniques and Calibration

$CTDO_2$ Measurements

27 March 2024

(1) Personnel

TANAKA Kiyoshi
MURAKAMI Kiyoshi (RF2206, RF2207)
HIGASHI Yoshikazu (RF2206, RF2207)
WADA Kouichi (RF2205, RF2207)
SEGAWA Takahiro (RF2205, RF2207)
CHIBA Yasuomi (RF2205, RF2206)
TANAKA Hidekazu (RF2205, RF2206)

(2) $CTDO_2$ measurement system

(*Software*: SEASAVEwin32 ver7.23.2)

Deck unit	***Serial number***	***Station***
SBE 11plus (SBE)	11P35251 – 0683	RF7040 – 7135
Under-water unit	***Serial number***	***Station***
SBE 9plus (SBE)	09P69709 –1103 (Pressure : 123135)	RF7040 – 7135
Temperature	***Serial number***	***Station***
SBE 3plus (SBE)	03P6159 (primary) 03P4321 (secondary)	RF7040 – 7135 RF7040 – 7135
SBE 35 (SBE)	0093	RF7040 – 7135
Conductivity	***Serial number***	***Station***
SBE 4C (SBE)	043697 (primary) 046059 (secondary)	RF7040 – 7135 RF7040 – 7135
Pump	***Serial number***	***Station***
SBE 5T (SBE)	056552 (primary) 058892 (primary) 057934 (secondary) 059398 (secondary)	RF7040 RF7041 – 7135 RF7040 – 7134 RF7135
Oxygen	***Serial number***	***Station***
RINKO III (JFE)	392 (foil number: 200633A) 356 (foil number:200633A)	RF7040 – 7135 RF7040 – 7135
Water sampler (36 position)	***Serial number***	***Station***
SBE 32 (SBE)	32 – 1270	RF7040 – 7135
Altimeter	***Serial number***	***Station***
VA500 (VA)	69758	RF7040 – 7135
Water sampling bottle		***Station***
Niskin Bottle (GO)		RF7040 – 7135

SBE: Sea- Bird Electronics, Inc., USA
JFE: JFE Advantech Co., Ltd., Japan
VA: VALEPORT, Inc., UK
GO: General Oceanics, Inc., USA

(3) Pre-cruise calibration

(3.1) Pressure

S/N 09P 69709-1103(123135), 25 Feb. 2022

c_1	=	-4.282684×10^4	t_1	=	3.006702×10
c_2	=	5.097742×10^{-1}	t_2	=	-8.607997×10^{-5}
c_3	=	1.312000×10^{-2}	t_3	=	3.727820×10^{-6}
d_1	=	3.583800×10^{-2}	t_4	=	3.699030×10^{-9}
d_2	=	0.000000	t_5	=	0.000000

Formula:

$$c = c_1 + c_2 \times U + c_3 \times U^2$$

$$d = d_1 + d_2 \times U$$

$$t_0 = t_1 + t_2 \times U + t_3 \times U^2 + t_4 \times U^3 + t_5 \times U^4$$

U (*degrees Celsius*) = *M* × (*12-bit pressure temperature compensation word*) + *B*

U: temperature in degrees Celsius

S/N 1103 coefficients in SEASOFT (configuration sheet dated on *25 Feb. 2022)*

$M = 1.28040 \times 10^{-2}$, $B = -9.31868$

Finally, pressure is computed as

$$P(psi) = c \times (1 - t_0^2 / t^2) \times \{1 - d \times (1 - t_0^2 / t^2)\}$$

t: pressure period (μsec)

The drift-corrected pressure is computed as

$$Drift\ corrected\ pressure(dbar) = slope \times (computed\ pressure\ in\ dbar) + offset$$

Slope = 0.99990, Offset = −0.5007

(3.2) Temperature (ITS-90): SBE 3plus

*S/N 03P*6159 *(primary), 20 Oct. 2021*

g	=	$4.32896843 \times 10^{-3}$	j	=	$2.03049914 \times 10^{-6}$
h	=	$6.34331696 \times 10^{-4}$	f_0	=	1000.0
i	=	$2.16892784 \times 10^{-5}$			

*S/N 03P*4321 *(secondary), 19 Jan. 2022*

g	=	$4.39112463 \times 10^{-3}$	j	=	$1.95502273 \times 10^{-6}$
h	=	$6.47351045 \times 10^{-4}$	f_0	=	1000.0
i	=	$2.30648901 \times 10^{-5}$			

Formula:

$$Temperature(ITS-90) = \frac{1}{g + h \times \ln(f_0/f) + i \times \ln^2(f_0/f) + j \times \ln^3(f_0/f)} - 273.15$$

f: Instrument freq.[Hz]

(3.3) Deep Ocean Standards Thermometer Temperature (ITS-90): SBE 35

S/N 0093, 27 Oct. 2020

a_0	=	$4.12756963 \times 10^{-3}$	a_3	=	$-9.36245277 \times 10^{-6}$
a_1	=	$-1.08163464 \times 10^{-3}$	a_4	=	$2.00979198 \times 10^{-7}$
a_2	=	$1.67453817 \times 10^{-4}$			

Formula:

$$Linearized\ temperature(ITS-90) = 1/\{a_0 + a_1 \times \ln(n) + a_2 \times \ln^2(n) + a_3 \times \ln^3(n) + a_4 \times \ln^4(n)\} - 273.15$$

n: instrument output

The slow time drift of the SBE 35

S/N 0093, 18 Nov. 2021 (2nd step: fixed point calibration)

Slope = 1.000003, Offset = -0.000148

Formula:

$$Temperature(ITS-90) = slope \times (Linearized\ temperature) + offset$$

(3.4) Conductivity: SBE 4C

S/N 043697 (primary), 28 Jan. 2022

g	=	-9.71159477	j	=	$-2.55900486 \times 10^{-5}$
h	=	1.23873705	CP_{cor}	=	-9.5700×10^{-8}
i	=	$1.40974545 \times 10^{-3}$	CT_{cor}	=	3.2500×10^{-6}

S/N 046059 (secondary), 31 Mar. 2022

g	=	-1.02654717×10	j	=	$2.24507825 \times 10^{-4}$
h	=	1.60537792	CP_{cor}	=	-9.5700×10^{-8}
i	=	$-1.61160297 \times 10^{-3}$	CT_{cor}	=	3.2500×10^{-6}

Conductivity of a fluid in the cell is expressed as:

$$C(S/m) = \left(g + h \times f^2 + i \times f^3 + j \times f^4\right) \Big/ \left\{10 \times \left(1 + CT_{cor} \times t + CP_{cor} \times p\right)\right\}$$

f: instrument frequency (kHz)
t: water temperature (degrees Celsius)
p: water pressure (dbar).

(3.5) Oxygen (RINKO III)

The RINKO III (JFE Advantech Co., Ltd., Japan) sensor is based on the ability of a selected substance to act as a dynamic fluorescence quencher. The RINKO III model is designed to be used with a CTD system that accepts an auxiliary analog sensor, and it is designed to operate down to 7000 m. The RINKO III output is expressed in voltage from 0 to 5 V.

(4) Quality control and data correction during the cruise

(4.1) Temporal change of deck pressure

The post-cruise drift corrected pressure was computed as follows:

$$Drift\ corrected\ pressure(dbar) = slope \times (computed\ pressure\ in\ dbar) + offset$$

S/N 09P69709 –1103, 27 Feb. 2023

Slope = 1.00000, Offset = −0.2490

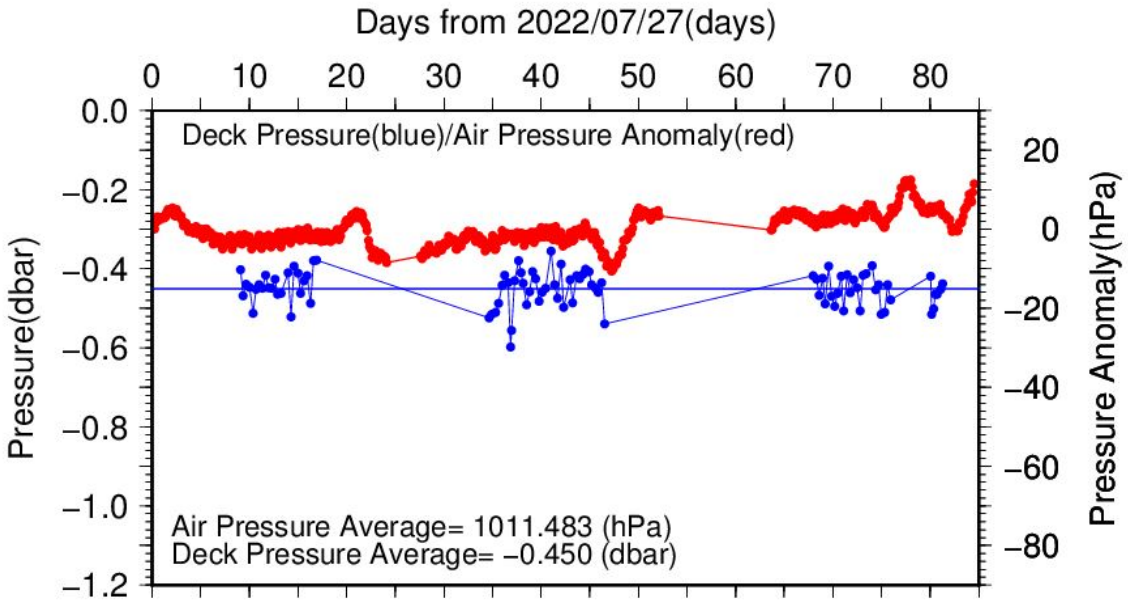

Figure C.1.1. Time series of the CTD deck pressure. Red line indicates atmospheric pressure anomaly. Blue line and dots indicate pre-cast deck pressure and average.

(4.2) Temperature sensor (SBE 3plus)

The practical corrections for the CTD temperature data can be made by using a SBE 35 and correcting the SBE 3plus so that it agrees with the SBE 35 (*McTaggart et al., 2010*; *Uchida et al., 2007*).

CTD temperature is corrected as follows:

$$Corrected\ temperature = T - (c_0 + c_1 \times P + c_2 \times P^2)$$

T: CTD temperature (degrees Celsius), *P:* pressure (dbar), and c_0, c_1, c_2: coefficients

Table C.1.1. Temperature correction summary (pressure ≥ 2000dbar). (Bold: accepted sensor)

S/N	*Num*	c_0*(K)*	c_1*(K/dbar)*	C_2*(K/dbar^2)*	*Stations*
03P6159	**230**	**6.406639×10^{-4}**	**0.000000**	**0.000000**	**RF7040 – 7064**
03P6159	443	6.949485×10^{-4}	-8.851556×10^{-8}	1.089389×10^{-11}	RF7065 (※) **RF7066 – 7067** RF7068 – 7102
03P6159	**369**	**5.199946×10^{-4}**	**0.000000**	**0.000000**	**RF7103 – 7135**
03P4321	230	7.108319×10^{-4}	0.000000	0.000000	RF7040 – 7064
03P4321	**415**	**-4.949481×10^{-6}**	**2.372874×10^{-7}**	**$-1.249677 \times 10^{-11}$**	**RF7065** (※) RF7066 – 7067

					RF7068 – 7102
03P4321	369	-6.060353×10^{-5}	2.505086×10^{-7}	$-1.368830 \times 10^{-11}$	RF7103 – 7135

※From station RF7066 to RF7067, S/N 03P6159 was accepted instead of S/N 03P4321 due to data failure. After RF7068, this data failure was resolved.

Table C.1.2. Temperature correction summary for S/N 03P 6159.

Stations	Pressure < 2000dbar			Pressure ≥ 2000 dbar		
	Num	Average (K)	Std (K)	Num	Average (K)	Std (K)
RF7040 – 7064	569	– 0.0003	0.0093	230	0.0000	0.0002
RF7065 – 7102	828	– 0.0001	0.0090	443	0.0000	0.0001
RF7103 – 7135	726	– 0.0003	0.0078	369	0.0000	0.0001

Table C.1.3. Temperature correction summary for S/N 03P 4321.

Stations	Pressure < 2000dbar			Pressure ≥ 2000 dbar		
	Num	Average (K)	Std (K)	Num	Average (K)	Std (K)
RF7040 – 7064	569	– 0.0009	0.0149	230	0.0000	0.0002
RF7065 – 7102	782	– 0.0012	0.0078	415	0.0000	0.0001
RF7103 – 7135	726	– 0.0008	0.0092	369	0.0000	0.0002

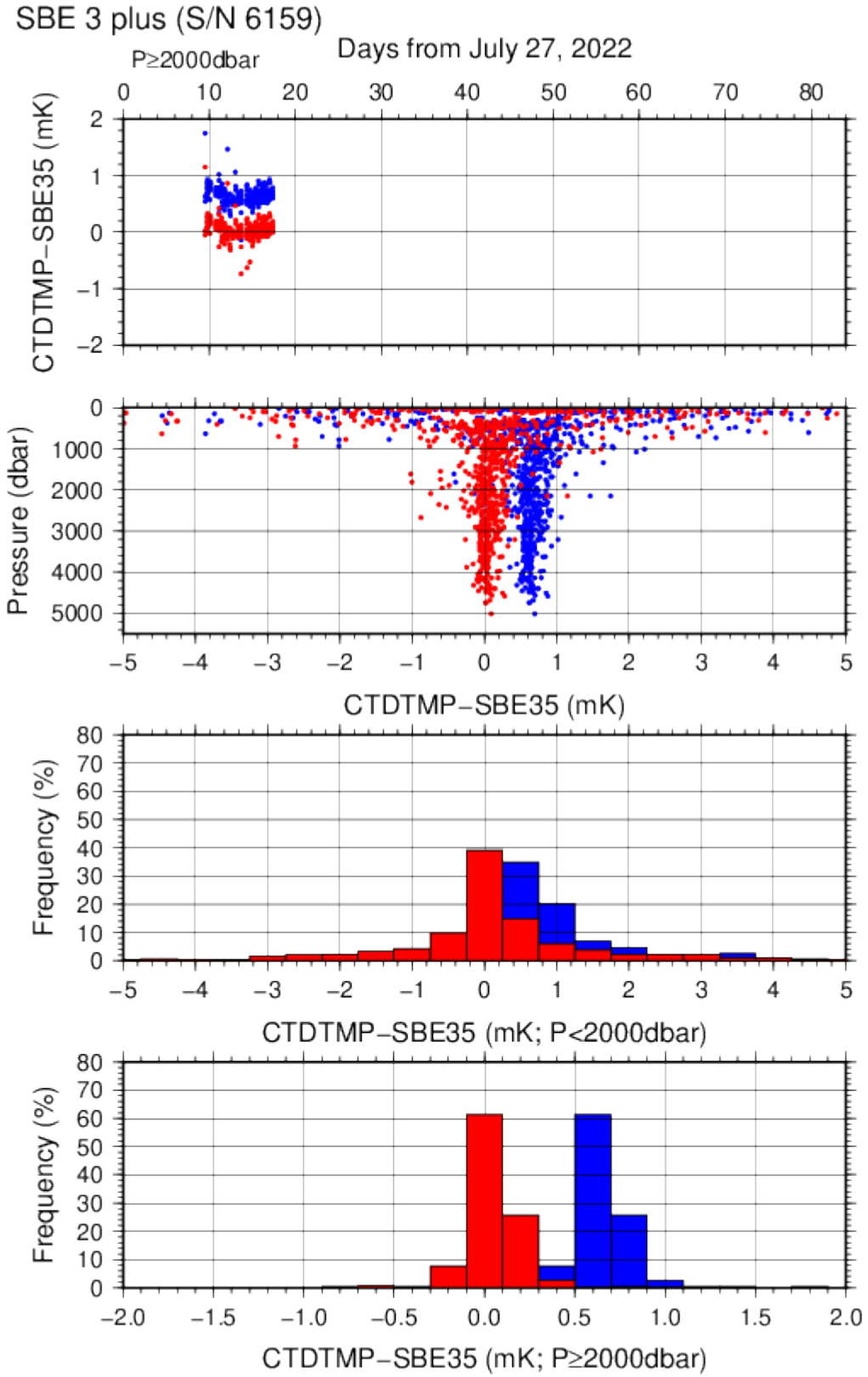

Figure C.1.2. Difference between the CTD temperature (*S/N 03P 6159*) and the Deep Ocean Standards thermometer (SBE 35) on RF22-05. Blue and red dots indicate before and after the correction using SBE 35 data, respectively. Lower two panels show histograms of the differences after correction.

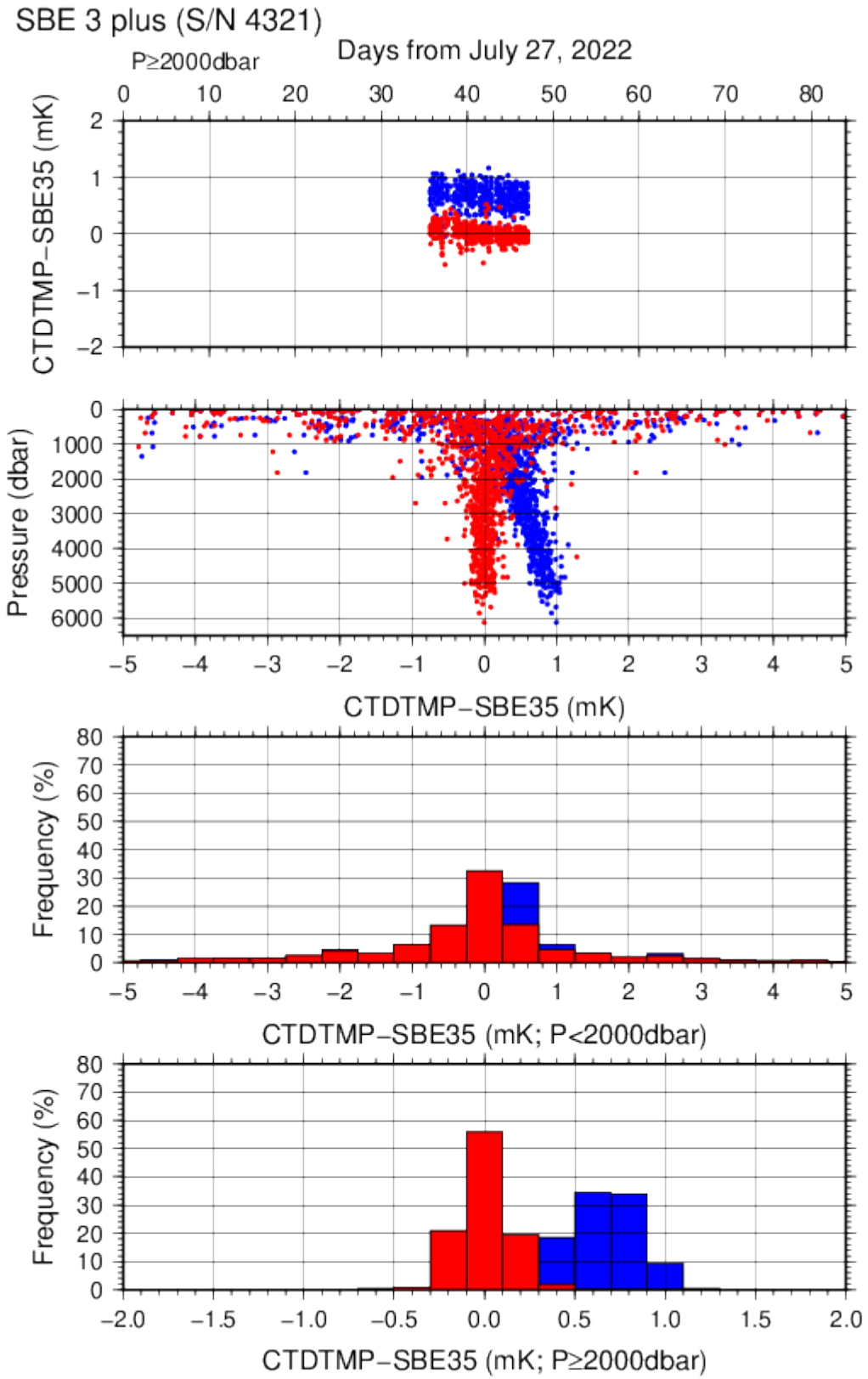

Figure C.1.3. Difference between the CTD temperature (*S/N 03P 4321*) and the Deep Ocean Standards thermometer (SBE 35) on RF22-06. Blue and red dots indicate before and after the correction using SBE 35 data, respectively. Lower two panels show histograms of the differences after correction.

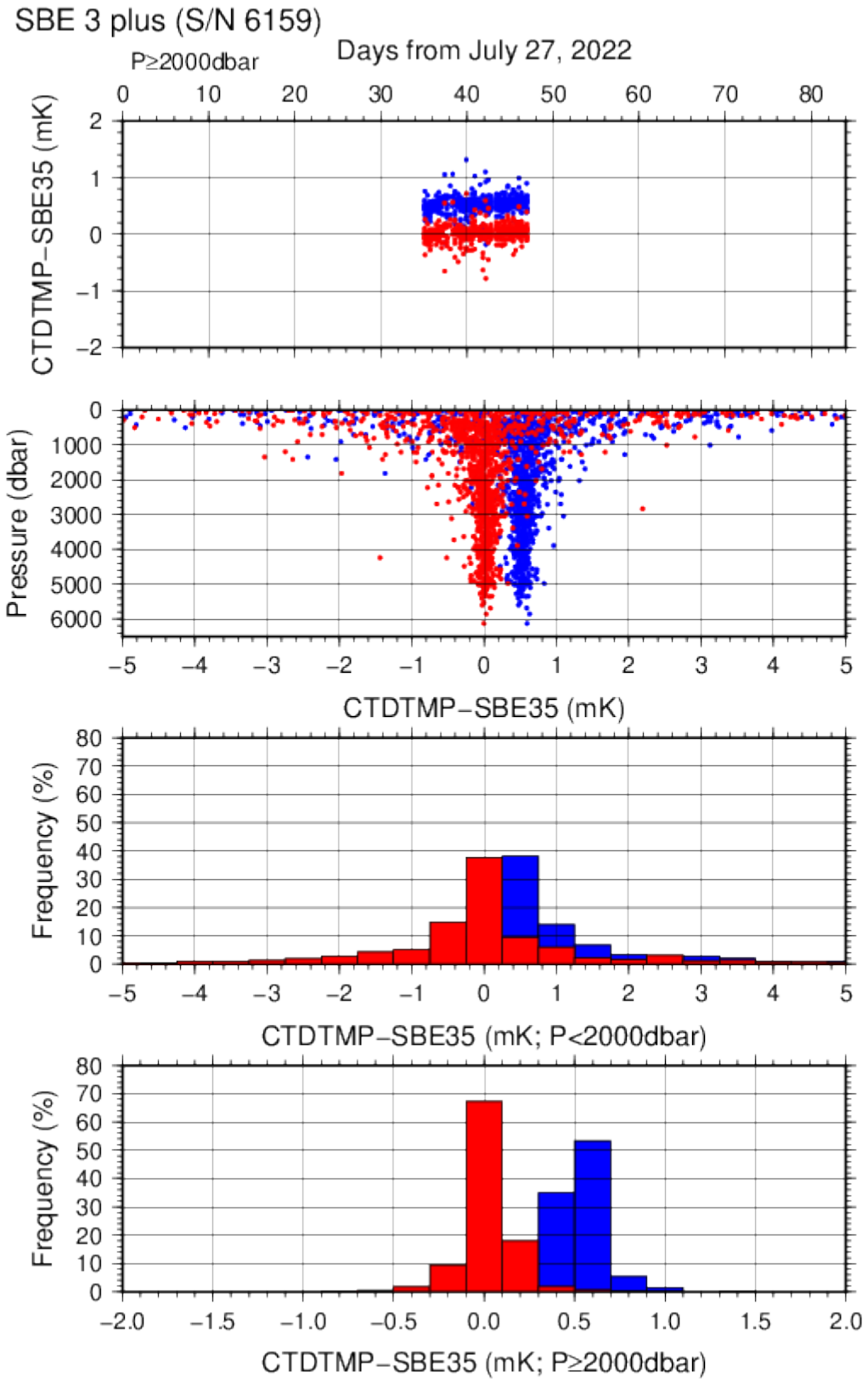

Figure C.1.4. Difference between the CTD temperature (*S/N 03P 6159*) and the Deep Ocean Standards thermometer (SBE 35) on RF22-06. Blue and red dots indicate before and after the correction using SBE 35 data, respectively. Lower two panels show histograms of the differences after correction.

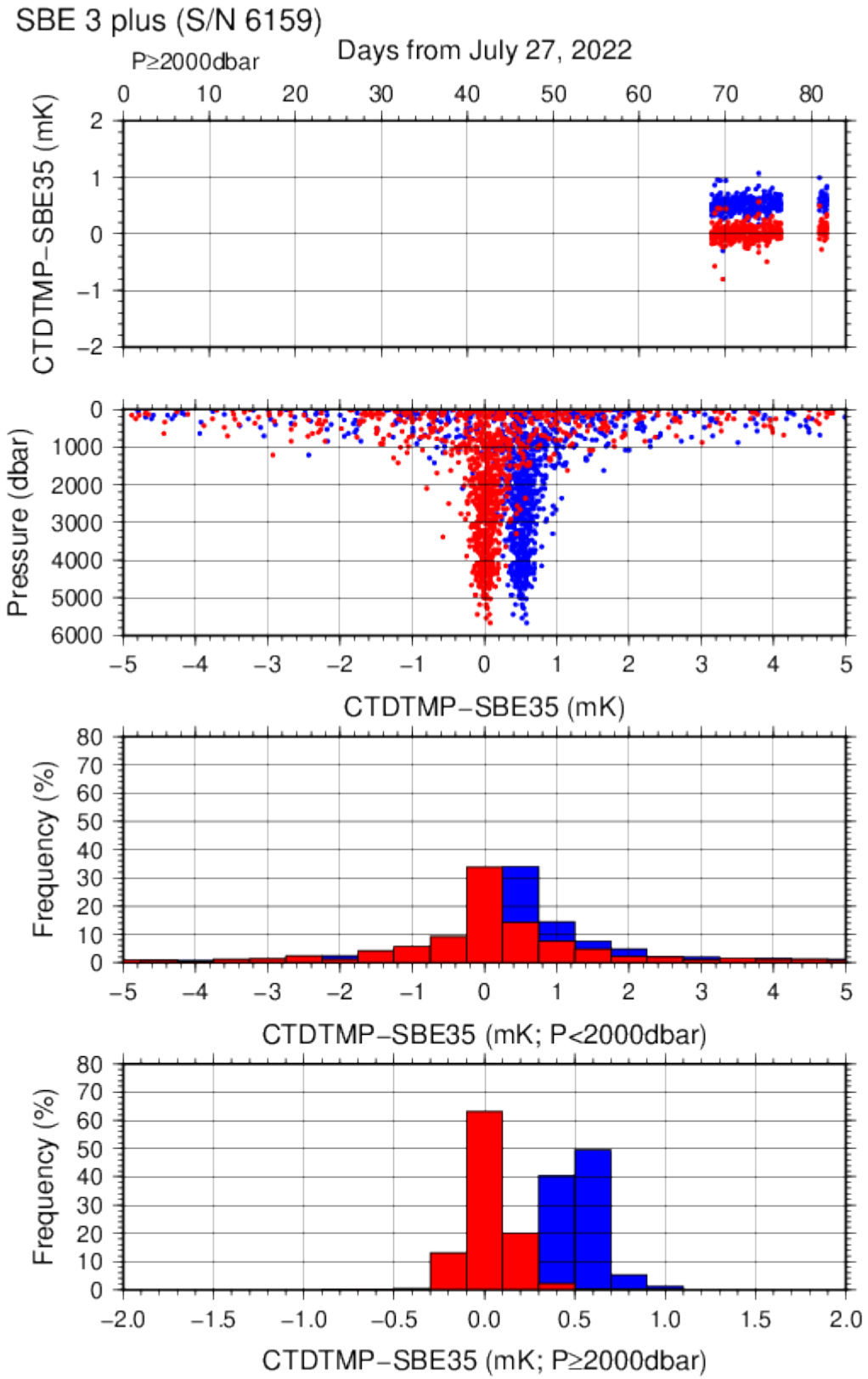

Figure C.1.5. Difference between the CTD temperature (*S/N 03P 6159*) and the Deep Ocean Standards thermometer (SBE 35) on RF22-07 Leg 1. Blue and red dots indicate before and after the correction using SBE 35 data, respectively. Lower two panels show histograms of the differences after correction.

(4.3) Conductivity sensor (SBE 4C)

The practical corrections for CTD conductivity data can be made by using bottle salinity data to correct the SBE 4C to agree with measured conductivity (*McTaggart et al., 2010*).

CTD conductivity was corrected as follows:

$$Corrected\ Conductivity = C - \left(\sum_{i=0}^{I} c_i \times C^i + \sum_{j=1}^{J} p_j \times P^j \right)$$

C: CTD conductivity, c_i and p_j: calibration coefficients
i, j: determined by use of the AIC (*Akaike*, 1974). In accord with *McTaggart et al.* (2010), the maximum of *I* and *J* are 2.

Table C.1.4. Conductivity correction coefficient summary. (Bold: accepted sensor)

S/N	*Num*	c_0(S/m)	c_1	c_2(m/S)	c_3(m/S^2)	*Stations*
			p_1(S/m/dbar)	p_2(S/m/dbar^2)	p_3(S/m/dbar^3)	
043697	**905**	**-4.3479×10^{-3}**	**1.8374×10^{-3}**	**-2.3936×10^{-4}**	**0.0000**	**RF7040 – 7064**
			1.6941×10^{-7}	**-2.3824×10^{-11}**	**0.0000**	
043697	1325	-1.7159×10^{-3}	7.7946×10^{-4}	-1.5948×10^{-4}	0.0000	RF7065 (※) **RF7066 – 7067** RF7068 – 7102
			1.6297×10^{-8}	0.0000	0.0000	
043697	**1193**	**4.7357×10^{-4}**	**-4.4053×10^{-4}**	**0.0000**	**0.0000**	**RF7103 – 7135**
			2.3972×10^{-8}	**0.0000**	**0.0000**	
046059	896	-2.8598×10^{-4}	1.6159×10^{-4}	0.0000	0.0000	RF7040 – 7064
			0.0000	0.0000	0.0000	
046059	**1270**	**-2.4270×10^{-3}**	**1.1184×10^{-3}**	**-1.2363×10^{-4}**	**0.0000**	**RF7065** (※) RF7066 – 7067 **RF7068 – 7102**
			1.5156×10^{-7}	**-3.1434×10^{-11}**	**2.1157×10^{-15}**	
046059	1111	5.2708×10^{-4}	-3.6327×10^{-4}	6.6707×10^{-5}	0.0000	RF7103 – 7135
			2.7612×10^{-8}	0.0000	0.0000	

※From station RF7066 to RF7067, S/N 043697 was accepted instead of S/N 046059 due to data failure. After RF7068, this data failure was resolved.

Table C.1.5. Conductivity correction and salinity correction summary for S/N 043697.

Stations	Pressure < 1900dbar					
	Conductivity			Salinity		
	Num	Average (S/m)	Std (S/m)	Num	Average	Std
RF7040 – 7064	621	0.0000	0.0011	621	0.0000	0.0075
RF7065 – 7102	849	0.0000	0.0007	849	0.0000	0.0051
RF7103 – 7135	749	0.0000	0.0008	749	0.0000	0.0062
Stations	Pressure ≥ 1900 dbar					
	Conductivity			Salinity		
	Num	Average (S/m)	Std (S/m)	Num	Average	Std
RF7040 – 7064	284	0.0000	0.0000	284	0.0000	0.0005
RF7065 – 7102	476	0.0000	0.0001	476	0.0000	0.0006
RF7103 – 7135	444	0.0000	0.0000	444	0.0000	0.0004

Table C.1.6. Conductivity correction and salinity correction summary for S/N 046059.

Stations	Pressure < 1900dbar					
	Conductivity			Salinity		
	Num	Average (S/m)	Std (S/m)	Num	Average	Std
RF7040 – 7064	618	0.0000	0.0011	618	0.0000	0.0081

RF7065 – 7102	818	0.0000	0.0007	818	0.0000	0.0050
RF7103 – 7135	691	0.0000	0.0008	691	0.0000	0.0059
Stations	Pressure ≥ 1900 dbar					
	Conductivity			Salinity		
	Num	Average (S/m)	Std (S/m)	Num	Average	Std
RF7040 – 7064	278	0.0000	0.0000	278	0.0000	0.0005
RF7065 – 7102	452	0.0000	0.0000	452	0.0000	0.0004
RF7103 – 7135	420	0.0000	0.0000	420	0.0000	0.0004

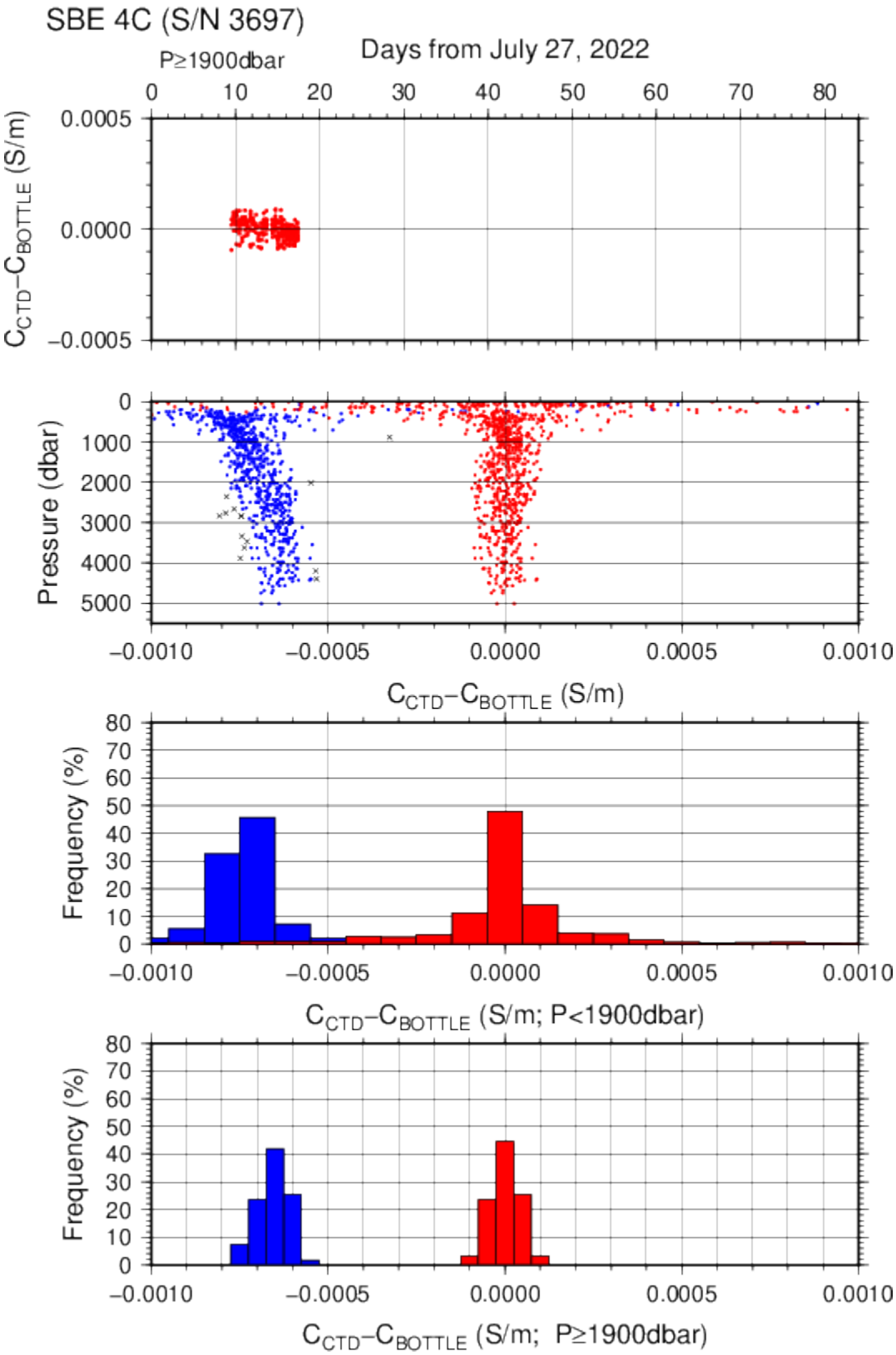

Figure C.1.6. Difference between the CTD conductivity (*S/N 043697*) and the bottle conductivity on RF22-05. Blue and red dots indicate before and after the calibration using bottle data, respectively. Lower two panels show histograms of the differences before and after calibration.

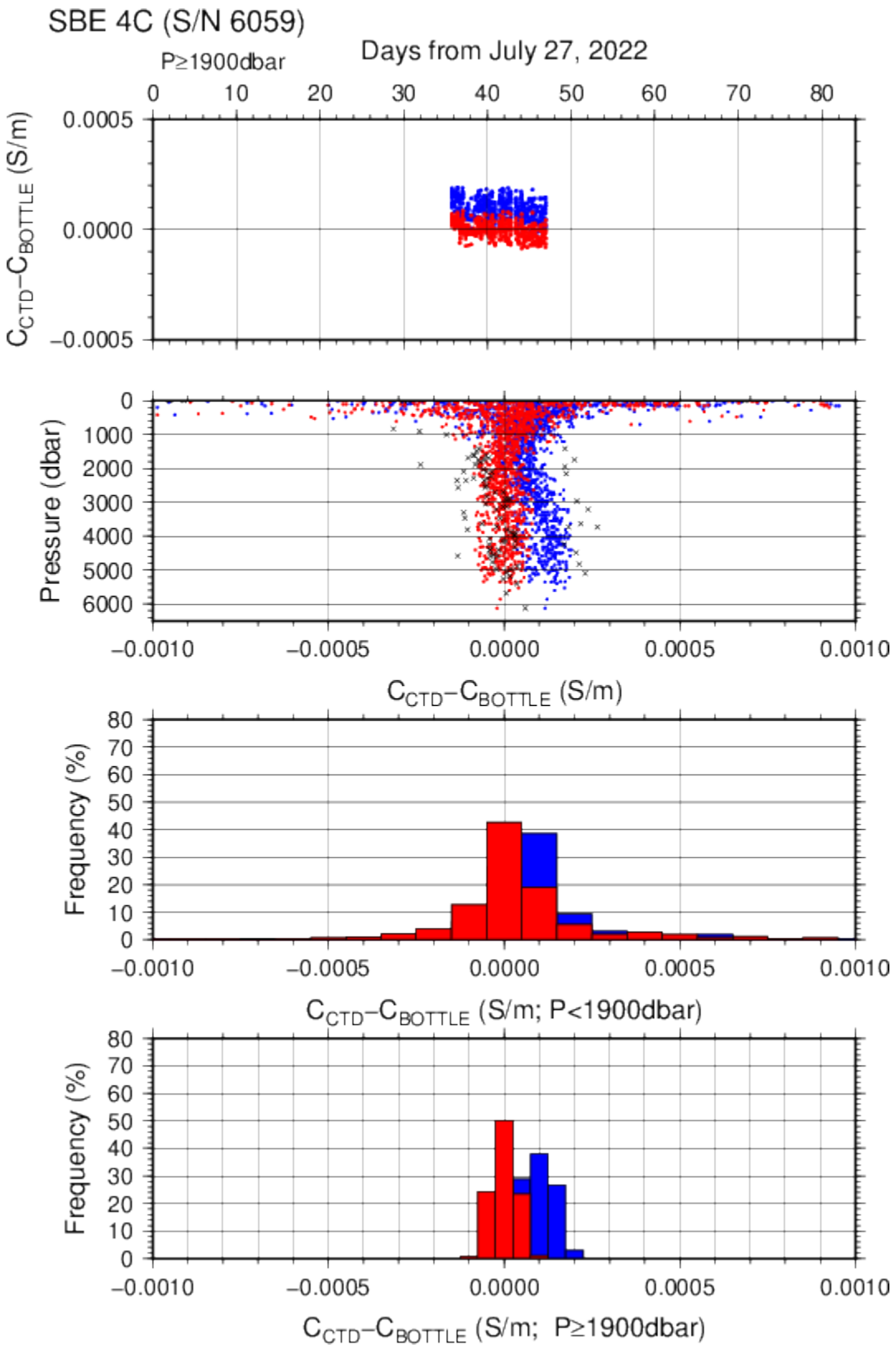

Figure C.1.7. Difference between the CTD conductivity (*S/N 046059*) and the bottle conductivity on RF22-06. Blue and red dots indicate before and after the calibration using bottle data, respectively. Lower two panels show histograms of the differences before and after calibration.

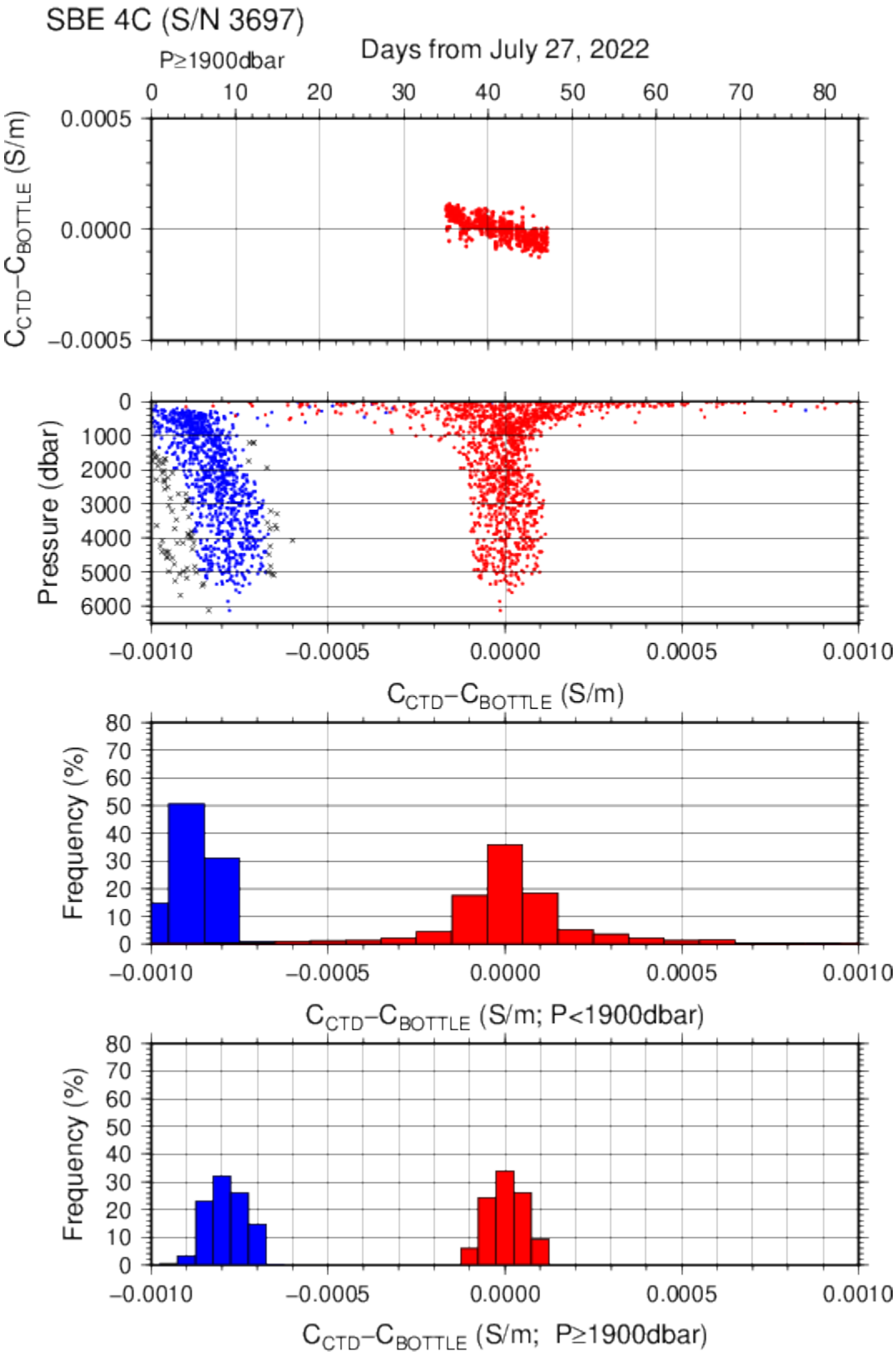

Figure C.1.8. Difference between the CTD conductivity (*S/N 043697*) and the bottle conductivity on RF22-06. Blue and red dots indicate before and after the calibration using bottle data, respectively. Lower two panels show histograms of the differences before and after calibration.

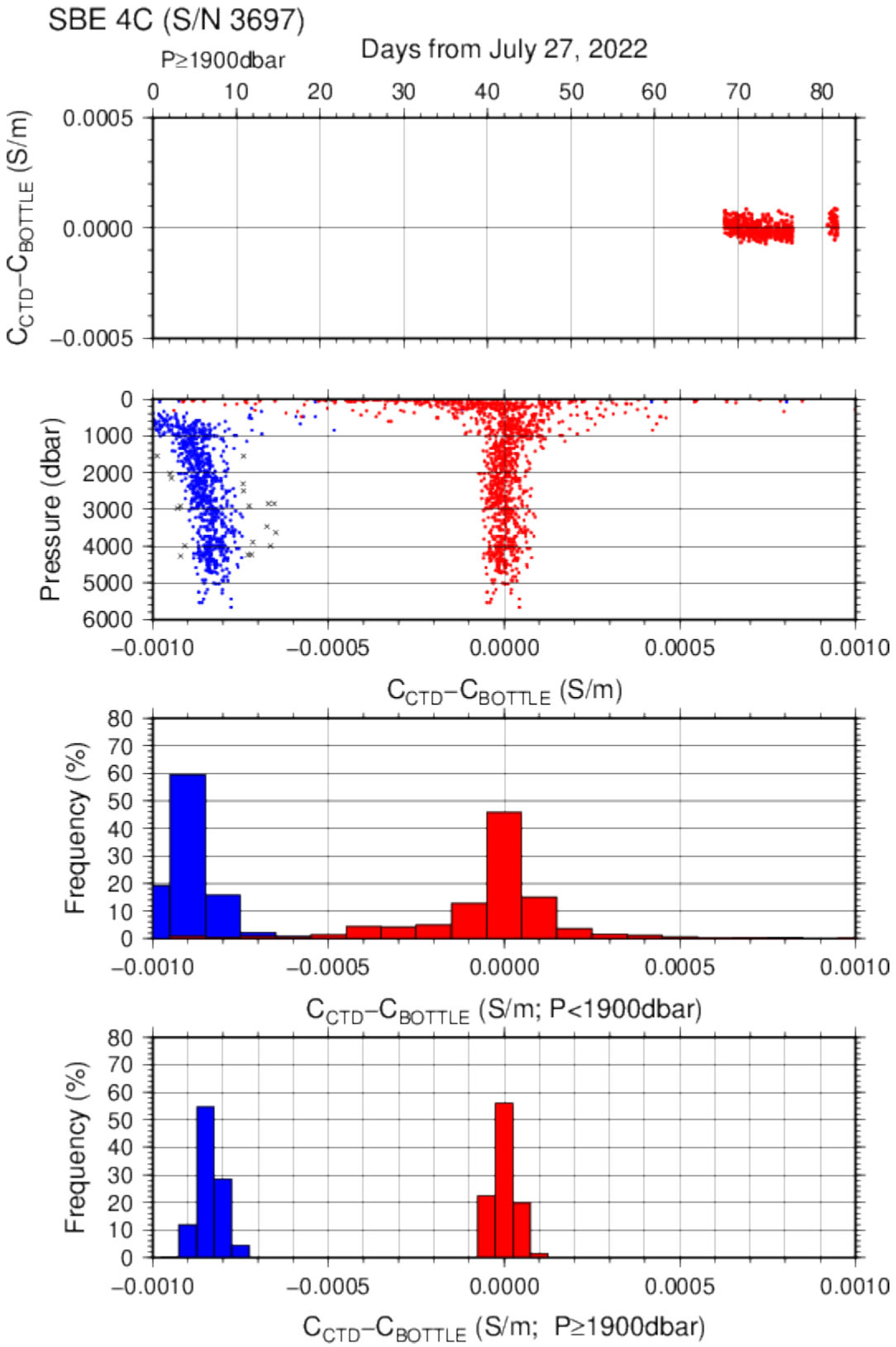

Figure C.1.9. Difference between the CTD conductivity (*S/N 043697*) and the bottle conductivity on RF22-07 Leg 1. Blue and red dots indicate before and after the calibration using bottle data, respectively. Lower two panels show histograms of the differences before and after calibration.

(4.4) Oxygen sensor (RINKO III)

The CTD oxygen concentration was calculated using the RINKO III output (voltage) with the Stern-Volmer equation in accord with the method of Uchida et al. (2008) and Uchida et al. (2010). The pressure hysteresis for the RINKO III output (voltage) was corrected in accord with Sea-bird Electronics (2009) and Uchida et al. (2010). The equations were as follows:

$$P_0 = 1.0 + c_4 \times t$$
$$P_c = c_5 + c_6 \times v + c_7 \times T + c_8 \times T \times v$$
$$K_{sv} = c_1 + c_2 \times t + c_3 \times t^2$$
$$coef = (1.0 + c_9 \times P/1000)^{1/3}$$
$$[O_2] = O_2^{sat} \times \{(P_0/P_c - 1.0)/K_{sv} \times coef\}$$

P: pressure (dbar), *t*: potential temperature, *v*: RINKO output voltage (volt)
T: elapsed time of the sensor from the beginning of first station in calculation group in day
O_2^{sat}: dissolved oxygen saturation by Garcìa and Gordon (1992) (μmol/kg)
$[O_2]$: dissolved oxygen concentration (μmol/kg)
c_1–c_9: determined by minimizing differences between CTD oxygen concentration and bottle dissolved oxygen concentration by quasi-newton method (*Shanno, 1970*).

Table C.1.7. Dissolved oxygen correction coefficient summary. (Bold: accepted sensor)

S/N	*Stations*	c_1	c_2	c_3	c_4	c_5
		c_6	c_7	c_8	c_9	
0392	RF7040 – 7064	1.67544	1.52969×10^{-2}	1.29452×10^{-4}	-2.06723×10^{-3}	-1.10424×10^{-1}
		3.12593×10^{-1}	1.02224×10^{-3}	-1.46624×10^{-4}	8.04862×10^{-2}	
0392	RF7065 – 7102	1.72710	2.11986×10^{-2}	1.87955×10^{-4}	-9.01896×10^{-4}	-1.26917×10^{-1}
		3.17603×10^{-1}	2.45262×10^{-4}	2.15964×10^{-4}	7.99771×10^{-2}	
0392	RF7103 – 7135	1.75666	2.04888×10^{-2}	2.50957×10^{-4}	-9.85855×10^{-4}	-1.31903×10^{-1}
		3.18994×10^{-1}	-5.52313×10^{-4}	5.46897×10^{-4}	7.90762×10^{-2}	
0356	**RF7040 – 7064**	**1.76099**	$\mathbf{1.76869 \times 10^{-2}}$	$\mathbf{1.54020 \times 10^{-4}}$	$\mathbf{-1.72809 \times 10^{-3}}$	$\mathbf{-1.18853 \times 10^{-1}}$
		$\mathbf{3.14640 \times 10^{-1}}$	$\mathbf{1.11683 \times 10^{-3}}$	$\mathbf{-1.91344 \times 10^{-4}}$	$\mathbf{7.98476 \times 10^{-2}}$	
0356	**RF7065 – 7102**	**1.78055**	$\mathbf{2.84361 \times 10^{-2}}$	$\mathbf{1.55622 \times 10^{-4}}$	$\mathbf{2.57797 \times 10^{-4}}$	$\mathbf{-1.31167 \times 10^{-1}}$
		$\mathbf{3.19775 \times 10^{-1}}$	$\mathbf{5.83281 \times 10^{-5}}$	$\mathbf{1.92499 \times 10^{-4}}$	$\mathbf{7.78531 \times 10^{-2}}$	
0356	**RF7103 – 7135**	**1.76373**	$\mathbf{2.34709 \times 10^{-2}}$	$\mathbf{1.43849 \times 10^{-4}}$	$\mathbf{-5.85406 \times 10^{-4}}$	$\mathbf{-1.21666 \times 10^{-1}}$
		$\mathbf{3.17354 \times 10^{-1}}$	$\mathbf{-3.38758 \times 10^{-4}}$	$\mathbf{3.47439 \times 10^{-4}}$	$\mathbf{7.85876 \times 10^{-2}}$	

Table C.1.8. Dissolved oxygen correction summary for S/N 0392.

Stations	Pressure < 950dbar			Pressure ≥ 950 dbar		
	Num	Average (μmol/kg)	Std (μmol/kg)	Num	Average (μmol/kg)	Std (μmol/kg)
RF7040 – 7064	449	0.04	1.02	372	-0.00	0.27
RF7065 – 7102	634	–0.00	0.82	640	0.00	0.31
RF7103 – 7135	538	–0.06	0.71	555	0.00	0.30

Table C.1.9. Dissolved oxygen correction summary for S/N 0356.

Stations	Pressure < 950dbar			Pressure ≥ 950 dbar		
	Num	Average (μmol/kg)	Std (μmol/kg)	Num	Average (μmol/kg)	Std (μmol/kg)
RF7040 – 7064	449	–0.01	0.94	372	-0.00	0.24
RF7065 – 7102	634	–0.04	0.79	640	-0.00	0.26
RF7103 – 7135	538	-0.02	0.55	555	0.00	0.22

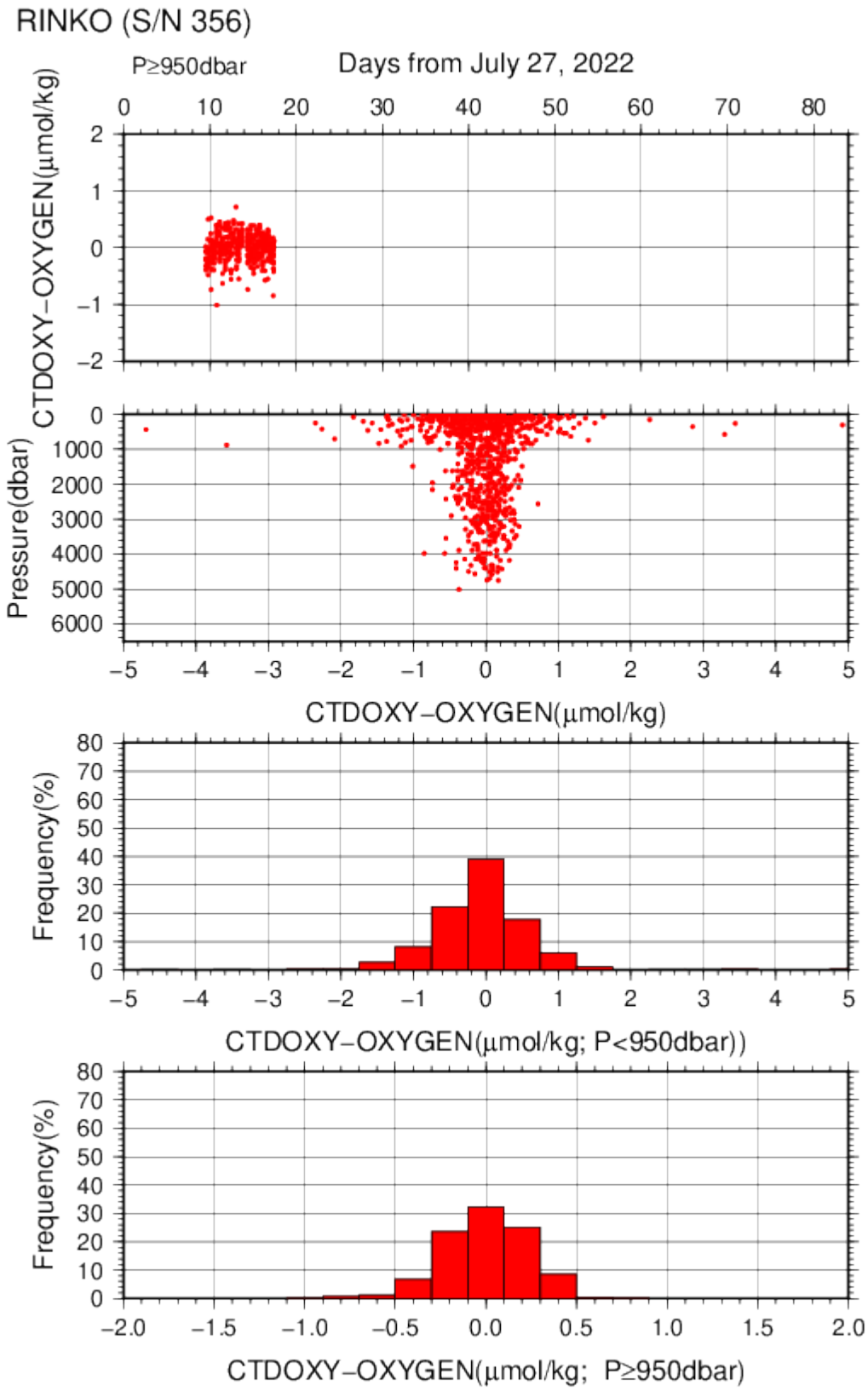

Figure C.1.10. Difference between the CTD oxygen (*S/N 0356*) and bottle dissolved oxygen at RF22-05. Red dots in upper two panels indicate the result of calibration. Lower two panels show histograms of the differences between calibrated oxygen concentration and bottle oxygen concentration.

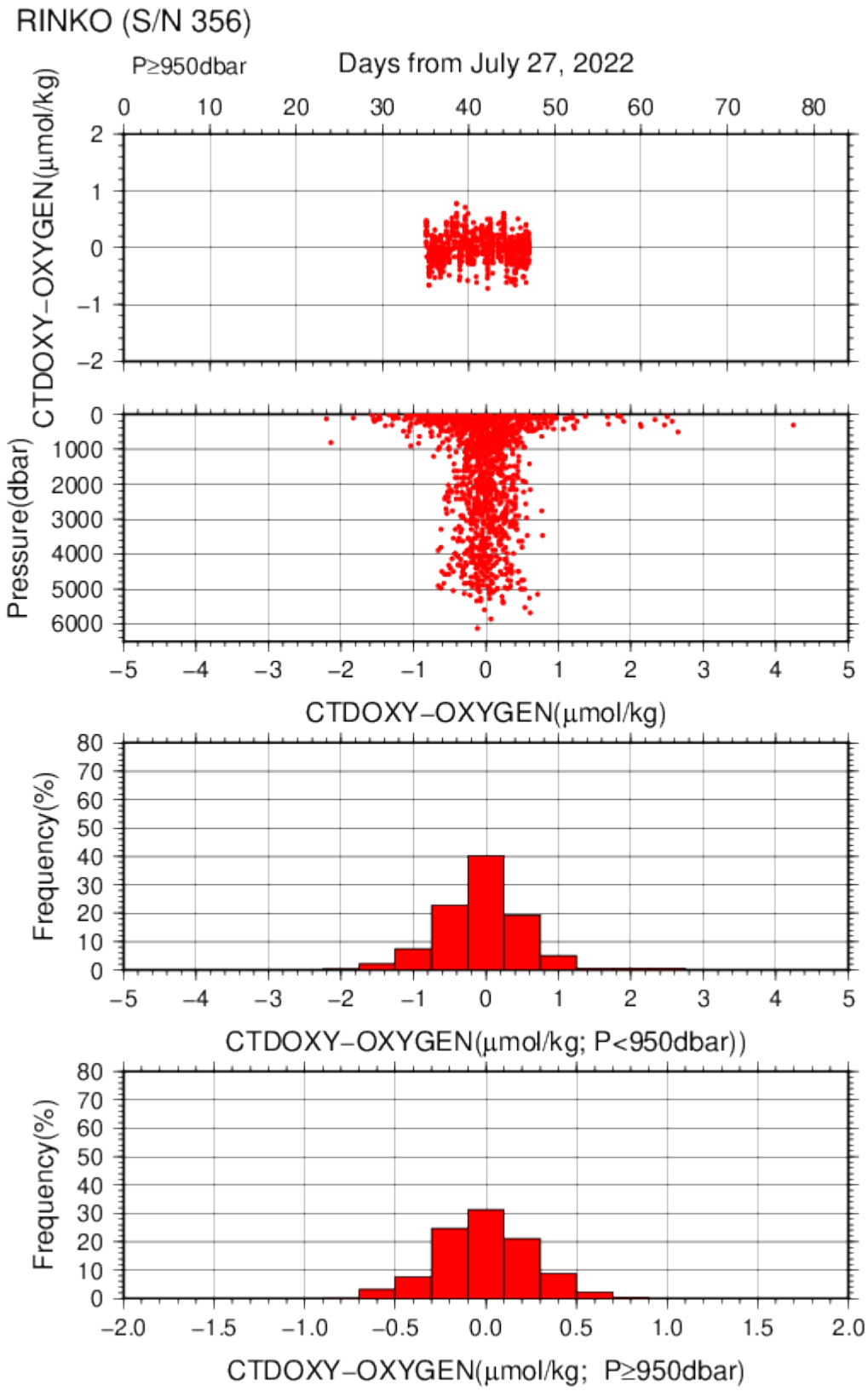

Figure C.1.11. Difference between the CTD oxygen (*S/N 0356*) and bottle dissolved oxygen at RF22-06. Red dots in upper two panels indicate the result of calibration. Lower two panels show histograms of the differences between calibrated oxygen concentration and bottle oxygen concentration.

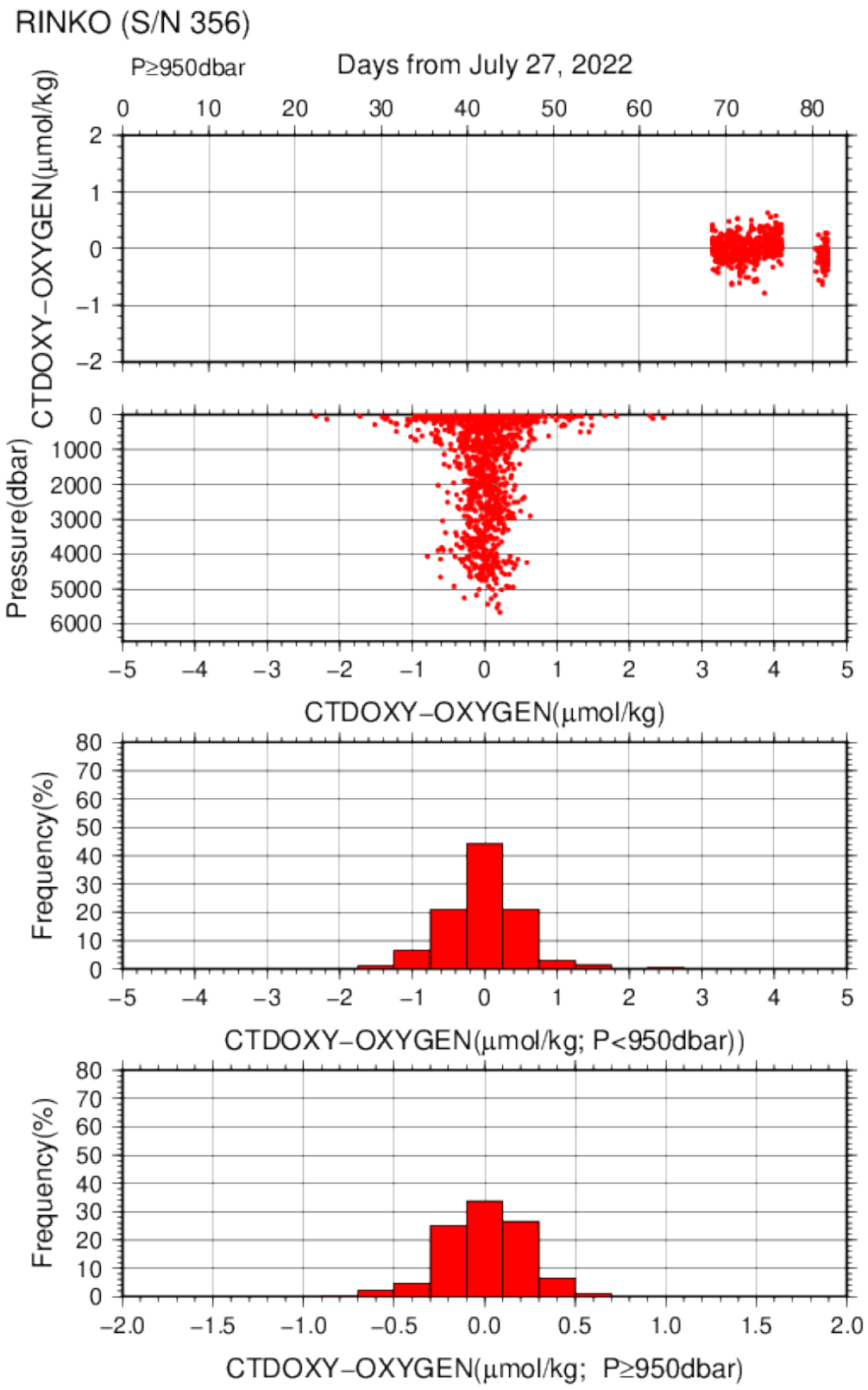

Figure C.1.12. Difference between the CTD oxygen (*S/N 0356*) and bottle dissolved oxygen at RF22-07 Leg1. Red dots in upper two panels indicate the result of calibration. Lower two panels show histograms of the differences between calibrated oxygen concentration and bottle oxygen concentration.

(4.5) Results of detection of sea floor by the altimeter (VA500)

The altimeter detected the sea floor at 91 of 93 stations and that of final detection of sea floor was 13.7 m. The summary of detection of VA500 was shown in Figure C.1.13.

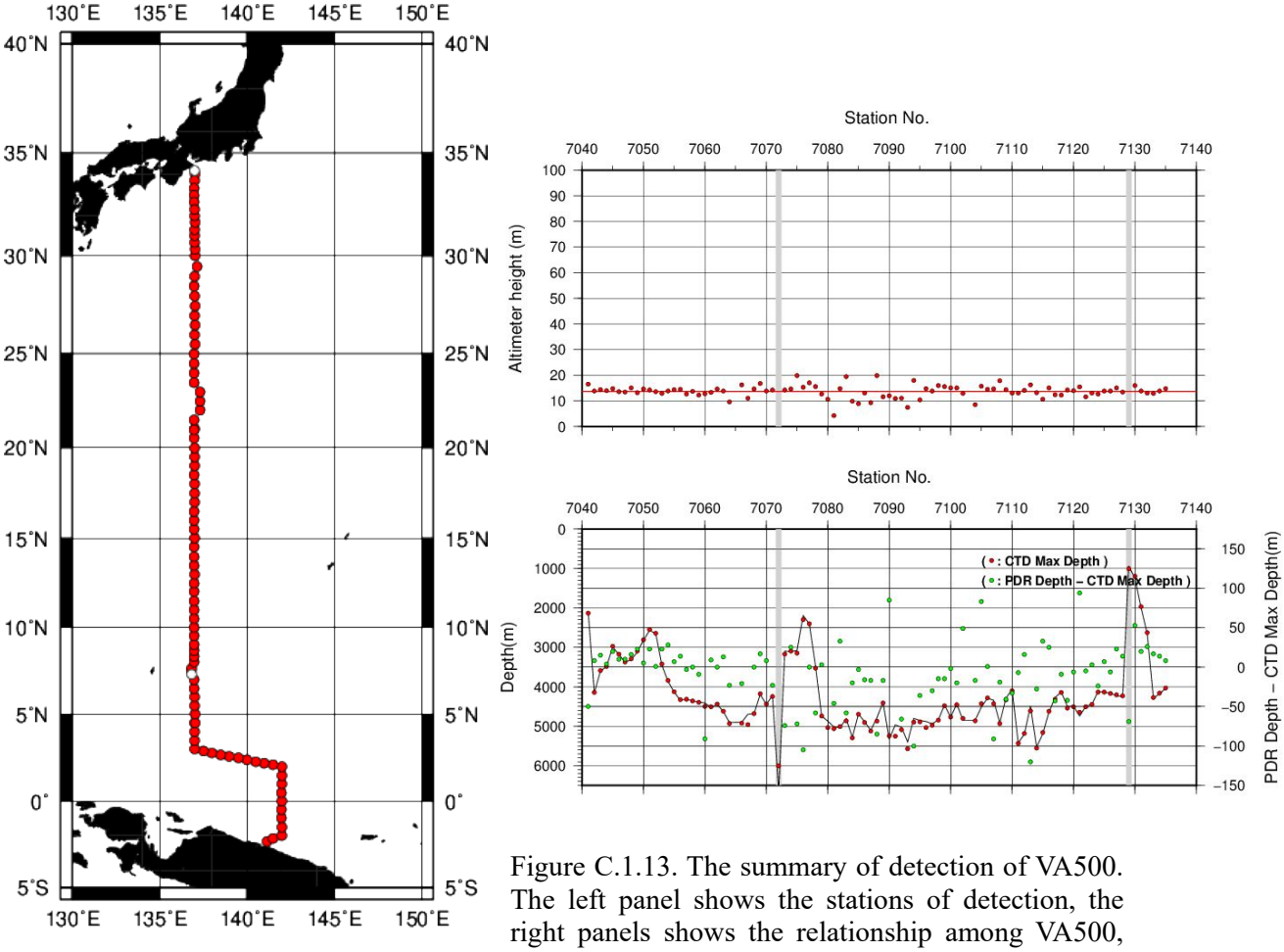

Figure C.1.13. The summary of detection of VA500. The left panel shows the stations of detection, the right panels shows the relationship among VA500, bathymetry（PDR Depth） and CTD depth. In the left panel, closed and open circles indicate react and no-react stations, respectively. In the right two panels, gray shade indicates no-react stations.

(5) Post-cruise calibration

After the cruise, post-cruise calibration of sensors was performed by the manufacturer, as shown below. We confirmed that the calibration of these sensors did not change significantly during the cruise.

(5.1) Temperature (ITS-90): SBE 3plus

S/N 03P6159 (primary), 13 May. 2023

g	=	$4.31677996 \times 10^{-3}$	j	=	$2.00080133 \times 10^{-6}$
h	=	$6.38544094 \times 10^{-4}$	f_0	=	1000.0
i	=	$2.17927463 \times 10^{-5}$			

S/N 03P4321 (secondary), 24 May. 2023

g	=	$4.34249577 \times 10^{-3}$	j	=	$2.09128339 \times 10^{-6}$
h	=	$6.40268544 \times 10^{-4}$	f_0	=	1000.0
i	=	$2.24531711 \times 10^{-5}$			

(5.2) Deep Ocean Standards Thermometer Temperature (ITS-90): SBE 35

S/N 0093, 27 Oct. 2020

a_0	=	$4.12756963 \times 10^{-3}$	a_3	=	$-9.36245277 \times 10^{-6}$
a_1	=	$-1.08163464 \times 10^{-3}$	a_4	=	$2.00979198 \times 10^{-7}$
a_2	=	$1.67453817 \times 10^{-4}$			

Formula:

$$Linearized\ temperature(ITS{-}90) = 1/\left\{a_0 + a_1 \times \ln(n) + a_2 \times \ln^2(n) + a_3 \times \ln^3(n) + a_4 \times \ln^4(n)\right\} - 273.15$$

n: instrument output

The slow time drift of the SBE 35

S/N 0093, 02 Feb. 2023 (2nd step: fixed point calibration)

Slope = 1.000007, Offset = –0.000205

Formula:

$$Temperature(ITS{-}90) = slope \times (Linearized\ temperature) + offset$$

(5.3) Conductivity: SBE 4C

S/N 043697 (primary), 23 May. 2023

g	=	–9.79179904	j	=	$2.71617766 \times 10^{-4}$
h	=	1.25556323	CP_{cor}	=	-9.5700×10^{-8}
i	=	$-2.74297983 \times 10^{-3}$	CT_{cor}	=	3.2500×10^{-6}

S/N 046059 (secondary), 22 May. 2023

g	=	$-1.02817639 \times 10^{-1}$	j	=	$4.22955067 \times 10^{-4}$
h	=	1.61242457	CP_{cor}	=	-9.5700×10^{-8}
i	=	$-3.91114555 \times 10^{-3}$	CT_{cor}	=	3.2500×10^{-6}

References

Akaike, H. (1974): A new look at the statistical model identification. *IEEE Transactions on Automatic Control, **19**:716–722.*

Garcìa, H. E., and L. I. Gordon (1992): Oxygen solubility in seawater: Better fitting equations. *Limnol. Oceanogr., **37**, 1307–1312*.

McTaggart, K. E., G. C. Johnson, M. C. Johnson, F. M. Delahoyde, and J. H. Swift (2010): The GO-SHIP Repeat Hydrography Manual: A Collection of Expert Reports and guidelines. IOCCP Report No ***14***, ICPO Publication Series No. 134, version 1, 2010.

Sea-Bird Electronics (2009): SBE 43 dissolved oxygen (DO) sensor – hysteresis corrections, *Application note no. 64-3, 7 pp.*

Shanno, David F. (1970): Conditioning of quasi-Newton methods for function minimization. *Math. Comput. **24**, 647–656. MR 42 #8905.*

Uchida, H., G. C. Johnson, McTaggart, K. E. (2010): CTD oxygen sensor calibration procedures. In: The GO-SHIP repeat hydrography manual: A Collection of Expert Reports and guidelines. IOCCP Report No ***14***, ICPO Publication Series No. 134, version 1, 2010.

Uchida, H., K. Ohyama, S. Ozawa, and M. Fukasawa (2007): In-situ calibration of the Sea-Bird 9plus CTD thermometer. *J. Atmos. Oceanic Technol., **24**, 1961–1967.*

Uchida, H., T. Kawano, I. Kaneko, and M. Fukasawa (2008): In-situ calibration of optode-based oxygen sensors. *J. Atmos. Oceanic Technol., **25**, 2271–2281*.

Bottle Salinity

25 September 2023

(1) Personnel

TANAKA Kiyoshi
MURAKAMI Kiyoshi (RF2206, RF2207)
HIGASHI Yoshikazu (RF2206, RF2207)
WADA Kouichi (RF2205, RF2207)
SEGAWA Takahiro (RF2205, RF2207)
CHIBA Yasuomi (RF2205, RF2206)
TANAKA Hidekazu (RF2205, RF2206)

(2) Salinity measurement

Salinometer: AUTOSAL 8400B (Guildline Instruments Ltd., Canada ; S/N 73556 for stations between RF7096 and RF7102, S/N 72103 for stations between RF7103 and RF7128, and S/N 73239 for all other stations)
Thermometer: 1502A Tweener thermometer readout (to monitor ambient temperature and bath temperature) (Fluke calibration, USA)
IAPSO Standard Seawater: P165 (K15=0.99986)

(3) Sampling and measurement

The measurement system was almost the same as the system described by Kawano (2010). Algorithm for practical salinity scale, 1978 (PSS-78; UNESCO, 1981) was employed to convert the conductivity ratios to salinities.

(4) Station occupied

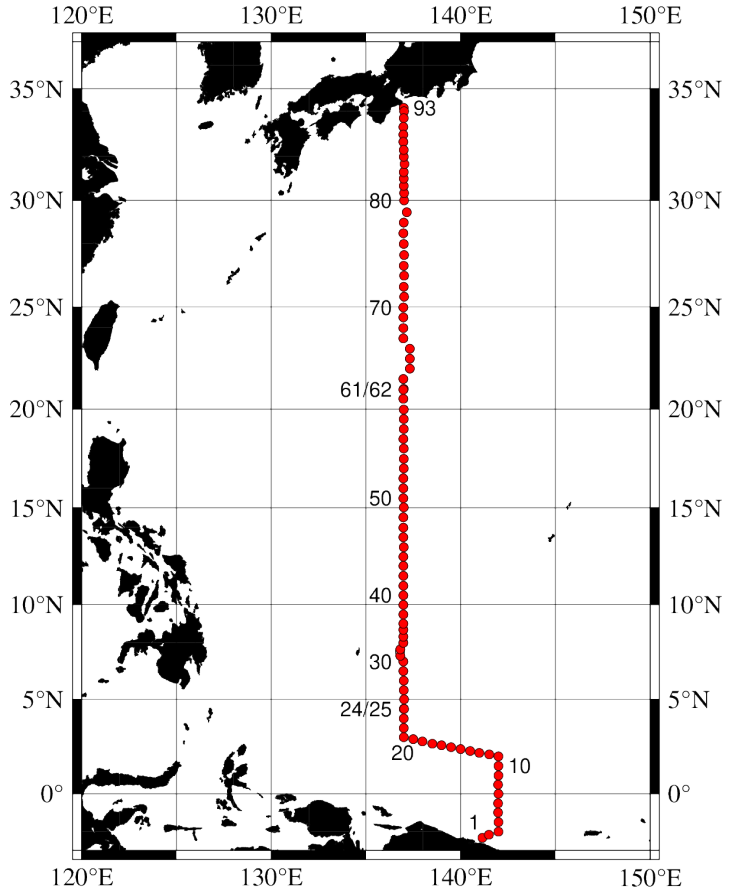

Figure C.2.1. Location of observation stations of bottle salinity.

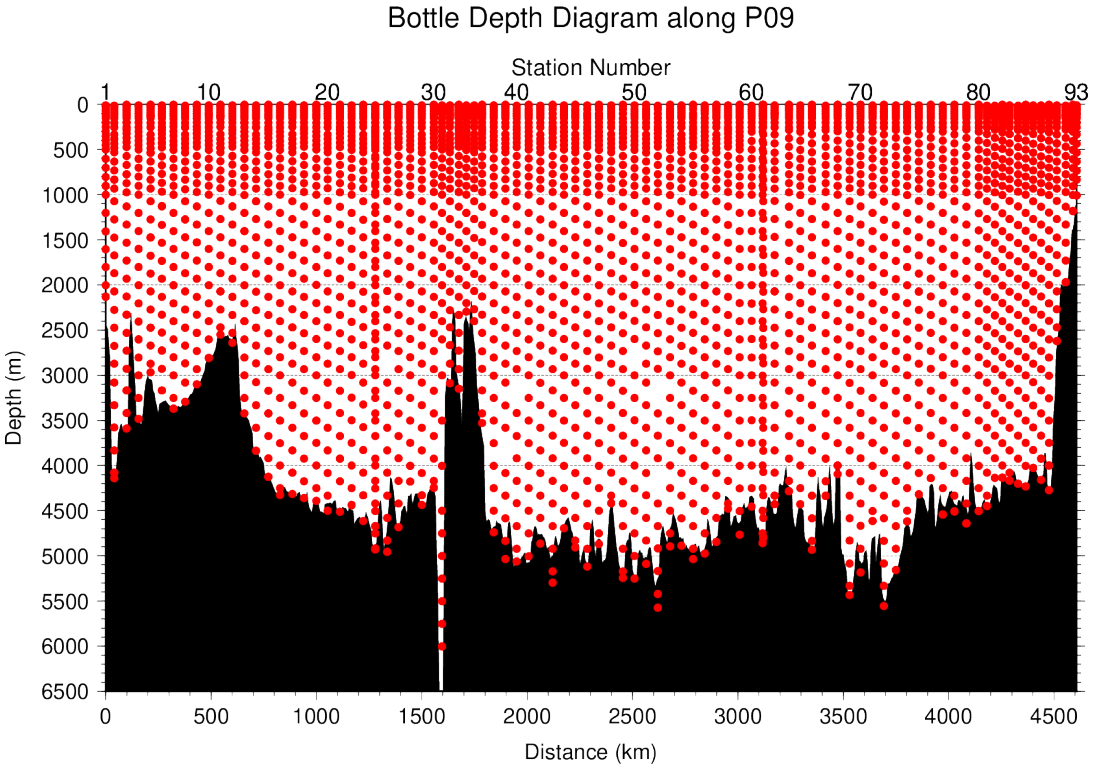

Figure C.2.2. Distance-depth distribution of sampling layers of bottle salinity.

(5) Result

(5.1) Ambient temperature, bath temperature and Standard Seawater measurements

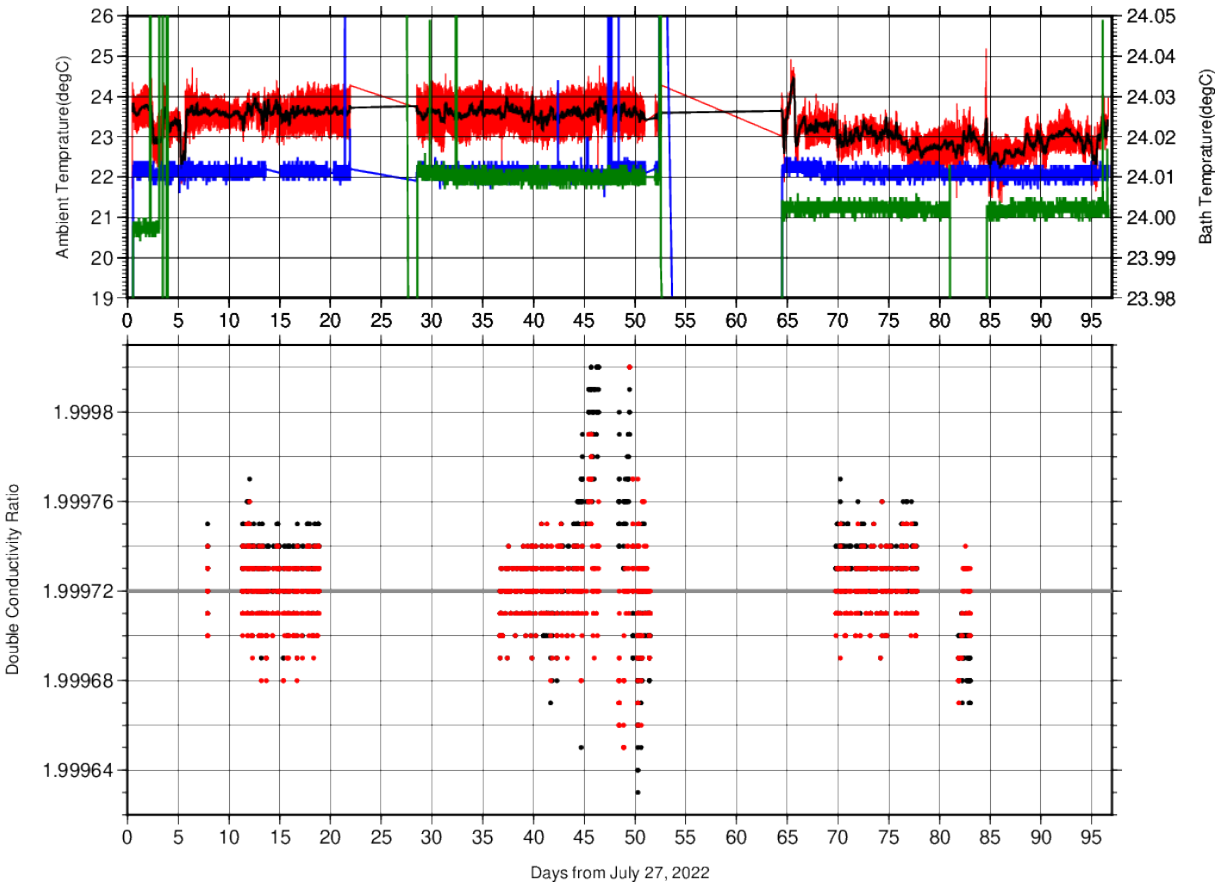

Figure C.2.3. The upper panel indicate time-series of ambient temperature and bath temperature during the cruise. (Red(black) line; ambient(average) temperature. Green line; bath temperature in Autosal S/N72103(RF2205,2207) and S/N73556(RF2206). Blue line; bath temperature in Autosal（S/N 73239）. The lower panel, black dots, and red dots indicate raw and corrected time-series of the double conductivity ratio of the standard seawater (P165).

(5.2) Replicate and duplicate samples

We took replicate (pair of water samples taken from a single Niskin bottle) and duplicate (pair of water samples taken from different Niskin bottles closed at the same depth) samples for bottle salinity throughout the cruise. Table C.2.1 summarizes the results of the analyses. Figure C.2.4 shows details of the results. The calculation of the standard deviation from the difference of sets was based on a procedure (SOP 23) in DOE (1994).

Table C.2.1. Summary of replicate and duplicate salinity analyses.

Measurement	Average difference ± S.D.
Replicate sample	0.0003 ± 0.0003 (N = 314)
Duplicate sample	0.0009 ± 0.0018 (N = 171)

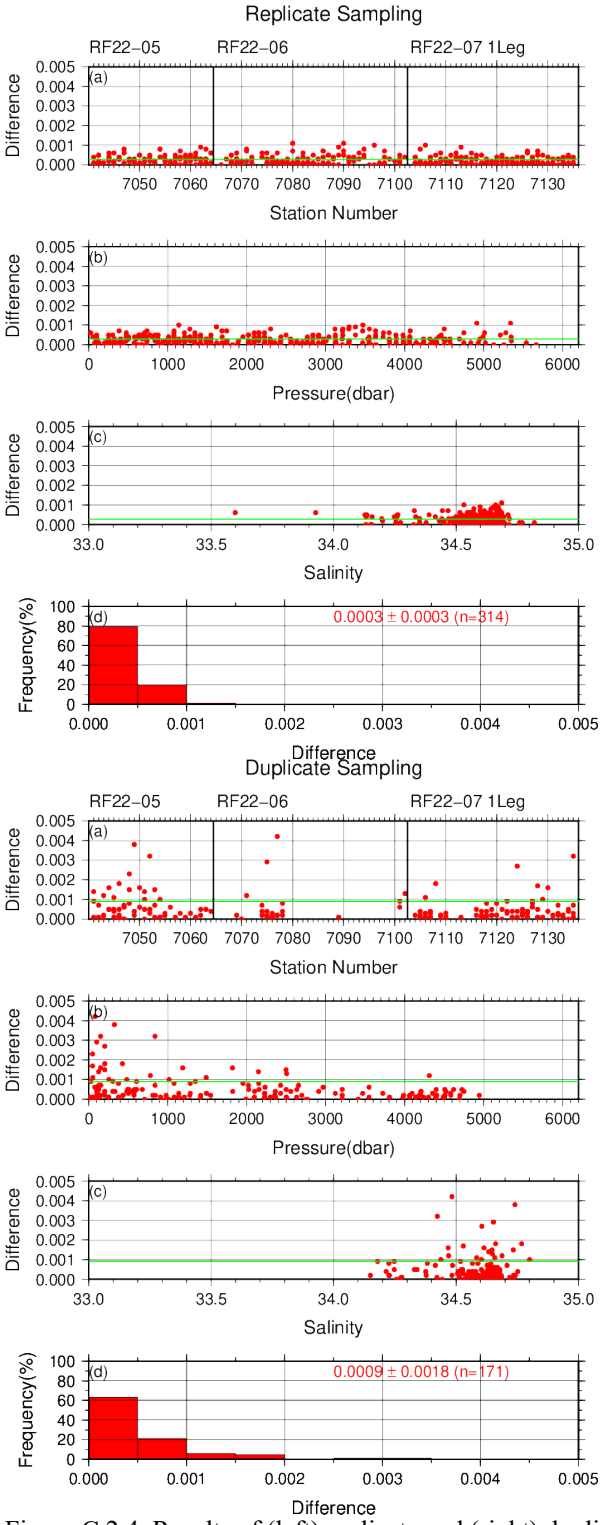

Figure C.2.4. Results of (left) replicate and (right) duplicate analyses during the cruise against (a) station number, (b) pressure, (c) salinity, and (d) histogram of the measurements. Green line indicates the mean of the differences of salinity of replicate/duplicate analyses.

(5.3) Summary of assigned quality control flags

Table C.2.2. Summary of assigned quality control flags

Flag	Definition	Number
2	Good	2826

3	Questionable	0
4	Bad (Faulty)	96
5	Not reported	4
6	Replicate measurements	319
Total number of samples		3245

References

DOE (1994), Handbook of methods for the analysis of the various parameters of the carbon dioxide system in sea water; version 2. *A. G. Dickson and C. Goyet (eds), ORNL/CDIAC-74.*

Kawano (2010), The GO-SHIP Repeat Hydrography Manual: A Collection of Expert Reports and Guidelines. *IOCCP Report No. 14, ICPO Publication Series No. 134, Version 1.*

UNESCO (1981), Tenth report of the Joint Panel on Oceanographic Tables and Standards. *UNESCO Tech. Papers in Mar. Sci., **36**, 25 pp.*

3. Bottle Oxygen

31 March 2023

(1) Personnel

KITAGAWA Takahiro
FUJII Takuya
NAKAMURA Motohiro (RF22-05, RF22-06)
HASHIMOTO Susumu (RF22-06, RF22-07)
OCHIAI Naoko (RF22-05, RF22-07)
FUJIWARA Hiroyuki (RF22-05)
UEHARA Tomohiro (RF22-06)
KAKUYA Keita (RF22-07)

(2) Station occupied

A total of 92 stations (RF 22-05 : 24, RF 22-06 : 36, RF 22-07 : 32) were occupied for dissolved oxygen measurements. Station location and sampling layers of bottle oxygen are shown in Figures C.3.1 and C.3.2, respectively.

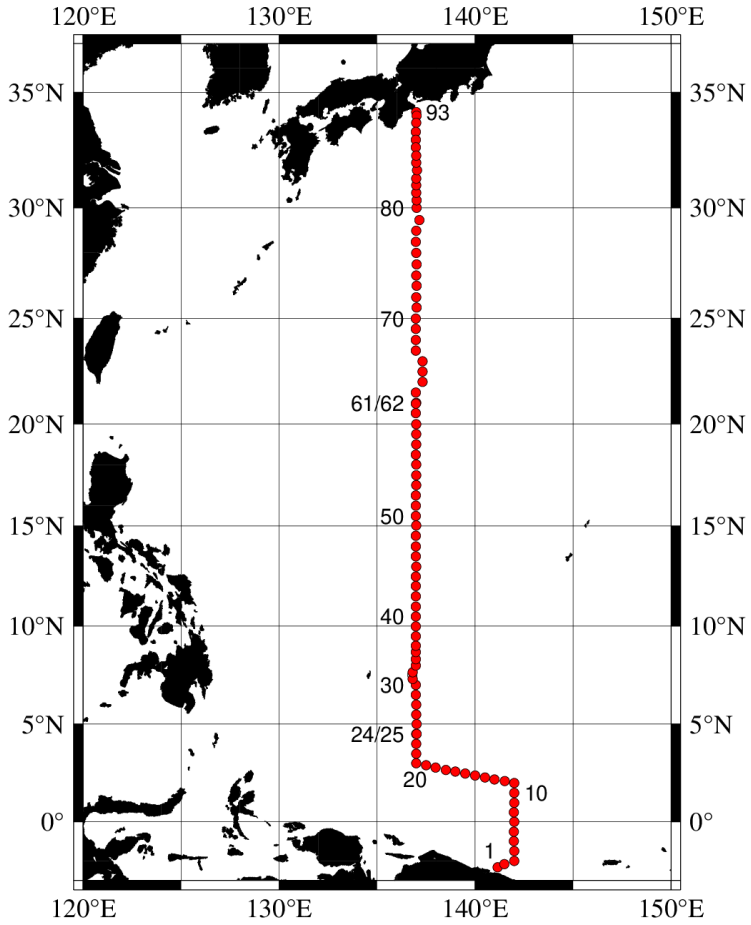

Figure C.3.1. Location of observation stations of bottle oxygen. Closed and open circles indicate sampling and no-sampling stations, respectively.

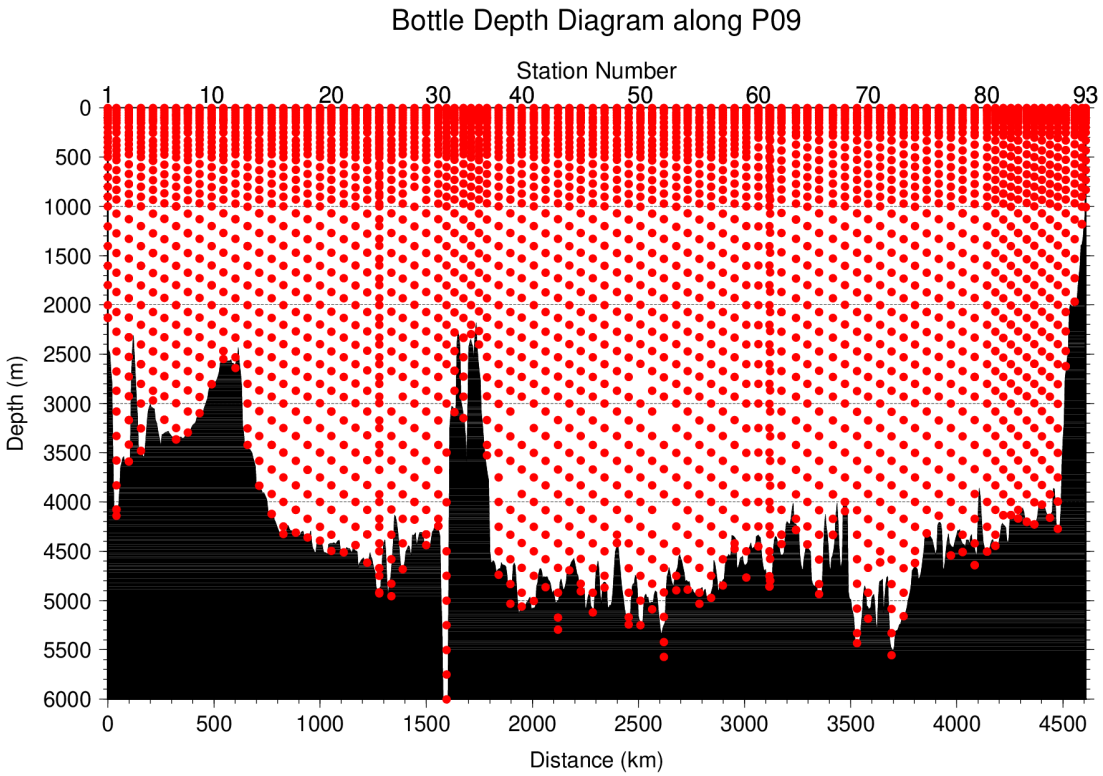

Figure C.3.2. Distance-depth distribution of sampling layers of bottle oxygen.

(3) Instrument

Detector: DOT-15X (KIMOTO ELECTRIC CO., LTD., Japan)
Burette: APB-610 (Kyoto Electronics Manufacturing Co., Ltd., Japan)

(4) Sampling and measurement

Methods of seawater sampling, measurement, and calculation of dissolved oxygen concentration were based on an IOCCP Report (Langdon, 2010). Details of the methods are shown in Appendix A1.
The reagents for the measurement were prepared according to recipes described in Appendix A2. Standard KIO_3 solutions were prepared gravimetrically using the highest purity standard substance KIO_3 (Lot. No. KCN5512, FUJIFILM Wako Pure Chemical Corporation, Japan). Table C.3.1 shows the batch list of prepared standard KIO_3 solutions.

Table C.3.1. Batch list of the standard KIO_3 solutions.

KIO_3 batch	**Cruise**	**Concentration and uncertainty (k=2) at 20 °C. Unit is mol L^{-1}.**	**Purpose of use**
20220117-2	RF22-05,06,07	0.0016666±0.0000007	Standardization (main use)
20211130-2	RF22-05,06,07	0.0016670±0.0000007	Mutual comparison

(5) Standardization

The concentration of the $Na_2S_2O_3$ titrant was determined with the standard KIO_3 solution 20220117-2 for RF22-05, RF22-06 and RF22-07, respectively, based on the methods of an IOCCP Report (Langdon, 2010). Figure C.3.3 shows the results of standardization during the cruise. The standard deviation of the concentration at 20 °C was determined through standardization and was used in the calculation of uncertainty.

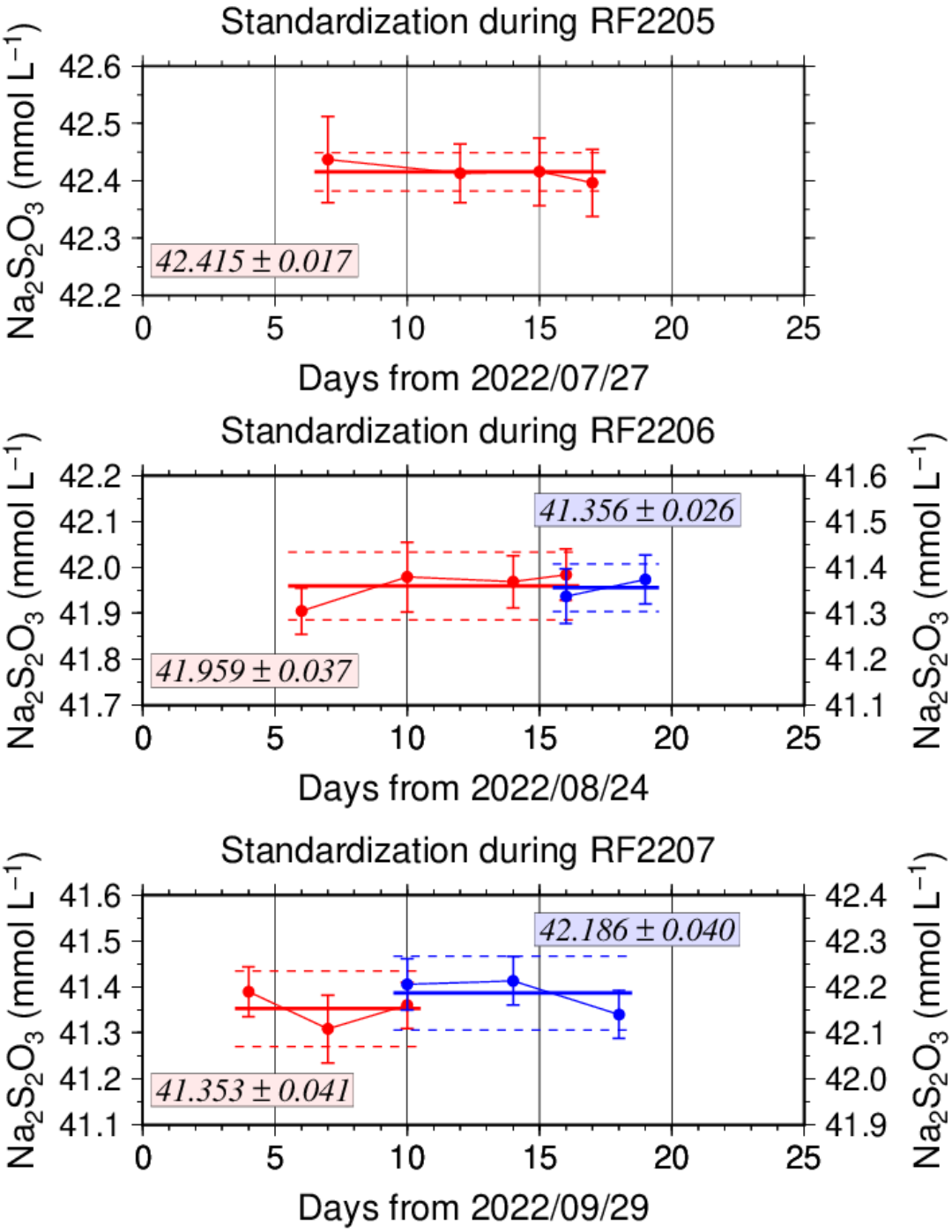

Figure C.3.3. Calculated concentration of $Na_2S_2O_3$ solution at 20 °C in standardization during RF22-05 (top) and RF22-06 (middle), RF22-07 (bottom). Different colors of plots indicate different batches of $Na_2S_2O_3$ solution; red (blue) plots correspond to the left (right) y-axis. Error bars of plots show uncertainty (k=2) of concentration of

$Na_2S_2O_3$ in the measurements. Thick and dashed lines denote the mean and twice the standard deviations for the batch measurements, respectively.

(6) Blank

(6.1) Reagent blank

The blank in an oxygen measurement (reagent blank in distilled water; $V_{reg\text{-}blk}$) was determined by the methods described in the IOCCP Report (Langdon, 2010) using pure water. The blank reflects not only the interfering substances (oxidants or reductants) in the reagents but also the differences between the measured end-point and the equivalence point due to unknown causes in the titrator (Figure C.3.4).

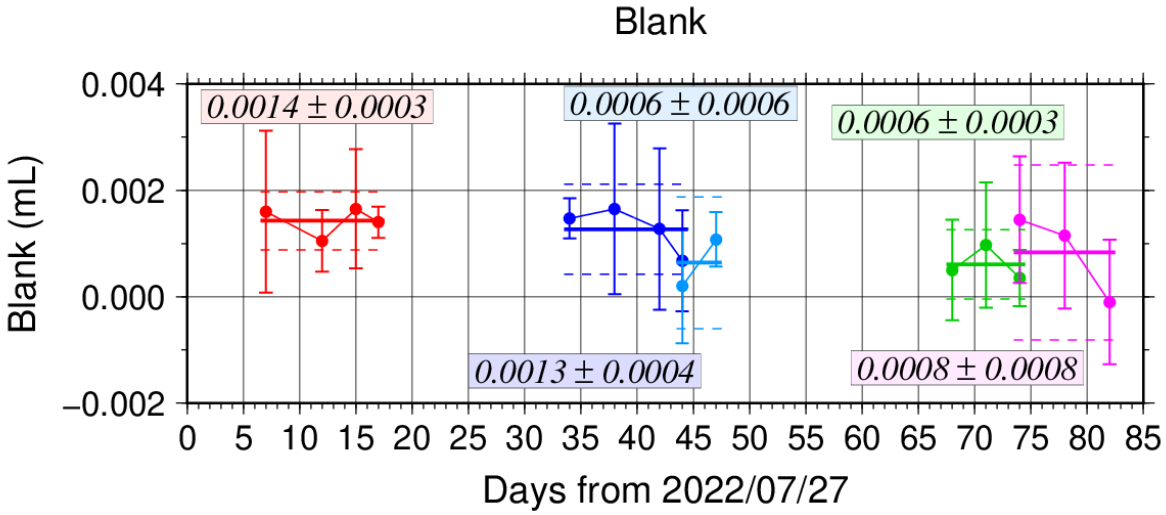

Figure C.3.4. Reagent blank ($V_{reg\text{-}blk}$) determination. Error bars of plots show standard deviations of the measurements. Thick and dashed lines denote the mean and the mean ±twice the standard deviation for the batch measurement, respectively.

(6.2) Seawater blank

We also determined seawater blank ($V_{sw\text{-}blk}$) which reflects interfering substances in seawater. Although this blank is not included in determination of oxygen concentration, measurement of the blank would be necessary to improve traceability and comparability in dissolved oxygen concentration. Details are described in Appendix A3.

(7) Quality Control

(7.1) Replicate and duplicate analyses

We took replicate (pair of water samples taken from a single Niskin bottle) and duplicate (pair of water samples taken from different Niskin bottles closed at the same depth) samples of dissolved oxygen throughout the cruise. Table C.3.2 summarizes the results of the analyses. Figure C.3.5 shows details of the results. The calculation of the standard deviation from the difference of sets was based on a procedure (SOP 23) in DOE (1994).

Table C.3.2. Summary of replicate and duplicate measurements.

Measurement	Ave. ± S.D. (μmol kg^{-1})
Replicate	0.18±0.17 (N=353)
Duplicate	0.24±0.24 (N=174)

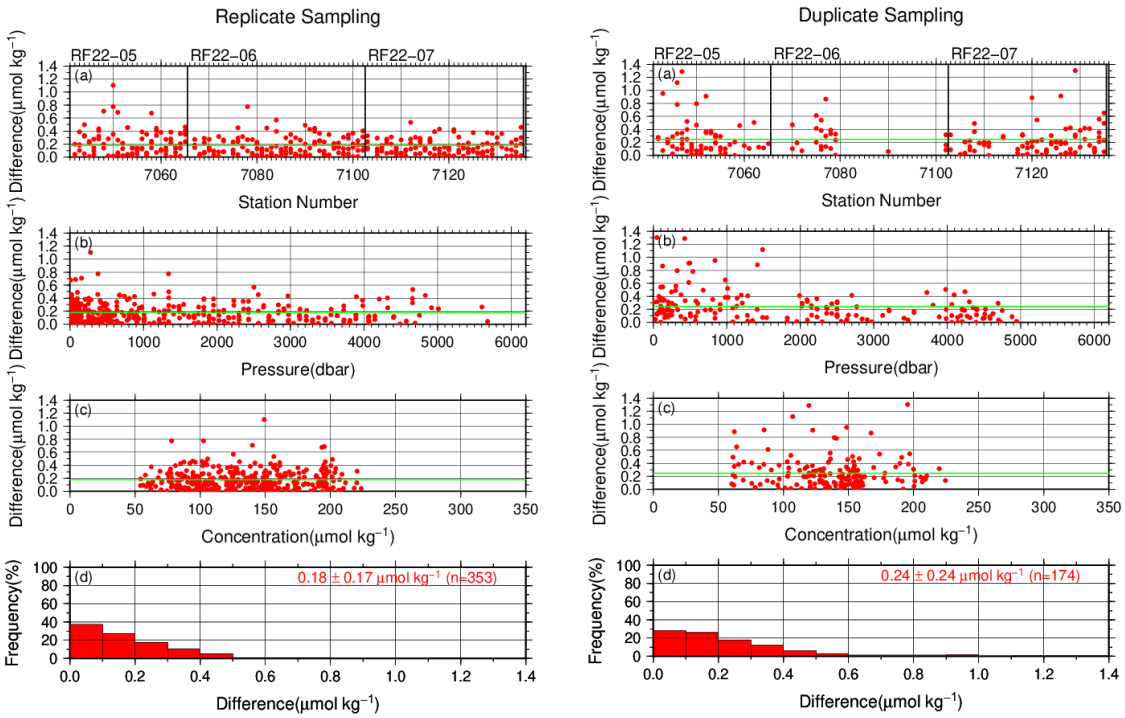

Figure C.3.5. Results of (left) replicate and (right) duplicate measurements during the cruise against (a) station number, (b) pressure, and (c) concentration of dissolved oxygen. Green lines denote the average of the measurements. Bottom panels (d) show histograms of the measurements.

(7.2) Comparisons between standard KIO_3 solutions

During the cruise, comparisons were made between different lots of standard KIO_3 solutions to confirm the accuracy of our oxygen measurements and the bias of a standard KIO_3 solution. A concentration of the standard KIO_3 solution "20211130-2" was determined using $Na_2S_2O_3$ solution standardized with the KIO_3 solution "20220117-2", and the difference between the measured value and the theoretical one. Good agreement between two standards confirmed that there was no systematic shift in oxygen measurements during the cruise (Figure C.3.6).

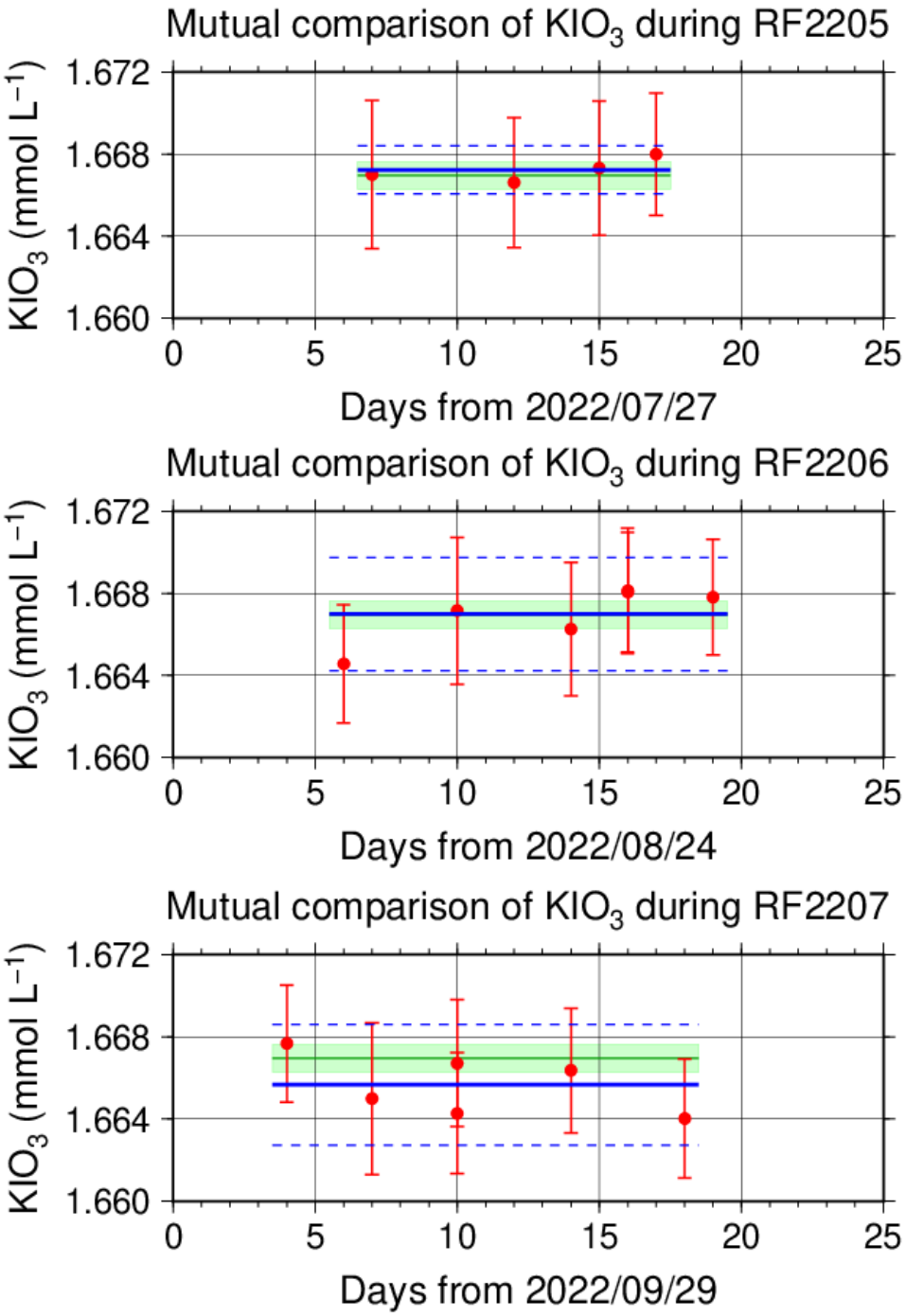

Figure C.3.6. Result of comparison of standard KIO_3 solutions during RF22-05 (top), RF22-06 (middle) and RF22-07 (bottom). Circles and error bars show mean of the measured value and its uncertainty (k=2), respectively. Thick and dashed lines in blue

denote the mean and the mean ± twice the standard deviations, respectively, for the measurements throughout the cruise. Green thin line and light green thick line denote the nominal concentration and its uncertainty (k=2) of standard KIO_3 solution "20211130-2", for RF22-05, RF22-06 and RF22-07, respectively.

(7.3) Quality control flag assignment

A quality flag value was assigned to oxygen measurements, as shown in Table C.3.3, using the code defined in IOCCP Report No.14 (Swift, 2010).

Table C.3.3. Summary of assigned quality control flags.

Flag	Definition	Number of samples
2	Good	2927
3	Questionable	2
4	Bad (Faulty)	12
5	Not reported	0
6	Replicate measurements	353
Total number of samples		3294

(8) Uncertainty

Oxygen measurement involves various uncertainties; determination of glass bottles volume, repeatability and systematic error of burette discharge, repeatability of pickling reagent discharges, determination of reagent blank, standardization of $Na_2S_2O_3$ solution, and uncertainty of KIO_3 concentration. After taking into consideration the above uncertainties that could be evaluated, the expanded uncertainty of bottle oxygen concentrations (T=20, S=34.5) was estimated, as shown in Table C.3.4. However, it is difficult to determine a strict uncertainty for oxygen concentration because there is no reference material for oxygen measurement.

Table C.3.4. Expanded uncertainty (k=2) of bottle oxygen during the cruise.

O_2 conc. (μmol kg^{-1})	Uncertainty (μmol kg^{-1})
20	0.31
30	0.32
50	0.34
70	0.37
100	0.41
150	0.51
200	0.62
250	0.74
300	0.87
400	1.12

Appendix

A1. Methods

(A1.1) Seawater sampling

Following procedure is based on a determination method in IOCCP Report (Langdon, 2010). Seawater samples were collected from 10-liters Niskin bottles attached the CTD-

system and a stainless steel bucket for the surface. Seawater for bottle oxygen measurement was transferred from the Niskin bottle and a stainless steel bucket to a volumetrically calibrated dry glass bottles. At least three times the glass volume water was overflowed. Then, pickling reagent-I 1 mL and reagent-II 1mL were added immediately, and sample temperature was measured using a thermometer. After a stopper was inserted carefully into the glass, it was shaken vigorously to mix the content and to disperse the precipitate finely. After the precipitate has settled at least halfway down the glass, the glass was shaken again. The sample glasses containing pickled samples were stored in a laboratory until they were titrated. To prevent air from entering the glass, deionized water (DW) was added to its neck after sampling.

(A1.2) Sample measurement

At least 15 minutes after the re-shaking, the samples were measured on board. Added 1 mL H_2SO_4 solution and a magnetic stirrer bar into the sample glass, samples were titrated with $Na_2S_2O_3$ solution whose molarity was determined with KIO_3 solution. During the titration, the absorbance of iodine in the solution was monitored using a detector. Also, temperature of $Na_2S_2O_3$ solution during the titration was recorded using a thermometer. Dissolved oxygen concentration (μmol kg^{-1}) was calculated from sample temperature at the fixation, CTD salinity, glass volume, and titrated volume of the $Na_2S_2O_3$ solution, and oxygen in the pickling reagents-I (1 mL) and II (1 mL) (7.6×10^{-8} mol; Murray *et al.*, 1968).

A2. Reagents recipes

Pickling reagent-I; Manganous chloride solution (3 mol L^{-1})
Dissolve 600 g of $MnCl_2 \cdot 4H_2O$ in DW, then dilute the solution with DW to a final volume of 1 L.

Pickling reagent-II; Sodium hydroxide (8 mol L^{-1}) / sodium iodide solution (4 mol L^{-1})
Dissolve 320 g of NaOH in about 500 mL of DW, allow to cool, then add 600 g NaI and dilute with DW to a final volume of 1 L.

H_2SO_4 solution; Sulfuric acid solution (5 mol L^{-1})
Slowly add 280 mL concentrated H_2SO_4 to roughly 500 mL of DW. After cooling the final volume should be 1 L.

$Na_2S_2O_3$ solution; Sodium thiosulfate solution (0.04 mol L^{-1})
Dissolve 50 g of $Na_2S_2O_3 \cdot 5H_2O$ and 0.4 g of Na_2CO_3 in DW, then dilute the solution with DW to a final volume of 5 L.

KIO_3 solution; Potassium iodate solution (0.001667 mol L^{-1})
Dry high purity KIO_3 for two hours in an oven at 130 °C. After weight out accurately KIO_3, dissolve it in DW in a 5 L flask. Concentration of potassium iodate is determined by a gravimetric method.

A3. Seawater blank

Blank due to redox species other than oxygen in seawater ($V_{sw\text{-}blk}$) can be a potential source of measurement error. Total blank ($V_{tot\text{-}blk}$) in seawater measurement can be represented as follows;

$$V_{tot\text{-}blk,} = V_{reg\text{-}blk} + V_{sw\text{-}blk}. \quad \text{(C3.A1)}$$

Because the reagent blank ($V_{reg\text{-}blk}$) determined for pure water is expected to be equal to that in seawater, the difference between blanks for seawater ($V_{tot\text{-}blk}$) and for pure water gives the $V_{sw\text{-}blk}$.

Here, $V_{sw\text{-}blk}$ was determined by following procedure. Seawater was collected in the calibrated volumetric glass without the pickling solution. Then 1 mL of the standard

KIO_3 solution, H_2SO_4 solution, and reagent solution-II and I each were added in sequence into the glass. After that, the sample was titrated to the end-point by $Na_2S_2O_3$ solution. Similarly, a glass contained 100 mL of DW added with 1 mL of the standard KIO_3 solution, H_2SO_4 solution, pickling reagent solution-II and I were titrated with $Na_2S_2O_3$ solution. The difference of the titrant volume of the seawater and DW glasses gave $V_{sw\text{-}blk}$.

The seawater blank has been reported from 0.4 to 0.8 μmol kg^{-1} in the previous study (Culberson *et al*., 1991). Additionally, these errors are expected to be the same to all investigators and not to affect the comparison of results from different investigators (Culberson, 1994). However, the magnitude and variability of the seawater blank have not yet been documented. Understanding of the magnitude and variability is important to improve traceability and comparability in oxygen concentration. The determined seawater blanks are shown in Table C.3.A1.

Table C.3.A1. Results of seawater blank determinations.

Station: RF7054 02°-16′N/140°-30′E		Station: RF7064 04°-31′N/137°-01′E		Station: RF7085 12°-30′N/137°-00′E	
Depth (m)	Blank (μmol kg^{-1})	Depth (m)	Blank (μmol kg^{-1})	Depth (m)	Blank (μmol kg^{-1})
25	0.24	50	0.13	50	0.55
50	0.28	125	0.21	125	0.44
101	0.33	151	0.77	125	0.71
202	0.56	972	0.35	152	0.51
202	0.67	1532	1.17	1001	0.81
431	0.63	2532	0.80	1600	0.91
731	0.52	3423	0.73	2600	0.98
1271	0.53	4171	0.67	3001	0.67
1873	0.60	4927	0.57	3501	0.76
2075	0.54			4250	0.88
2472	0.65			4693	0.94
3078	0.68			4693	0.88

Station: RF7102 21°-00′N/137°-01′E		Station: RF7121 29°-30′N/137°-10′E		Station: RF7135 32°-20′N/137°-00′E	
Depth (m)	Blank (μmol kg^{-1})	Depth (m)	Blank (μmol kg^{-1})	Depth (m)	Blank (μmol kg^{-1})
26	0.77	74	0.47	26	0.78
100	0.64	149	0.60	51	0.61
100	0.72	149	0.68	51	0.66
200	0.99	280	0.75	434	0.65
432	0.80	772	0.64	1072	0.71
1266	0.92	1929	0.75	1670	0.78
2074	1.05	2529	0.71	2070	0.68
3080	0.97	3170	0.76	2472	0.77
3581	1.41	3668	0.71	2871	0.77
4072	1.38	4170	0.81	3333	0.75
4797	1.17	4640	0.75	4026	0.81
4797	1.00	4640	0.76	4026	0.75

Reference

Culberson, A.H. (1994), Dissolved oxygen, in WHPO Pub. 91-1 Rev. 1, November 1994, Woods Hole, Mass., USA.

Culberson, A.H., G. Knapp, M.C. Stalcup, R.T. Williams, and F. Zemlyak (1991), A comparison of methods for the determination of dissolved oxygen in seawater, WHPO Pub. 91-2, August 1991, Woods Hole, Mass., USA.

Langdon, C. (2010), Determination of dissolved oxygen in seawater by Winkler titration using the amperometric technique, *IOCCP Report No.14, ICPO Pub. 134, 2010 ver.1*

Murray, C. N., J. P. Riley and T. R. S. Wilson (1968), The solubility of oxygen in Winkler reagents used for the determination of dissolved oxygen. *Deep-Sea Res*. 15, 237–238.

Swift, J. H. (2010), Reference-quality water sample data: Notes on acquisition, record keeping, and evaluation. *IOCCP Report No.14, ICPO Pub. 134, 2010 ver.1*.

4. Nutrients

31 March 2023

(1) Personnel

KITAGAWA Takahiro
FUJII Takuya
NAKAMURA Motohiro (RF22-05, RF22-06)
HASHIMOTO Susumu (RF22-06, RF22-07)
OCHIAI Naoko (RF22-05, RF22-07)
FUJIWARA Hiroyuki (RF22-05)
UEHARA Tomohiro (RF22-06)
KAKUYA Keita (RF22-07)

(2) Station occupied

A total of 92 stations (RF 22-05 : 24, RF 22-06 : 36, RF 22-07 : 32) were occupied for nutrients measurements. Station location and sampling layers of nutrients are shown in Figures C.4.1 and C.4.2.

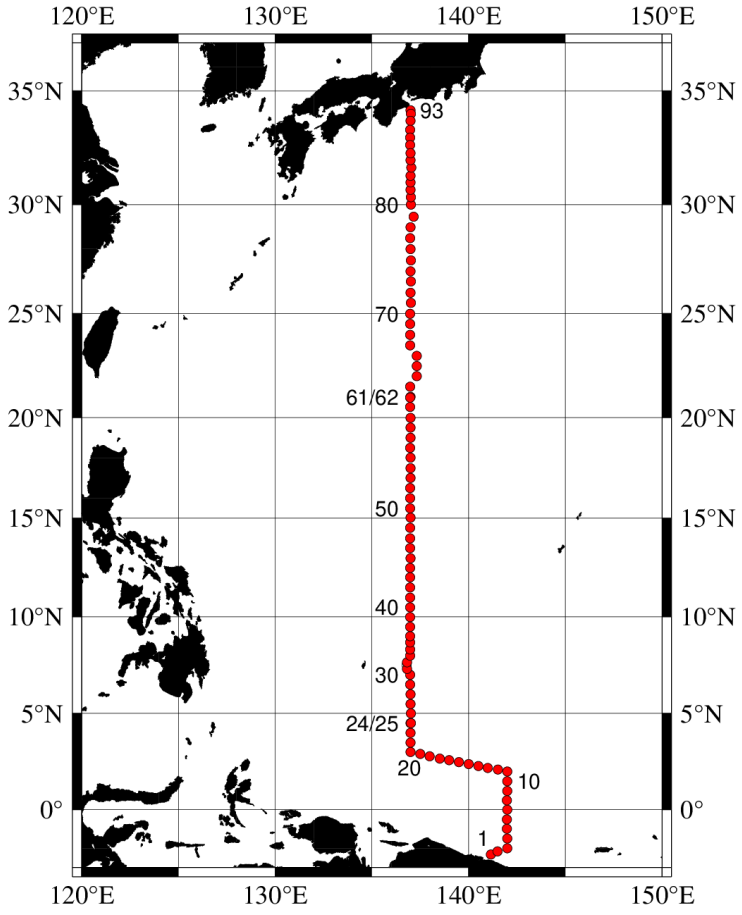

Figure C.4.1. Location of observation stations of nutrients. Closed and open circles indicate sampling and no-sampling stations, respectively.

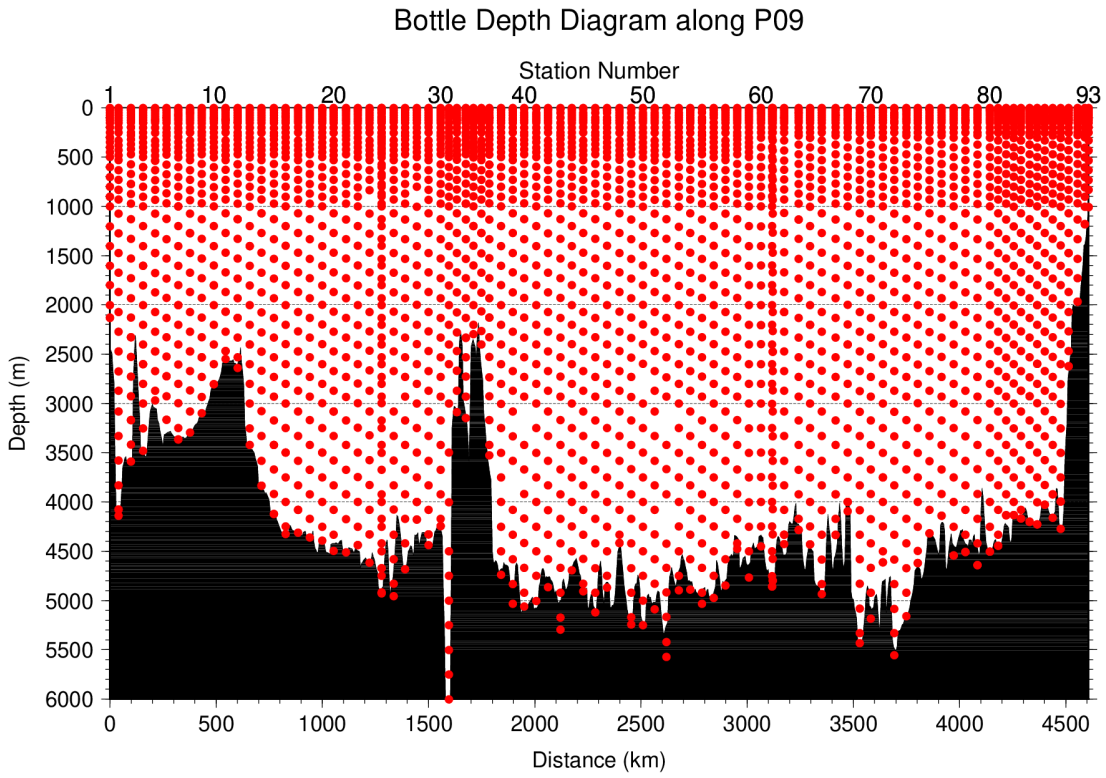

Figure C.4.2. Distance-depth distributions of sampling layers of nutrients.

(3) Instrument

The nutrients analyses were carried out on a four-channel Auto Analyzer III (BL TEC K.K., Japan) for four nutrients nitrate+nitrite, nitrite, phosphate, and silicate.

(4) Sampling and measurement

Methods of seawater sampling, measurement, and data processing of nutrient concentration were described in Appendixes A1, A2, and A3, respectively. The reagents for the measurement were prepared according to recipes shown in Appendix A4.

(5) Nutrients standards

(5.1) Volumetric laboratory ware of in-house standards

All volumetric wares were gravimetrically calibrated. The weights obtained in the calibration weighing were corrected for the density of water and for air buoyancy. Polymethylpenten volumetric flasks were gravimetrically calibrated at the temperature of use within 4–6 °C. All pipettes have nominal calibration tolerances of 0.1 % or better. These were gravimetrically calibrated in order to verify and improve upon this nominal tolerance.

(5.2) Reagents of standard

The batches of the reagents used for standards are listed in Table C.4.1.

Table C.4.1. List of reagents for the standards used in the cruise.

	Name	CAS No	Lot. No	Industries
Nitrate	Potassium nitrate 99.995 suprapur®	7757-79-1	B1706365	Merck KGaA
Nitrite	Sodium nitrite GR for analysis ACS, Reag. Ph Eur	7632-00-0	A1611049	Merck KGaA
Phosphate	Potassium dihydrogen phosphate anhydrous 99.995 suprapur®	7778-77-0	B1871308	Merck KGaA
Silicate	Silicon standard solution 1000 mg/l Si*	-	HC01345036	Merck KGaA

* Traceable to NIST-SRM3150

(5.3) Low nutrient seawater (LNSW)

Surface water with sufficiently low nutrient concentration was taken and filtered using 10 μm pore size membrane filter in our previous cruise. This water was stored in 15 liter flexible container with paper box.

(5.4) In-house standard solutions

Nutrient concentrations for A, B and C standards were set as shown in Table C.4.2. A and B standards were prepared with deionized water (DW). C standard (full scale of working standard) was mixture of B-1 and B-2 standards, and was prepared with LNSW. C-1 standard, whose concentrations of nutrient were nearly zero, was prepared as LNSW slightly added with DW to be equal with mixing ratio of LNSW and DW in C standard. The C-2 to -5 standards were prepared with mixture of C-1 and C standards in stages as 1/4, 2/4, 3/4, and 4/4 (i.e., pure “C standard”) concentration for full scale, respectively. The actual concentration of nutrients in each standard was calculated based on the solution temperature and factors of volumetric laboratory wares calibrated prior to use. Nominal zero concentration of nutrient was determined in measurement of DW after refraction error correction. The calibration curves for each run were obtained using 5 levels of C-1 to -5 standards. These standard solutions were periodically renewed as shown in Table C.4.3.

Table C.4.2. Nominal concentrations of nutrients for A, B, and C standards at 20 °C. Unit is μmol L^{-1}.

	A	B	C
Nitrate	27524	550	43.9
Nitrite	12020	240	1.9
Phosphate	2125	42.4	3.39
Silicate	35606	2134	170

Table C.4.3. Schedule of renewal of in-house standards.

Standard	Renewal
A-1 std. (NO_3)	Maximum 2 months
A-2 std. (NO_2)	No renewal
A-3 std. (PO_4)	Maximum 2 months
A-4 std. (Si)	Commercial prepared solution
B-1 std. (mixture of A-1, A-3, and A-4 stds.)	Maximum 8 days
B-2 std. (diluted A-2 std.)	Maximum 15 days
C-std. (mixture of B-1 and B-2 stds.)	Every measurement
C-1 to -5 stds.	Every measurement

(6) Certified reference material

Certified reference material for nutrients in seawater (hereafter CRM), which was prepared by the General Environmental Technos company (KANSO Technos, Japan), was used for every analysis at each hydrographic station. Use of CRMs for the analysis of seawater ensures stable comparability and uncertainty of data. CRMs used in the cruise are shown in Table C.4.4.

Table C.4.4. Certified concentration and uncertainty (k=2) of CRMs. Unit is μmol kg^{-1}.

	Nitrate	Nitrite	Phosphate	Silicate
CRM-CK	0.02±0.03*	0.011±0.008*	0.048±0.012	0.73±0.08*
CRM-CJ	16.2±0.2	0.031±0.007	1.19±0.02	38.5±0.4
CRM-CM	33.2±0.3	0.018±0.006*	2.38±0.03	100.5±0.5
CRM-CN	43.6±0.4	0.010±0.004*	2.94±0.03	152.7±0.8

* Reference value because concentration is under limit of quantitation

The CRMs were analyzed every run but were newly opened every two runs. Although this usage of CRM might be less common, we have confirmed a stability of the opened CRM bottles to be tolerance in our observation. The CRM bottles were stored at a laboratory in the ship, where the temperature was maintained at around 25 °C.
It is noted that nutrient data in our report are calibrated not on CRM but on in-house standard solutions. Therefore, to calculate data based on CRM, it is necessary that values of nutrient concentration in our report are correlated with CRM values measured in the same analysis run. The result of CRM measurements is attached as 49UP20220727_P09_nut_CRM_measurement.csv.

(7) Quality Control

(7.1) Replicate and duplicate analyses

We took replicate (pair of water samples taken from a single Niskin bottle) and duplicate (pair of water samples taken from different Niskin bottles closed at the same depth) samples of nutrients throughout the cruise. Table C.4.5 summarizes the results of the analyses. Figures C.4.3–C.4.5 show details of the results. The calculation of the standard deviation from the difference of sets of samples was based on a procedure (SOP 23) in DOE (1994).

Table C.4.5. Average and standard deviation of difference of replicate and duplicate measurements throughout the cruise. Unit is μmol kg^{-1}.

Samples	Nitrate+nitrite	Phosphate	Silicate
Replicate	0.034±0.036 (N=352)	0.002±0.002 (N=353)	0.062±0.060 (N=348)
Duplicate	0.043±0.050 (N=174)	0.003±0.003 (N=174)	0.097±0.092 (N=174)

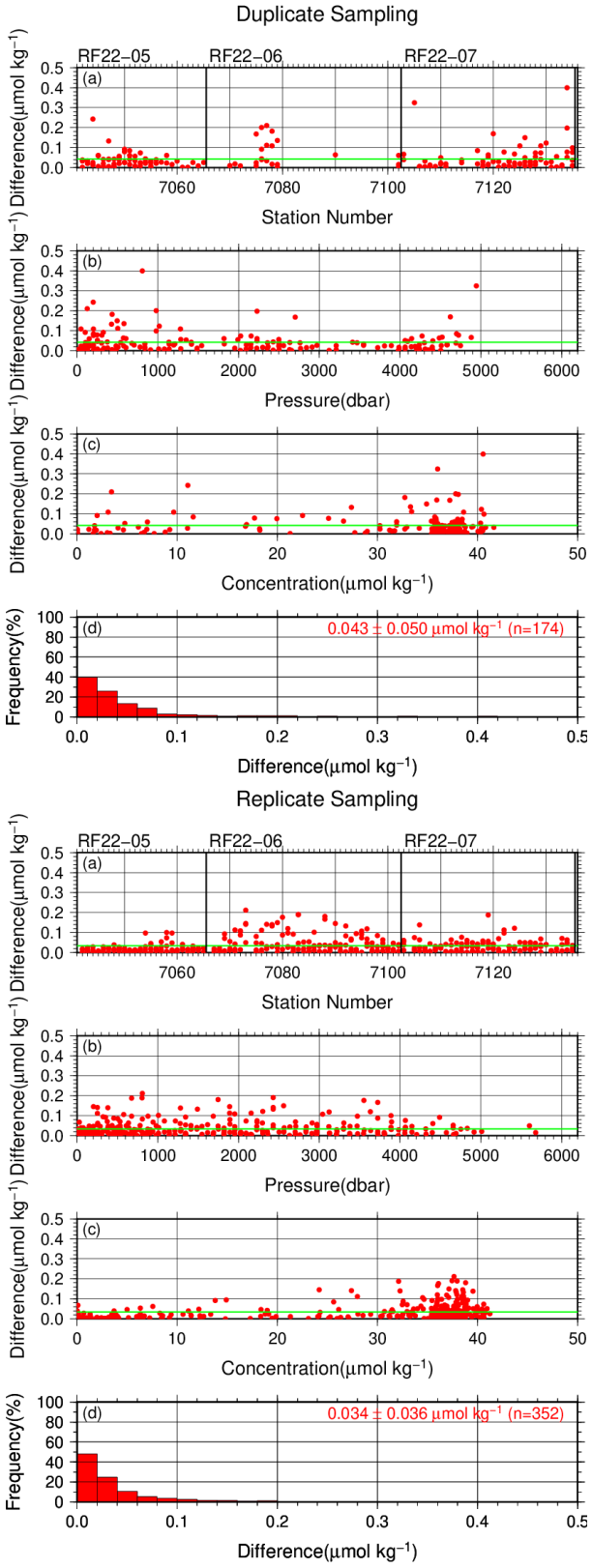

Figure C.4.3. Results of (left) replicate and (right) duplicate measurements of nitrate+nitrite throughout the cruise versus (a) station number, (b) sampling pressure, (c) concentration, and (d) histogram of the measurements. Green lines indicates the mean of the differences of concentrations based on replicate/duplicate analyses.

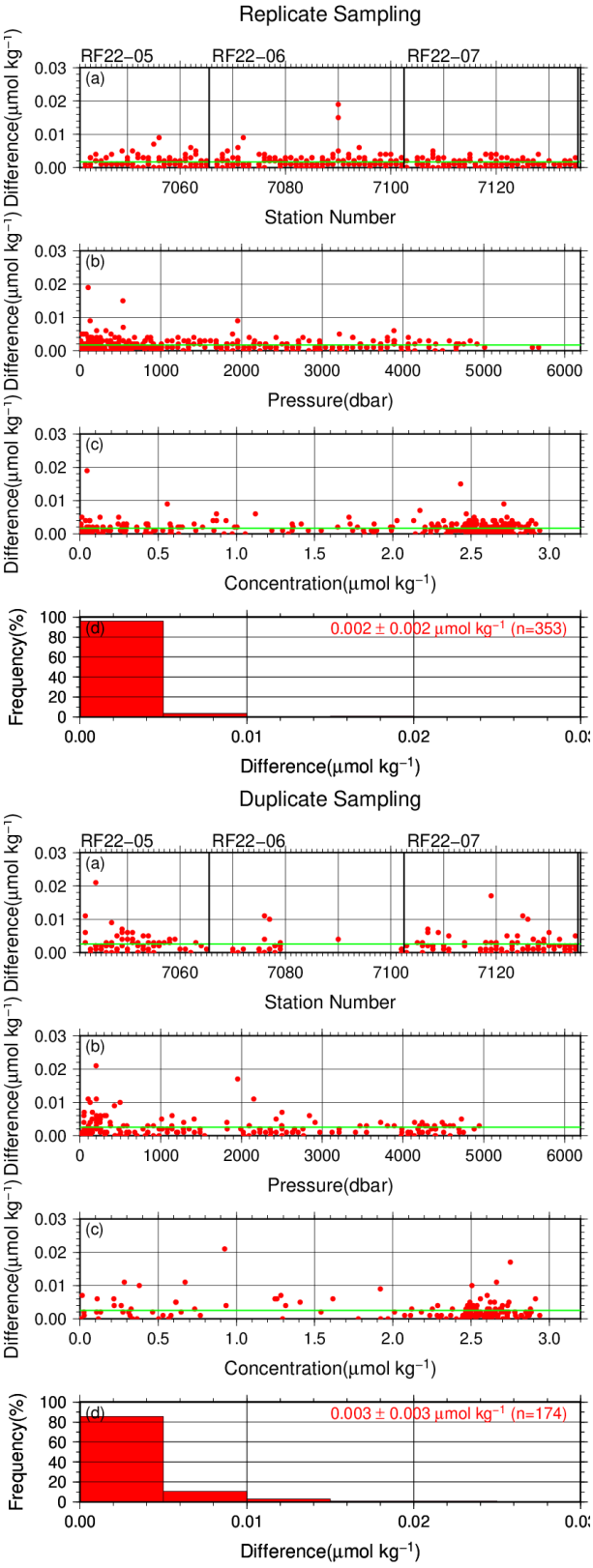

Figure C.4.4. Same as Figure C.4.3, but for phosphate.

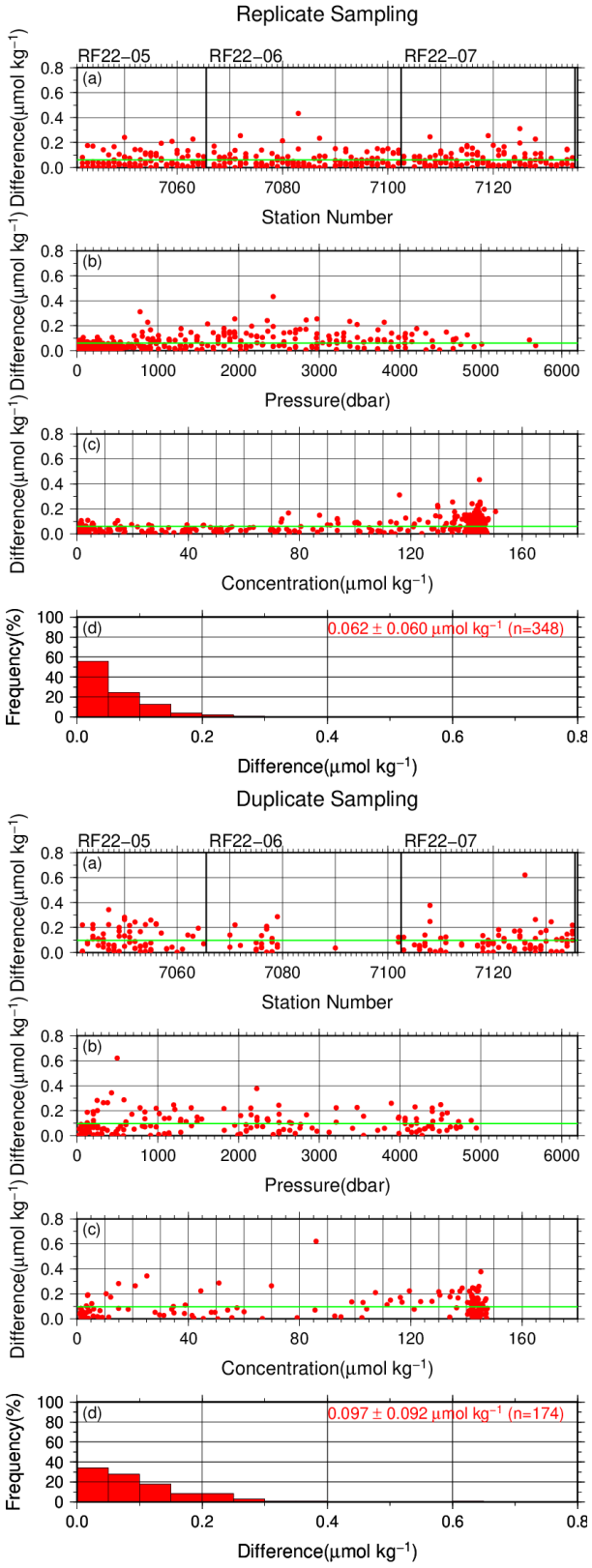

Figure C.4.5. Same as Figure C.4.3, but for silicate.

(7.2) Measurement of CRMs

Table C.4.6 summarizes the CRM measurements during the cruise. The CRM concentrations were assigned with in-house standard solutions. Figures C.4.6–C.4.9 show the measured concentrations of CRM-CN throughout the cruise.

Table C.4.6. Summary of (upper) mean concentration and its standard deviation (unit: μmol kg^{-1}), (middle) coefficient of variation (%), and (lower) total number of CRMs measurements throughout the cruise.

	Nitrate+nitrite	Nitrite	Phosphate	Silicate
CRM-CK	0.10±0.03 34.20 % (N=138)	0.042±0.005 10.73 % (N=138)	0.065±0.005 7.92 % (N=138)	0.85±0.07 7.77 % (N=138)
CRM-CJ	16.27±0.05 0.32 % (N=139)	0.051±0.001 2.72 % (N=139)	1.201±0.006 0.49 % (N=139)	38.86±0.10 0.25 % (N=139)
CRM-CM	33.26±0.08 0.23 % (N=138)	0.026±0.002 5.93 % (N=137)	2.383±0.007 0.28 % (N=138)	101.56±0.15 0.15 % (N=138)
CRM-CN	43.66±0.10 0.22 % (N=138)	0.017±0.002 8.76 % (N=138)	2.941±0.008 0.26 % (N=138)	154.36±0.20 0.13 % (N=138)

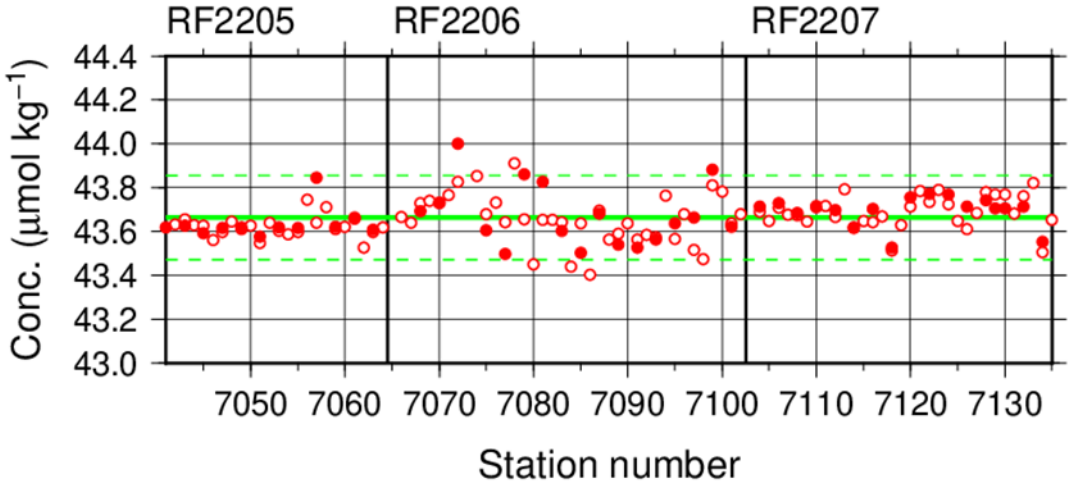

Figure C.4.6. Time-series of measured concentration of nitrate+nitrite of CRM-CN throughout the cruise. Closed and open circles indicate the newly and previously opened bottle, respectively. Thick and dashed lines denote the mean and the mean ± twice the standard deviations of the measurements throughout the cruise, respectively.

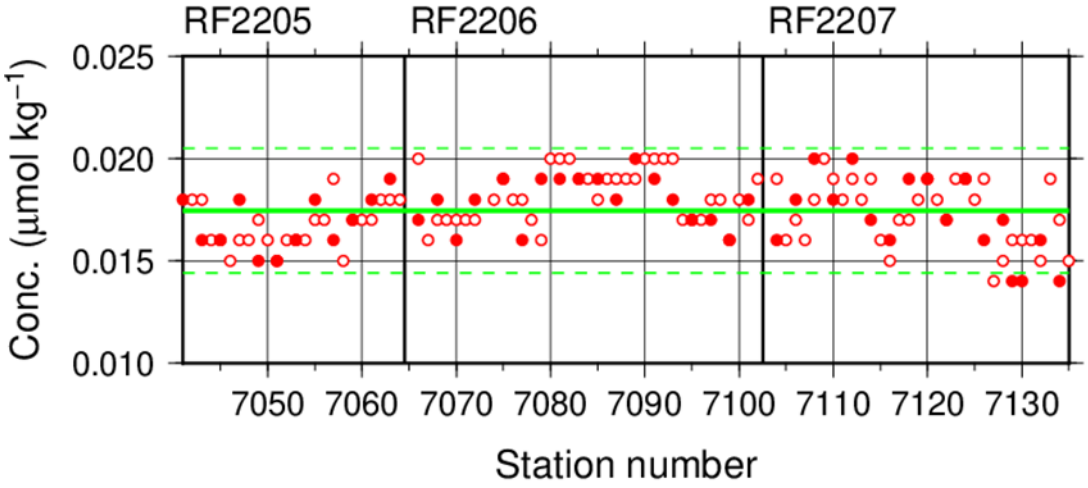

Figure C.4.7. Same as Figure C.4.6, but for nitrite.

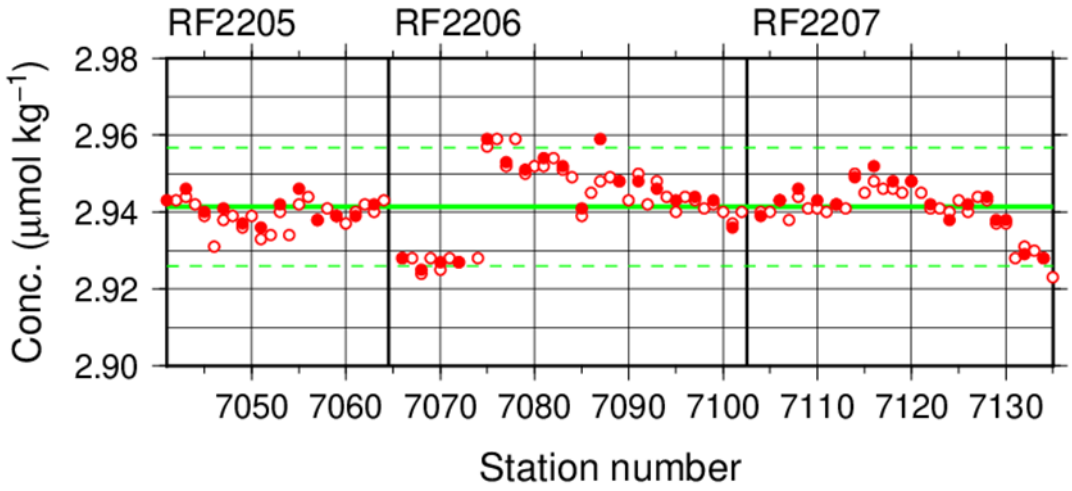

Figure C.4.8. Same as Figure C.4.6, but for phosphate.

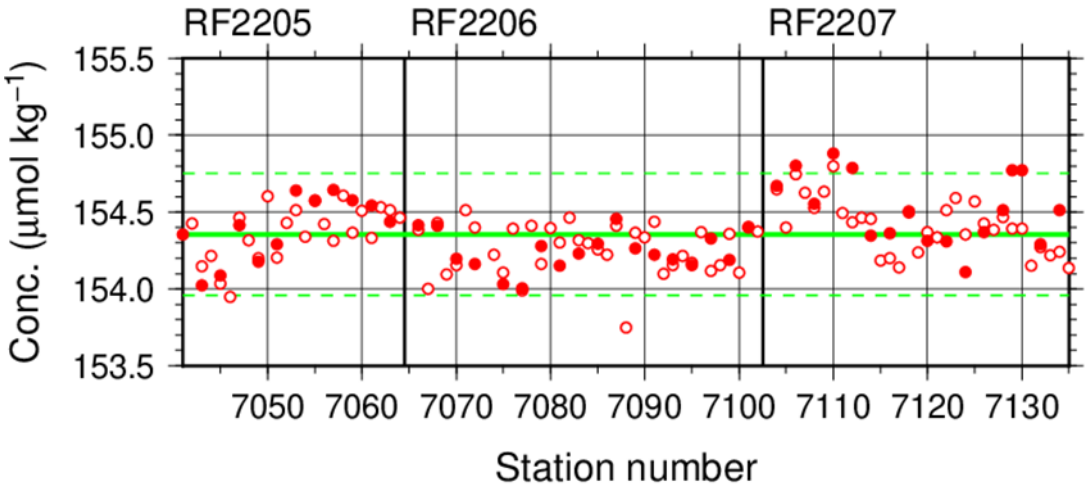

Figure C.4.9. Same as Figure C.4.6, but for silicate.

(7.3) Precision of analysis in a run

To monitor the precision of the analyses, the same samples were repeatedly measured in a sample array during a run. For this purpose, a C-5 standard solution was randomly inserted in every 2–10 samples as a "check standard" (the number of standards was about 8–9) in the run. The precision was estimated in terms of the coefficient of variation of the measurements. Table C.4.7 summarizes the results. The time series are shown in Figures C.4.10–C.4.13.

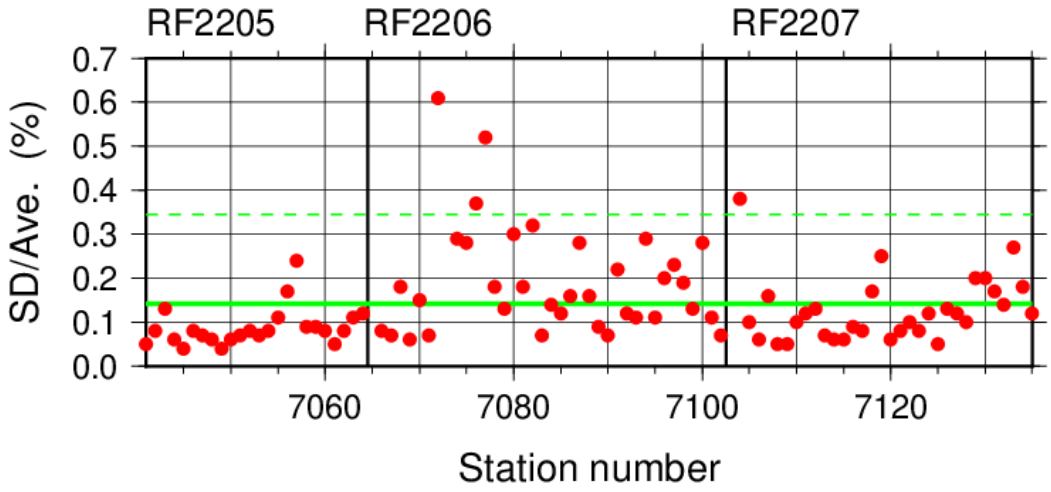

Figure C.4.10. Time-series of the coefficients of variation of "check standard" measurements of nitrate+nitrite throughout the cruise. Thick and dashed lines denote the mean and the mean ± twice the standard deviations of the measurements throughout the cruise, respectively.

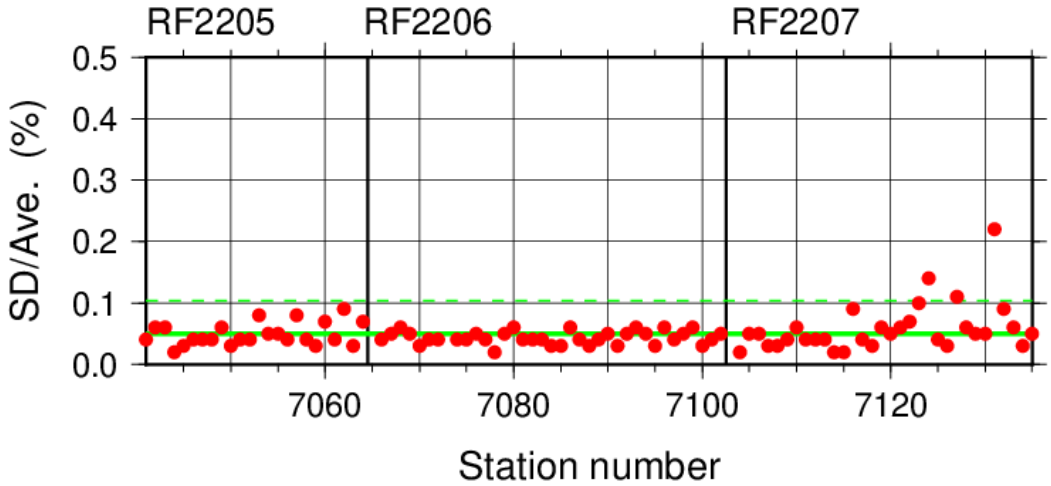

Figure C.4.11. Same as Figure C.4.10, but for nitrite.

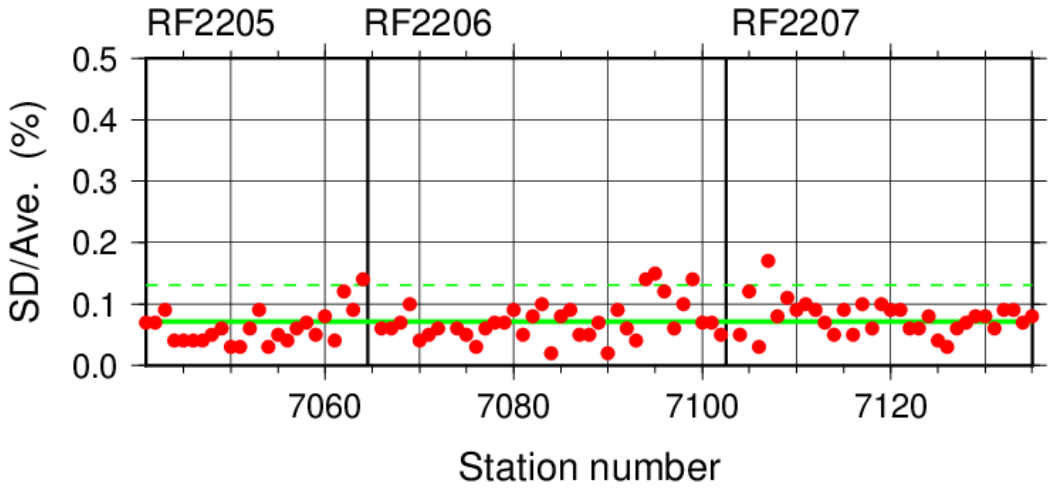

Figure C.4.12. Same as Figure C.4.10, but for phosphate.

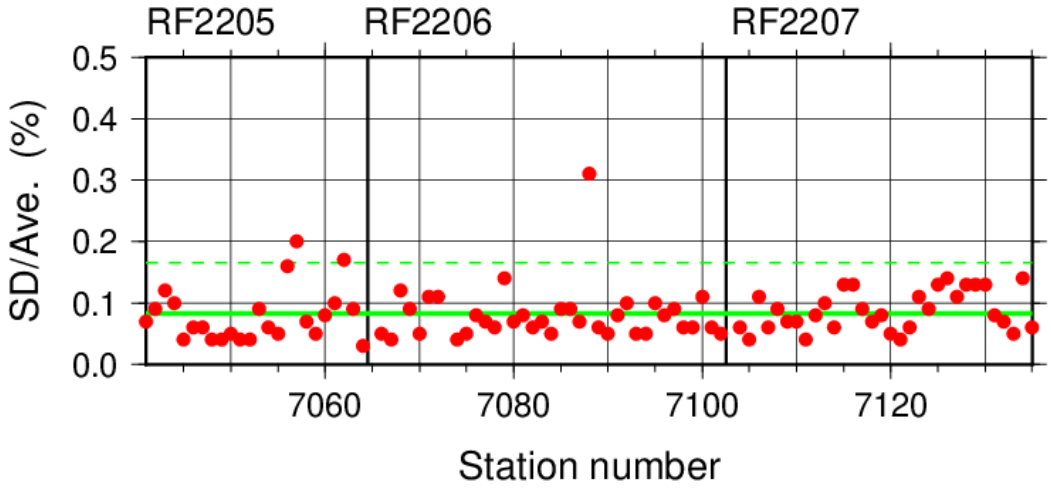

Figure C.4.13. Same as Figure C.4.10, but for silicate.

Table C.4.7. Summary of precisions of nutrient assays during the cruise.

	Nitrate+nitrite	Nitrite	Phosphate	Silicate
Median	0.11 %	0.04 %	0.07 %	0.07 %
Mean	0.14 %	0.05 %	0.07 %	0.08 %
Minimum	0.04 %	0.02 %	0.02 %	0.03 %
Maximum	0.61 %	0.22 %	0.17 %	0.31 %
Number	92	92	92	92

(7.4) Carryover

Carryover coefficients were determined during each analytical run. The C-5 standard (high standard) was followed by two C-1 standards (low standards). Figures C.4.14–17 show the time series of the carryover coefficients.

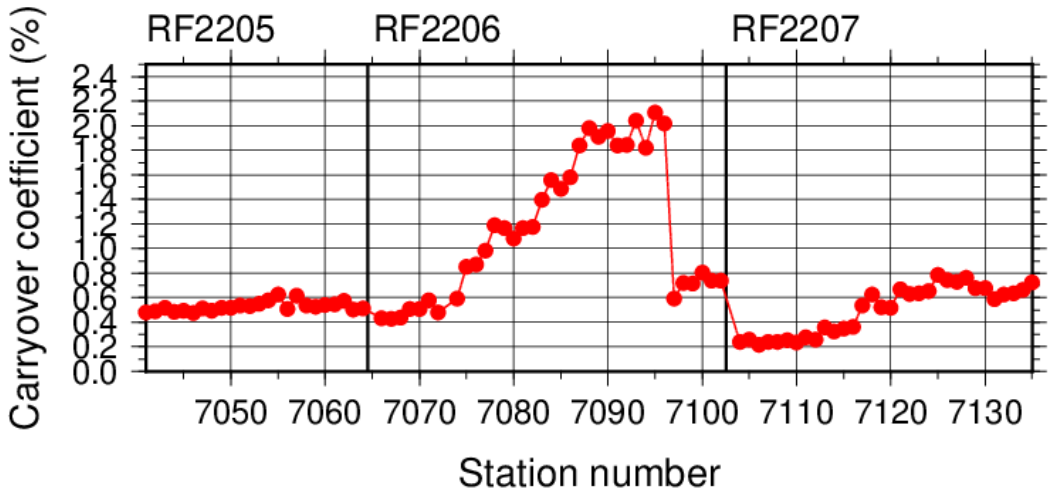

Figure C.4.14. Time-series of carryover coefficients in measurement of nitrate+nitrite throughout the cruise.

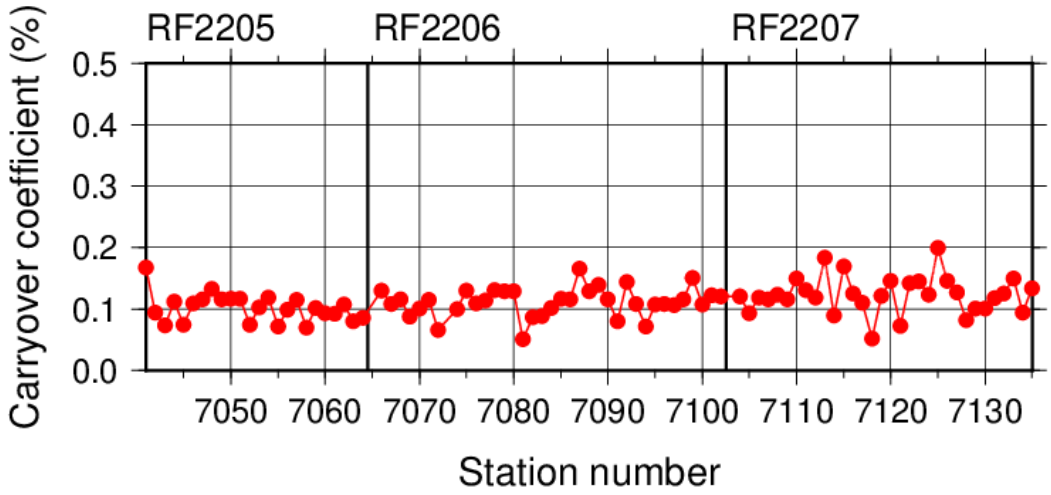

Figure C.4.15. Same as Figure C.4.14, but for nitrite.

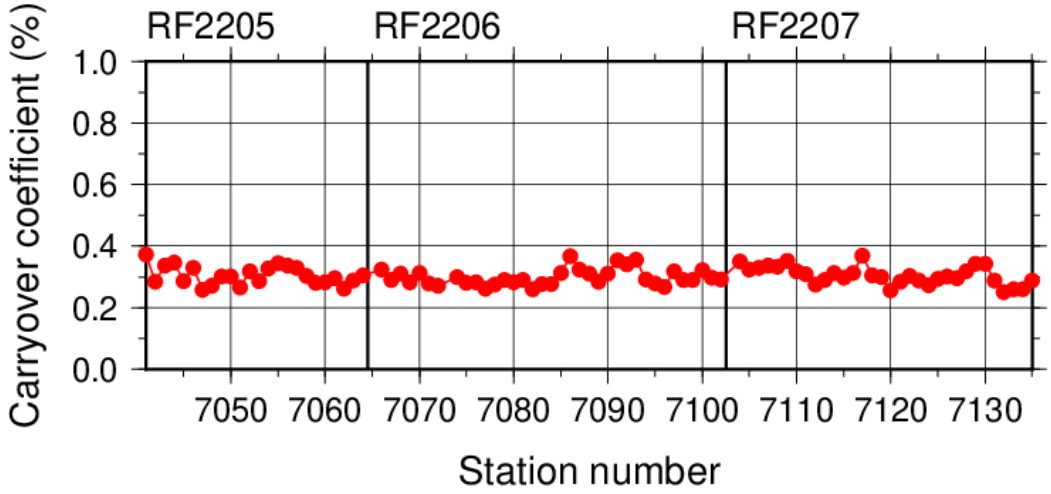

Figure C.4.16. Same as Figure C.4.14, but for phosphate.

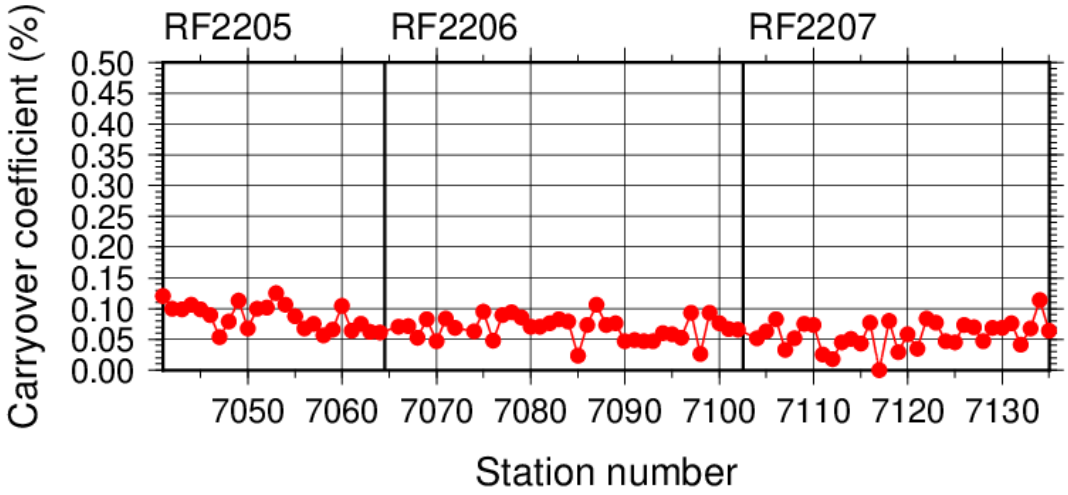

Figure C.4.17. Same as Figure C.4.14, but for silicate.

(7.5) Limit of detection/quantitation of measurement

Limit of detection (LOD) and quantitation (LOQ) of nutrient measurement were estimated from standard deviation (σ) of repeated measurements of nutrients concentration in C-1 standard as 3σ and 10σ, respectively. Summary of LOD and LOQ are shown in Table C.4.8.

Table C.4.8. Limit of detection (LOD) and quantitation (LOQ) of nutrient measurement in the cruise. Unit is μmol kg^{-1}.

	LOD	LOQ
Nitrate+nitrite	0.047	0.156
Nitrite	0.001	0.004
Phosphate	0.007	0.024
Silicate	0.102	0.340

(7.6) Quality control flag assignment

A quality flag value was assigned to nutriment measurements as shown in Table C.4.9, using the code defined in IOCCP Report No.14 (Swift, 2010).

Table C.4.9. Summary of assigned quality control flags.

Flag	Definition	Nitrate+nitrite	Nitrite	Phosphate	Silicate
2	Good	2929	2927	2922	2896
3	Questionable	1	1	2	0
4	Bad (Faulty)	11	12	16	49
5	Not reported	0	0	0	0
6	Replicate measurements	352	353	353	348
Total number of samples		3293	3293	3293	3293

(8) Uncertainty

(8.1) Uncertainty associated with concentration level: U_c

Generally, an uncertainty of nutrient measurement is expressed as a function of its concentration level which reflects that some components of uncertainty are relatively large in low concentration. Empirically, the uncertainty associated with concentrations level (U_c) can be expressed as follows;

$$U_c\ (\%) = a + b \cdot (1/C_x) + c \cdot (1/C_x)^2, \quad \text{(C4.1)}$$

where C_x is the concentration of sample for parameter X.

Using the coefficients of variation of the CRM measurements throughout the cruise, uncertainty associated with concentrations of nitrate+nitrite, phosphate, and silicate were determined as follows:

$$U_{c\text{-}no3}\ (\%) = 0.0513 + 2.70 \cdot (1/C_{no3}) + 0.0229 \cdot (1/C_{no3})^2 \quad \text{(C4.2)}$$

$$U_{c\text{-}po4}\ (\%) = -0.0897 + 0.398 \cdot (1/C_{po4}) \quad \text{(C4.3)}$$

$$U_{c\text{-}sil}\ (\%) = 0.0378 + 3.71 \cdot (1/C_{sil}) + 0.372 \cdot (1/C_{sil})^2, \quad \text{(C4.4)}$$

where C_{no3}, C_{po4}, and C_{sil} represent concentrations of nitrate+nitrite, phosphate, and silicate, respectively, in μmol kg^{-1}. Figures C.4.18–C.4.20 show the calculated uncertainty graphically.

Figure

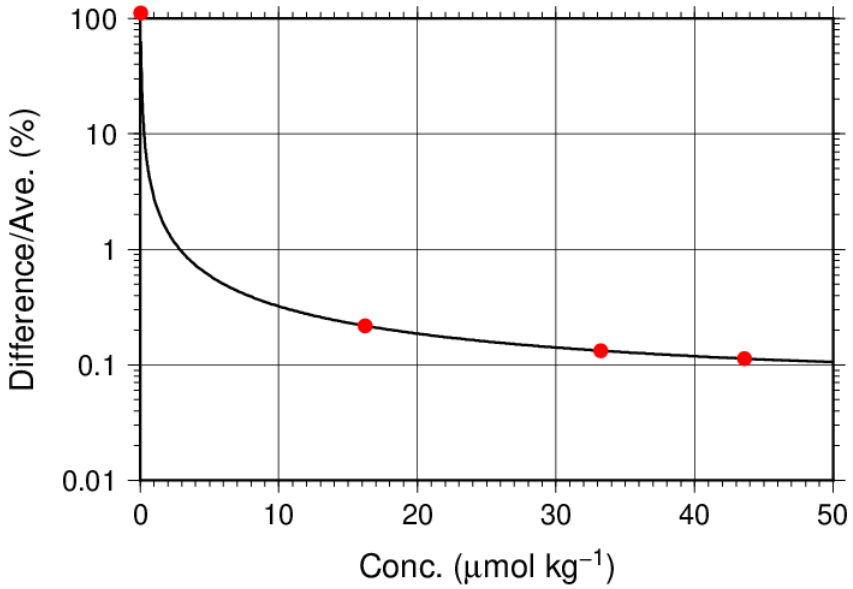

C.4.18. Uncertainty of nitrate+nitrite associated with concentrations.

Figure

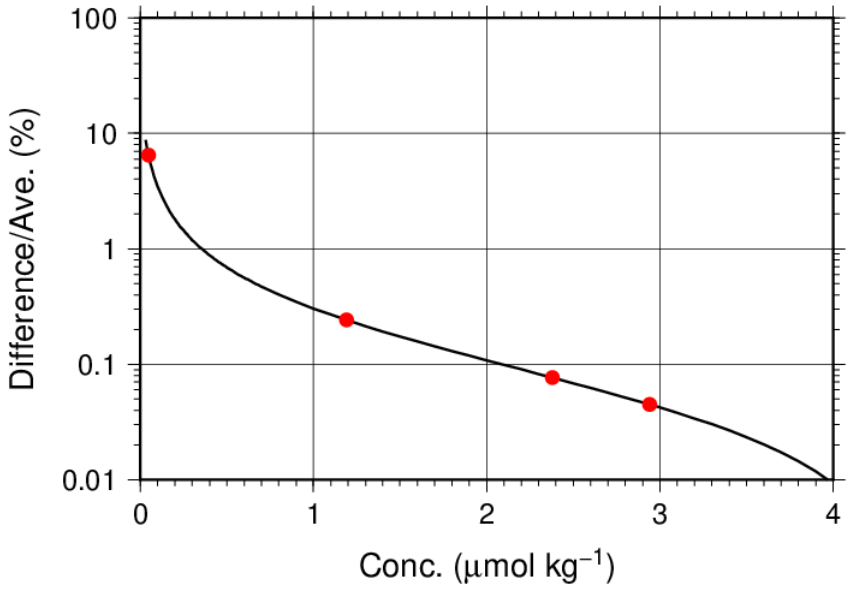

C.4.19. Same as Figure C.4.18, but for phosphate.

Figure

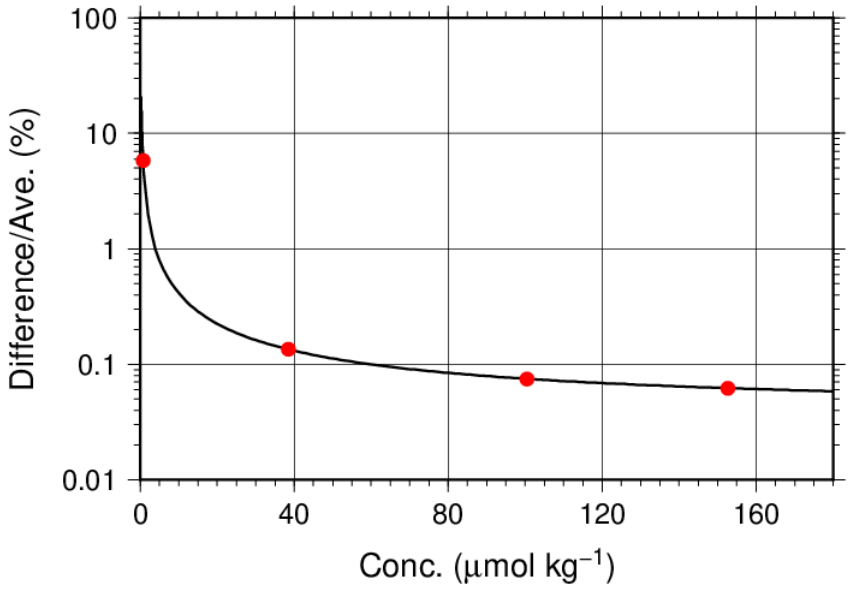

C.4.20. Same as Figure C.4.18, but for silicate.

(8.2) Uncertainty of analysis between runs: U_s

Uncertainty of analysis among runs (U_s) was evaluated based on the coefficient of variation of measured concentrations of CRM-CN with the highest concentration among the CRM lots throughout the cruise, as shown in subsection (7.2). The reason for using the CRM lot to state U_s is to exclude the effect of uncertainty associated with lower concentration described previously. As is clear from the definition of U_c, U_s is equal to U_c at nutrients concentrations of the lot. It is important to note that U_s includes all of uncertainties during the measurements throughout stations, namely uncertainties of concentrations of in-house standard solutions prepared for each run, uncertainties of slopes and intercepts of the calibration curve in each run, precision of measurement in a run (U_a), and between-bottle homogeneity of the CRM.

(8.3) Uncertainty of analysis in a run: U_a

Uncertainty of analysis in a run (U_a) was evaluated based on the coefficient of variation of repeated measurements of the "check standard" solution, as shown in subsection (7.3). The U_a reflects the conditions associated with chemistry of colorimetric measurement of nutrients, and stability of electronic and optical parts of the instrument throughout a run. Under a well-controlled condition of the measurements, U_a might show Poisson distribution with a mean as shown in Figures C.4.10–C.4.13 and Table C.4.7 and treated as a precision of measurement. U_a is a part of U_c at the concentration as stated in a previous section for U_c.

However, U_a may show larger value which was not expected from Poisson distribution of U_a due to the malfunction of the instruments, larger ambient temperature change, human errors in handling samples and chemistries, and contaminations of samples in a run. In the cruise, we observed that U_a of our measurement was usually small and well-controlled in most runs as shown in Figures C.4.10–C.4.13 and Table C.4.7. However, in a few runs, U_a showed high values which were over the mean ± twice the standard deviations of U_a, suggesting that the measurement system might have some problems.

(8.4) Uncertainty of CRM concentration: U_r

In the certification of CRM, the uncertainty of CRM concentrations (U_r) was stated by the manufacturer (Table C.4.4) as expanded uncertainty at k=2. This expanded uncertainty reflects the uncertainty of the Japan Calibration Service System (JCSS) solutions, characterization in assignment, between-bottle homogeneity, and long term stability. We have ensured comparability between cruises by ensuring that at least two lots of CRMs overlap between cruises. In comparison of nutrient concentrations between cruises using KANSO CRMs in an organization, it was not necessary to include U_r in the conclusive uncertainty of concentration of measured samples because comparability of measurements was ensured in an organization as stated previously.

(8.5) Conclusive uncertainty of nutrient measurements of samples: *U*

To determine the conclusive uncertainty of nutrient measurements of samples (U), we use two functions depending on U_a value acquired at each run as follows:
When U_a was small and measurement was well-controlled condition, the conclusive uncertainty of nutrient measurements of samples, U, might be as below:

$$U = U_c. \quad \text{(C4.5)}$$

When U_a was relative large and the measurement might have some problems, the conclusive uncertainty of nutrient measurements of samples, U, can be expanded as below:

$$U = \sqrt{U_c^2 + U_a^2}. \quad \text{(C4.6)}$$

When U_a was relative large and the measurement might have some problems, the equation of U is defined as to include U_a to evaluate U, although U_a partly overlaps with U_c. It means that the equation overestimates the conclusive uncertainty of samples. On the other hand, for low concentration there is a possibility that the equation not only overestimates but also underestimates the conclusive uncertainty because the functional shape of U_c in lower concentration might not be the same and cannot be verified. However, we believe that the applying the above function might be better way to evaluate the conclusive uncertainty of nutrient measurements of samples because we can do realistic evaluation of uncertainties of nutrient concentrations of samples which were obtained under relatively unstable conditions, larger U_a as well as the evaluation of them under normal and good conditions of measurements of nutrients.

Appendix

A1. Seawater sampling

Seawater samples were collected from 10-liters Niskin bottle attached CTD-system and a stainless steel bucket for the surface. Samples were drawn into 10 mL polymethylpenten vials using sample drawing tubes. The vials were rinsed three times before water filling and were capped immediately after the drawing.
No transfer was made and the vials were set on an auto sampler tray directly. Samples were analyzed immediately after collection.

A2. Measurement

(A2.1) General

Auto Analyzer III is based on Continuous Flow Analysis method and consists of sampler, pump, manifolds, and colorimeters. As a baseline, we used artificial seawater (ASW).

(A2.2) Nitrate+nitrite and nitrite

Nitrate+nitrite and nitrite were analyzed according to the modification method of Armstrong (1967). The sample nitrate was reduced to nitrite in a glass tube which was filled with granular cadmium coated with copper (RF22-05) or in a cadmium coil which was coated with a metallic copper (RF22-06 and RF22-07). The sample stream with its equivalent nitrite was treated with an acidic, sulfanilamide reagent and the nitrite forms nitrous acid which reacts with the sulfanilamide to produce a diazonium ion. N-1-naphthylethylene-diamine was added to the sample stream then coupled with the diazonium ion to produce a red, azo dye. With reduction of the nitrate to nitrite, sum of nitrate and nitrite were measured; without reduction, only nitrite was measured. Thus, for the nitrite analysis, no reduction was performed and the alkaline buffer was not necessary. The flow diagrams for each parameter are shown in Figures C.4.A1, C.4.A2.and C.4.A3. If the reduction efficiency of the cadmium column became lower than 95 %, the column or the coil was replaced.

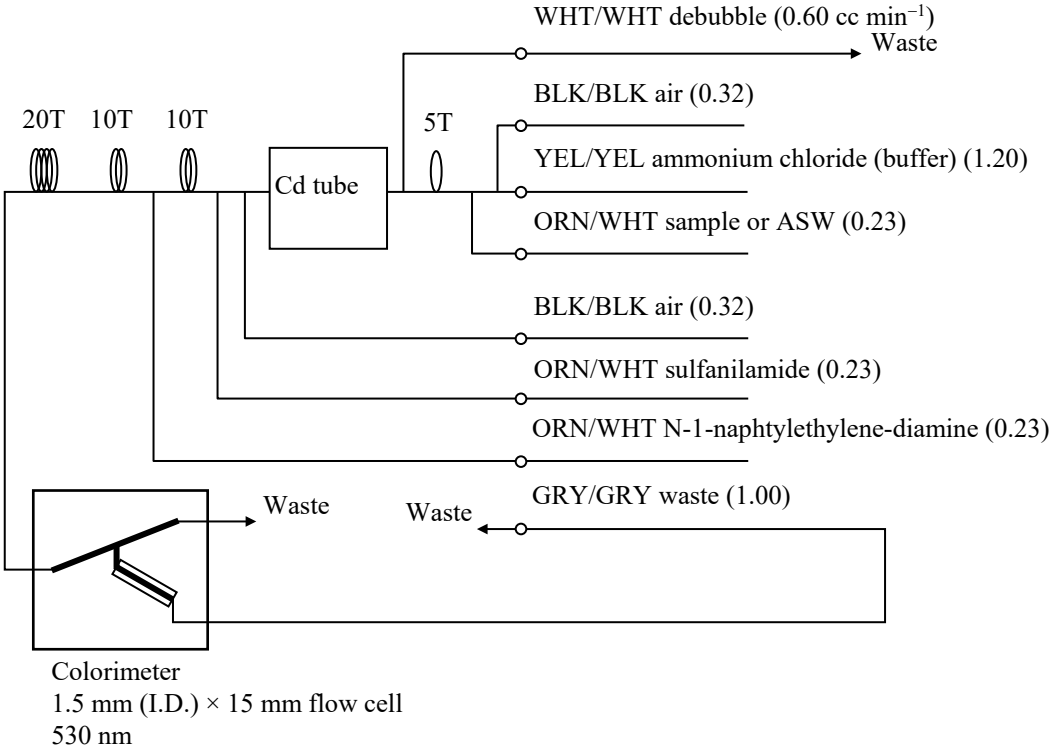

Figure C.4.A1. Nitrate+nitrite (ch. 1) flow diagram (RF22-05).

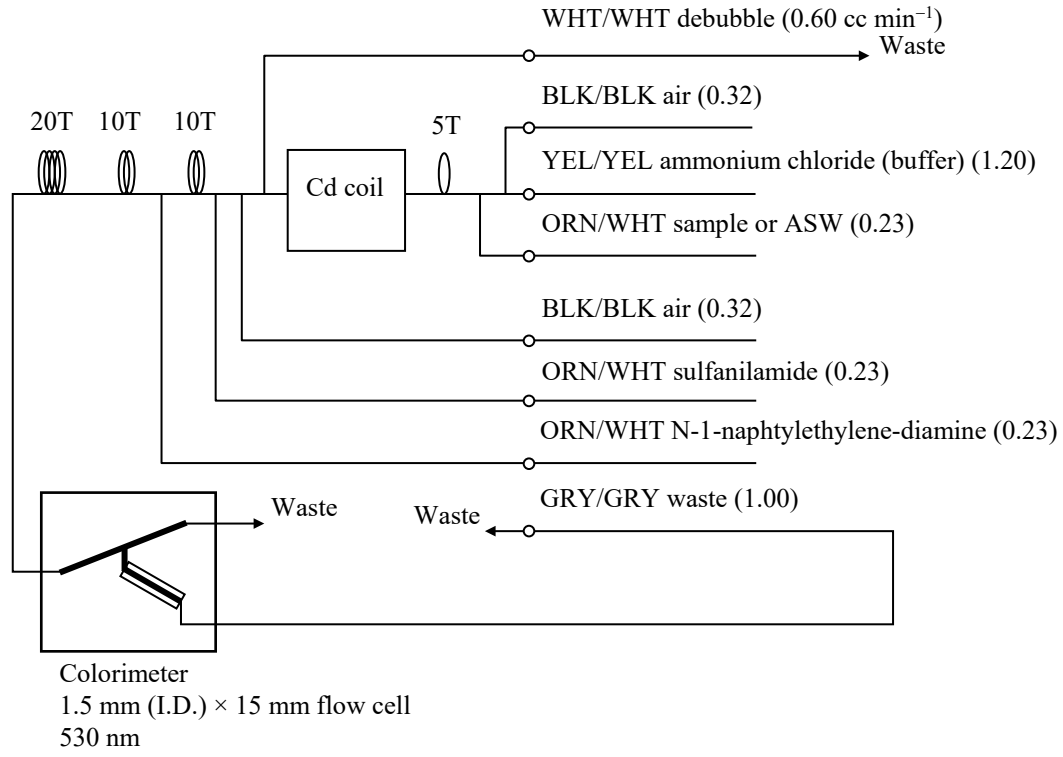

Figure C.4.A2. Nitrate+nitrite (ch. 1) flow diagram (RF22-06 and RF22-07).

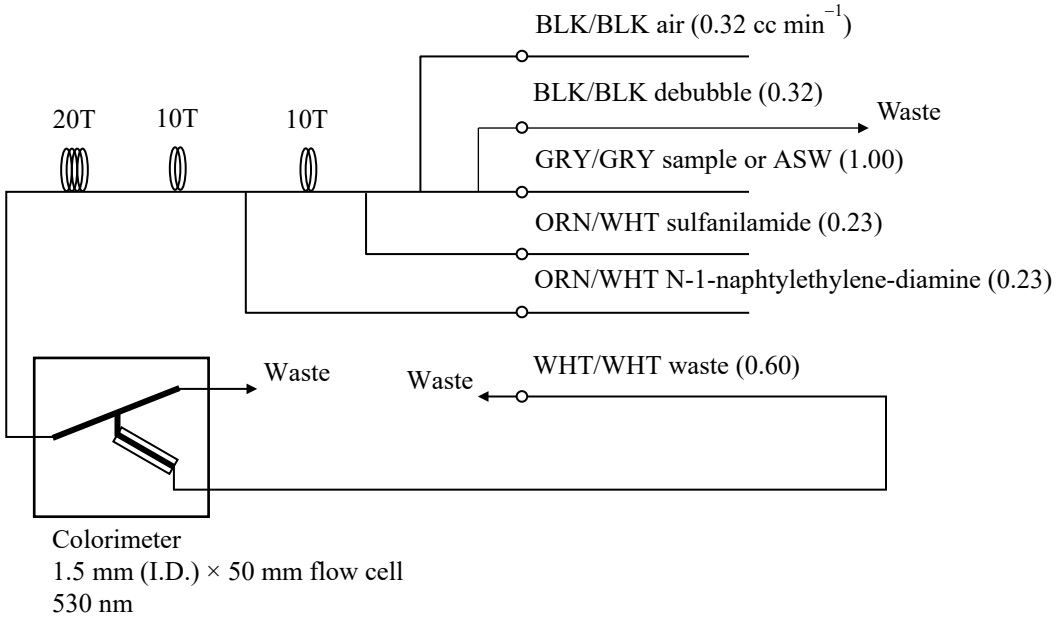

Figure C.4.A3. Nitrite (ch. 2) flow diagram.

(A2.3) Phosphate

The phosphate analysis was a modification of the procedure of Murphy and Riley (1962). Molybdic acid was added to the seawater sample to form phosphomolybdic acid which was in turn reduced to phosphomolybdous acid using L-ascorbic acid as the reductant. The flow diagram for phosphate is shown in Figure C.4.A4.

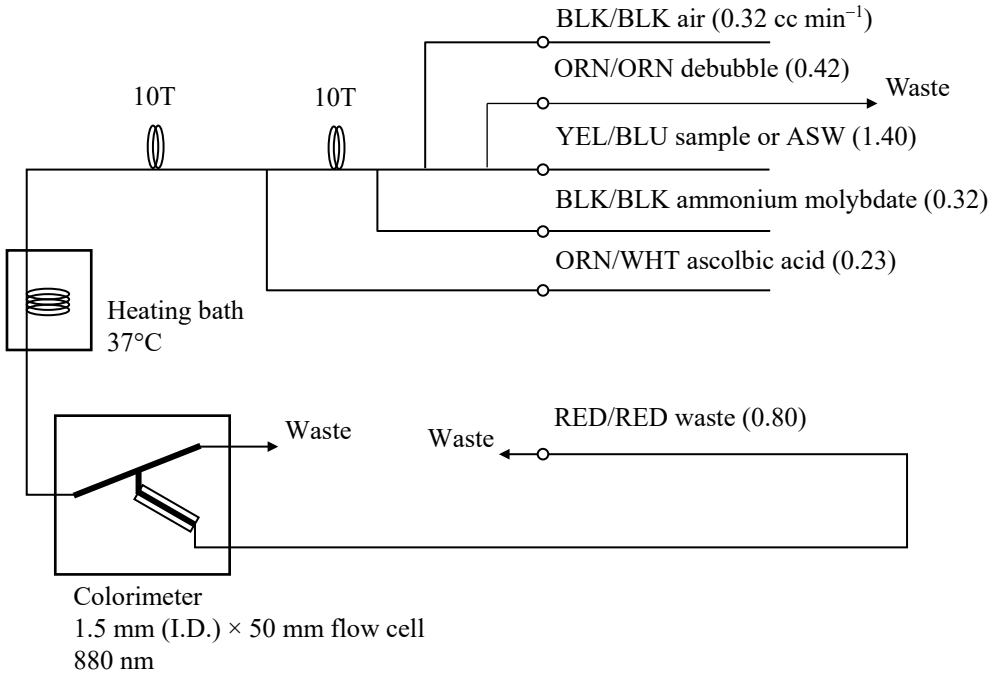

Figure C.4.A4. Phosphate (ch. 3) flow diagram.

(A2.4) Silicate

The silicate was analyzed according to the modification method of Grasshoff *et al.* (1983), wherein silicomolybdic acid was first formed from the silicate in the sample and added molybdic acid, then the silicomolybdic acid was reduced to silicomolybdous acid, or "molybdenum blue," using L-ascorbic acid as the reductant. The flow diagram for silicate is shown in Figure C.4.A5.

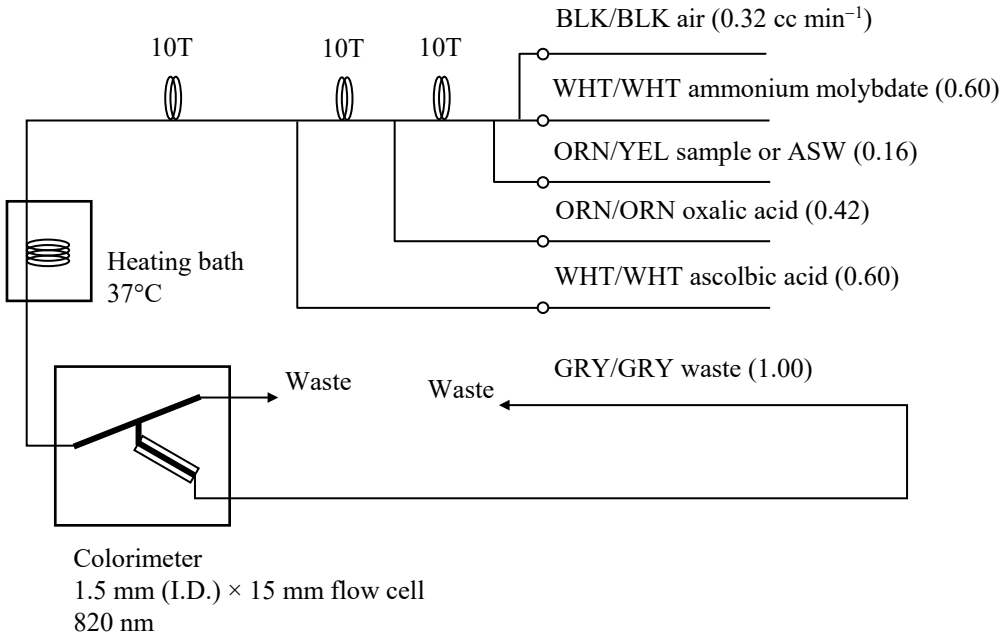

Figure C.4.A5. Silicate (ch. 4) flow diagram.

A3. Data processing

Raw data from Auto Analyzer III were recorded at 1-second interval and were treated as follows;

a. Check the shape of each peak and position of peak values taken, and then change the positions of peak values taken if necessary.
b. Baseline correction was done basically using linear regression.
c. Reagent blank correction was done basically using linear regression.
d. Carryover correction was applied to peak heights of each sample.
e. Sensitivity correction was applied to peak heights of each sample.
f. Refraction error correction was applied to peak heights of each seawater sample.
g. Calibration curves to get nutrients concentration were assumed quadratic expression.
h. Concentrations were converted from μmol L^{-1} to μmol kg^{-1} using seawater density.

A4. Reagents recipes

(A4.1) Nitrate+nitrite

Ammonium chloride (buffer), 0.7 μmol L^{-1} (0.04 % w/v);
Dissolve 190 g ammonium chloride, NH_4Cl, in ca. 5 L of DW, add about 5 mL ammonia(aq) to adjust pH of 8.2–8.5.
Sulfanilamide, 0.06 μmol L^{-1} (1 % w/v);
Dissolve 5 g sulfanilamide, 4-$NH_2C_6H_4SO_3H$, in 430 mL DW, add 70 mL concentrated HCl. After mixing, add 1 mL Brij-35 (22 % w/w).
N-1-naphtylethylene-diamine dihydrochloride (NEDA), 0.004 μmol L^{-1} (0.1 % w/v);
Dissolve 0.5 g NEDA, $C_{10}H_7NH_2CH_2CH_2NH_2 \cdot 2HCl$, in 500 mL DW.

(A4.2) Nitrite

Sulfanilamide, 0.06 μmol L^{-1} (1 % w/v); Shared from nitrate reagent.
N-1-naphtylethylene-diamine dihydrochloride (NEDA), 0.004 μmol L^{-1} (0.1 % w/v); Shared from nitrate reagent.

(A4.3) Phosphate

Ammonium molybdate, 0.005 μmol L^{-1} (0.6 % w/v);

Dissolve 3 g ammonium molybdate(VI) tetrahydrate, $(NH_4)_6Mo_7O_{24}\cdot 4H_2O$, and 0.05 g potassium antimonyl tartrate, $C_8H_4K_2O_{12}Sb_2\cdot 3H_2O$, in 400 mL DW and add 40 mL concentrated H_2SO_4. After mixing, dilute the solution with DW to final volume of 500 mL and add 2 mL sodium dodecyl sulfate (15 % solution in water).

L(+)-ascorbic acid, 0.08 μmol L^{-1} (1.5 % w/v);

Dissolve 4.5 g L(+)-ascorbic acid, $C_6H_8O_6$, in 300 mL DW. After mixing, add 10 mL acetone. This reagent was freshly prepared before every measurement.

(A4.4) Silicate

Ammonium molydate, 0.005 μmol L^{-1} (0.6 % w/v);

Dissolve 3 g ammonium molybdate(VI) tetrahydrate, $(NH_4)_6Mo_7O_{24}\cdot 4H_2O$, in 500 mL DW and added concentrated 2 mL H_2SO_4. After mixing, add 2 mL sodium dodecyl sulfate (15 % solution in water).

Oxalic acid, 0.4 μmol L^{-1} (5 % w/v);

Dissolve 25 g oxalic acid dihydrate, $(COOH)_2\cdot 2H_2O$, in 500 mL DW.

L(+)-ascorbic acid, 0.08 μmol L^{-1} (1.5 % w/v); Shared from phosphate reagent.

(A4.5) Baseline

Artificial seawater (salinity is ~34.7);

Dissolve 160.6 g sodium chloride, NaCl, 35.6 g magnesium sulfate heptahydrate, $MgSO_4\cdot 7H_2O$, and 0.84 g sodium hydrogen carbonate, $NaHCO_3$, in 5 L DW.

References

Armstrong, F. A. J., C. R. Stearns and J. D. H. Strickland (1967), The measurement of upwelling and subsequent biological processes by means of the Technicon TM Autoanalyzer TM and associated equipment, *Deep-Sea Res.*, 14(3), 381–389.

Grasshoff, K., Ehrhardt, M., Kremling K. et al. (1983), Methods of seawater analysis. 2nd rev, *Weinheim: Verlag Chemie, Germany, West.*

Murphy, J. and Riley, J.P. (1962), Analytica chimica *Acta*, *27, 31-36.*

Swift, J. H. (2010), Reference-quality water sample data: Notes on acquisition, record keeping, and evaluation. *IOCCP Report No.14, ICPO Pub. 134, 2010 ver.1*.

5. Phytopigments (chlorophyll-a and phaeopigment)

31 March 2023

(1) Personnel

KITAGAWA Takahiro
FUJII Takuya
NAKAMURA Motohiro (RF22-05, RF22-06)
HASHIMOTO Susumu (RF22-06, RF22-07)
OCHIAI Naoko (RF22-05, RF22-07)
FUJIWARA Hiroyuki (RF22-05)
UEHARA Tomohiro (RF22-06)
KAKUYA Keita (RF22-07)

(2) Station occupied

A total of 42 stations (RF 22-05 : 11, RF 22-06 : 17, RF 22-07 : 14) were occupied for phytopigment measurements. Station location and sampling layers of phytopigment are shown in Figures C.5.1 and C.5.2.

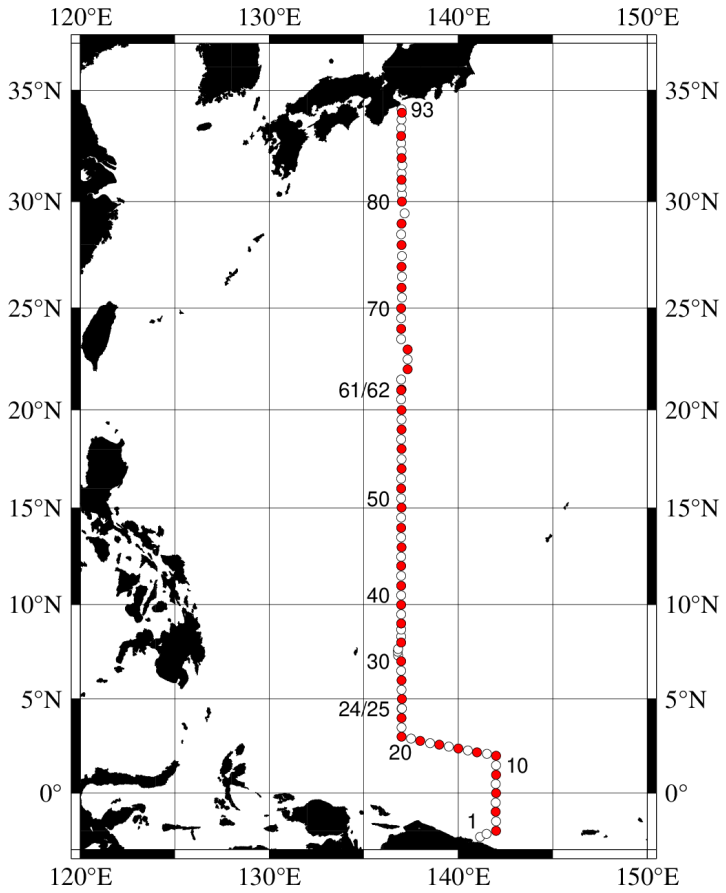

Figure C.5.1. Location of observation stations of chlorophyll-*a*. Closed and open circles indicate sampling and no-sampling stations, respectively.

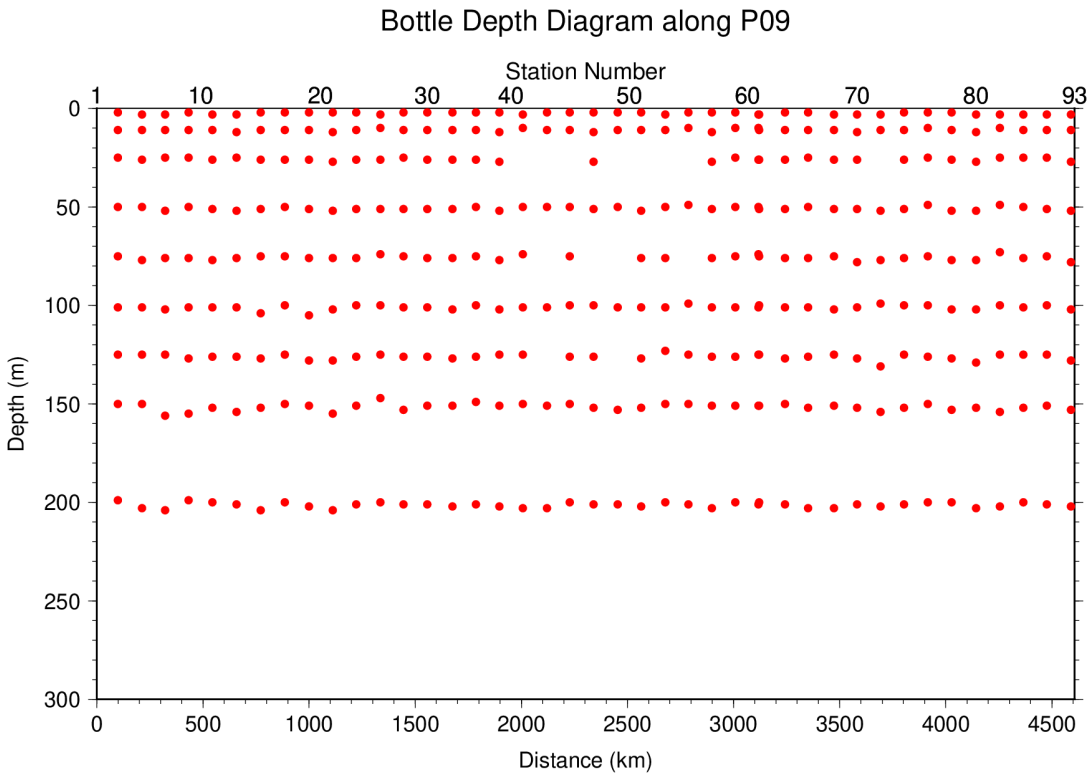

Figure C.5.2. Distance-depth distribution of sampling layers of chlorophyll-*a*.

(3) Reagents

N,N-dimethylformamide (DMF)

Hydrochloric acid (HCl), 0.5 mol L^{-1}

Chlorophyll-*a* standard from *Anacystis nidulans* algae (Lot. No. BCCD8179, Sigma-Aldrich, United States)

Rhodamine WT (Lot. No. A213E476, Turner Designs, United States)

(4) Instruments

Fluorometer: Trilogy (Turner Designs, United States)

Spectrophotometer: UV-1800 (Shimadzu, Japan)

(5) Standardization

(5.1) Determination of chlorophyll-*a* concentration of standard solution

To prepare the pure chlorophyll-*a* standard solution, reagent powder of chlorophyll-*a* standard was dissolved in DMF. A concentration of the chlorophyll-*a* solution was determined with the spectrophotometer as follows:

$$\text{chl. } a \text{ concentration } (\mu g\ mL^{-1}) = A_{chl} / a^{*}_{phy} \qquad (C5.1)$$

where A_{chl} is the difference between absorbance at 663.8 nm and 750 nm, and a^{*}_{phy} is specific absorption coefficient (UNESCO, 1994). The specific absorption coefficient is 88.74 L g^{-1} cm^{-1} (Porra *et al.*, 1989).

(5.2) Determination of R and f_{ph}

Before measurements, sensitivity of the fluorometer was calibrated with pure DMF and a rhodamine 1 ppm solution (diluted with deionized water).

The chlorophyll-*a* standard solution, whose concentration was precisely determined in subsection (5.1), was measured with the fluorometer, and after acidified with 1–2 drops 0.5 mol L^{-1} HCl the solution was also measured. The acidification coefficient (R) of the fluorometer was also calculated as the ratio of the unacidified and acidified readings of chlorophyll-*a* standard solution. The linear calibration factor (f_{ph}) of the fluorometer was calculated as the slope of the acidified reading against chlorophyll-*a* concentration. The R and f_{ph} in the cruise are shown in Table C.9.1.

Table C.5.1. R and f_{ph} in the cruises.

Cruises number	RF22-05	RF22-06	RF22-07
Acidification coefficient (R)	1.6219	1.6933	1.6607
Linear calibration factor (f_{ph})	1409.7	1577.7	1474.5

(6) Seawater sampling and measurement

Water samples were collected from 10-liters Niskin bottle attached the CTD-system and a stainless steel bucket for the surface. A 200 mL seawater sample was immediately filtered through 25 mm GF/F filters by low vacuum pressure below 15 cmHg, the particulate matter collected on the filter. Phytopigments were extracted in vial with 9 mL of DMF. The extracts were stored for 24 hours in the refrigerator at −30 °C until analysis.

After the extracts were put on the room temperature for at least one hour in the dark, the extracts were decanted from the vial to the cuvette. Fluorometer readings for each cuvette were taken before and after acidification with 1–2 drops 0.5 mol L^{-1} HCl. Chlorophyll-*a* and phaeopigment concentrations (μg mL^{-1}) in the sample are calculated as follows:

$$\text{chl } a \text{ conc.} = \frac{F_0 - F_a}{f_{ph} \cdot (R - 1)} \cdot \frac{v}{V} \qquad \text{(C5.2)}$$

$$\text{phaeo. conc.} = \frac{R \cdot F_0 - F_a}{f_{ph} \cdot (R - 1)} \cdot \frac{v}{V} \qquad \text{(C5.3)}$$

F_0: reading before acidification
F_a: reading after acidification
R: acidification coefficient (F_0/F_a) for pure chlorophyll-*a*
f_{ph}: linear calibration factor
v: extraction volume
V: sample volume.

(7) Quality control flag assignment

Quality flag value was assigned to oxygen measurements as shown in Table C.5.2, using the code defined in IOCCP Report No.14 (Swift, 2010).

Table C.5.2 Summary of assigned quality control flags.

Flag	Definition	Chl. *a*	Phaeo.
2	Good	362	362
3	Questionable	0	0

4	Bad (Faulty)	2	2
5	Not reported	0	0
	Total number	364	364

References

Porra, R. J., W. A. Thompson and P. E. Kriedemann (1989), Determination of accurate coefficients and simultaneous equations for assaying chlorophylls *a* and *b* extracted with four different solvents: verification of the concentration of chlorophyll standards by atomic absotption spectroscopy. *Biochem. Biophy. Acta,* 975, 384-394.

Swift, J. H. (2010), Reference-quality water sample data: Notes on acquisition, record keeping, and evaluation. *IOCCP Report No.14, ICPO Pub. 134, 2010 ver.1*.

UNESCO (1994), Protocols for the joint global ocean flux study (JGOFS) core measurements: Measurement of chlorophyll *a* and phaeopigments by fluorometric analysis, *IOC manuals and guides 29, Chapter 14.*

9. Lowered Acoustic Doppler Current Profiler

27 March 2024

(1) Personnel

MURAKAMI Kiyoshi (RF2206, RF2207)
WADA Kouichi (RF2205, RF2207)

(2) Instrument and measurement

Direct flow measurement from sea surface to sea bed was carried out using a Lowered Acoustic Doppler Current Profiler (LADCP). The instrument, RDI Workhorse Monitor 300 kHz (S/N 16468, 14108; Teledyne RD Instruments, USA), was attached on the CTD frame, orientating downward. The CPU firmware version was 50.41.

One ping raw data were recorded. Settings for the collecting data were as listed in Table C.9.1. A total of 92 operations were made with the CTD observations. The performance of the LADCP (S/N 16468) was good between Stn.1 (RF7041) and Stn.64 (RF7106). Beam 1 broke down at Stn.65 (RF7107), resulting in missing measurements. Using LADCP (S/N 14108) from Stn.66 (RF7108), it was good.

Table C9.1. Setting for the correcting data.

Bin length	8 m
Bin number	25
Error Threshold	2000 mm/s
Ping interval	1.0 sec

(3) Data process and result

Vertical profiles of absolute velocity are obtained by the inversion method (*Visbeck*, 2002). Both the up and down casts were used for the calculation. Because the first bin from LADCP is influenced by the turbulence generated by CTD frame, the weighted mean coefficient for the calculation was set to 0.1. The GPS navigation data were used in the calculation of the reference velocities and the bottom-track data were used for the correction of the reference velocities. Shipboard ADCP (SADCP) data averaged for 5 minutes were also included in the calculation. The CTD data were used for the sound speed and depth calculation. IGRF (International Geomagnetic Reference Field) 11th generation data were used for calculating magnetic deviation to correct the direction of velocity. In the calculation processing, we used Matlab routines (version 8b: 5 April 2004) provided by M. Visbeck and G. Krahmann. Because the uncertainty of velocity observed by SADCP is about 10 cm/s, we regard the error velocity from LADCP upper 1000 m as about 10 cm/s. Figures C.9.1 and C.9.2 show the results of the zonal velocity (eastward is positive) and the meridional velocity (northward is positive), respectively. The major currents in the western Pacific such as the Kuroshio (29°N to 31°N), the Equatorial Counter Current (3°N to 6°N), and the Equatorial Under Current (2°S to 3°N) appeared in the figures. Figure C.9.3 shows measurement errors of velocity estimated by the inversion method by the inversion method; some measurement points have error velocities exceeding 50 cm/s at depths greater than 1000 m, but the measurements are normal.

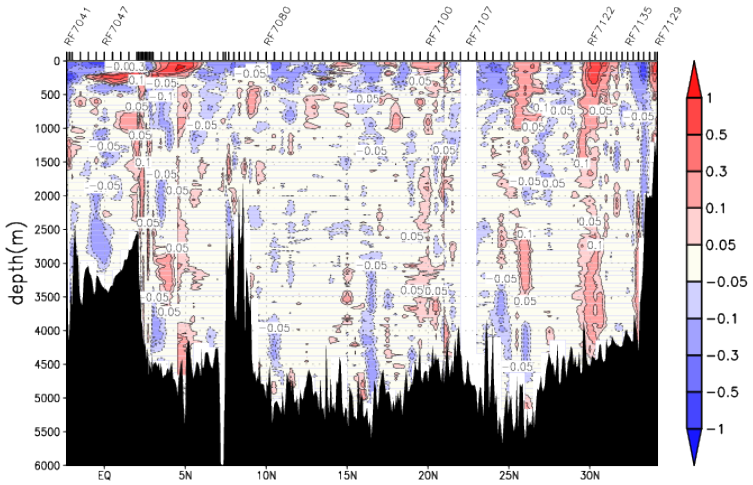

Figure C.9.1. The cross-section of zonal velocity (m/s, eastward is positive). Blanks are missing data from stn.65.

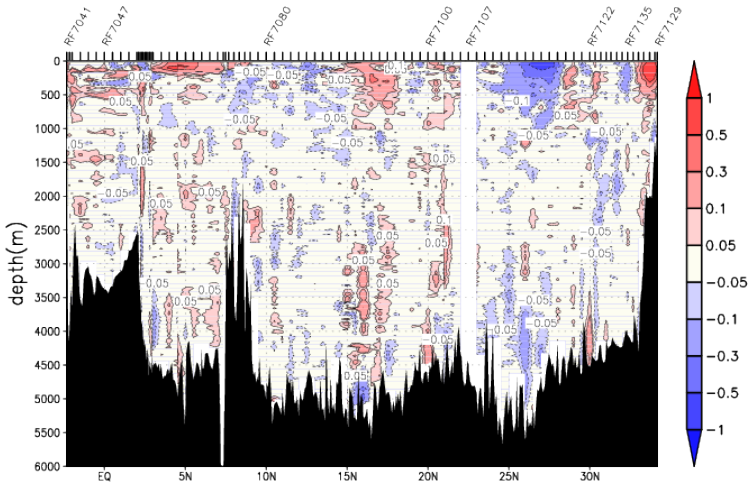

Figure C.9.2 The cross-section of meridional velocity (m/s, northward is positive). Blanks are missing data from stn.65.

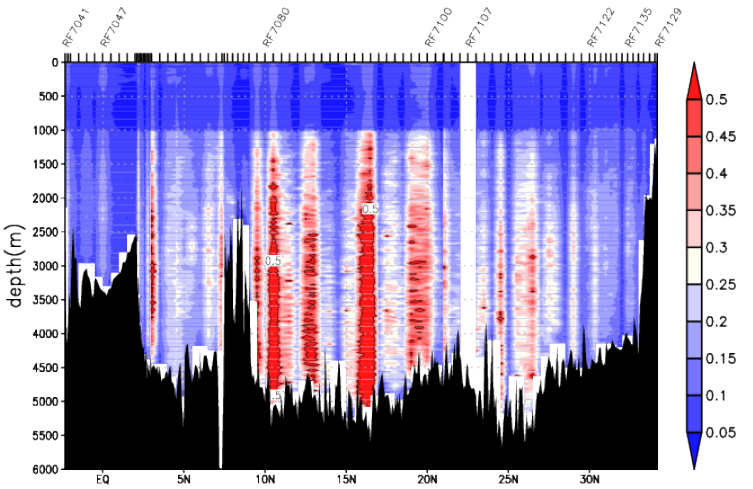

Figure C.9.3. Cross-section of measurement error in velocity (m/s) estimated by the inversion method. Blanks are missing data from stn.65.

Reference

Visbeck, M. (2002): Deep velocity profiling using Lowered Acoustic Doppler Current Profilers: Bottom track and inverse solutions. *J. Atmos. Oceanic Technol*., ***19***, 794-807.